R.P.I. Technical Report MP-30

A Progress Report for
July 1, 1972 to December 31, 1972

ANALYSIS AND DESIGN OF A CAPSULE LANDING SYSTEM AND SURFACE VEHICLE CONTROL SYSTEM FOR MARS EXPLORATION

National Aeronautics and Space Administration

Grant NGL 33-018-091

Submitted by the Special Projects Committee

D.K. Frederick
P.K. Lashmet
G.N. Sandor
C.N. Shen
E.J. Smith
S.W. Yerazunis

School of Engineering
Rensselaer Polytechnic Institute

ABSTRACT

Investigation of problems related to the design and control of a mobile planetary vehicle to implement a systematic plan for the exploration of Mars has been undertaken. Problem areas receiving attention include: vehicle configuration, control, dynamics, systems and propulsion; systems analysis; terrain modeling and path selection; and chemical analysis of specimens. The following specific tasks have been under study: vehicle model design, mathematical modeling of dynamic vehicle, experimental vehicle dynamics, obstacle negotiation, electromechanical controls, collapsibility and deployment, construction of a wheel tester, wheel analysis, payload design, system design optimization, effect of design assumptions, accessory optimal design, on-board computer subsystem, laser range measurement, discrete obstacle detection, obstacle detection systems, terrain modeling, path selection system simulation and evaluation, gas chromatograph/mass spectrometer system concepts, chromatograph model evaluation and improvement.

These tasks are defined in detail and the progress which has been achieved during the period July 1, 1972 to December 31, 1973 is summarized. Projections of work to be undertaken in certain areas during the period December 31, 1972 to June 30, 1973 are included.

TABLE OF CONTENTS

Analysis and Design of a Capsule Landing System and Surface Vehicle Control System for Mars Exploration

I. Introduction

Current national goals in space exploration include a detailed study and examination of the planet Mars. The effectiveness of Mars exploration missions would be enhanced according to the extent to which the investigative devices which are landed are mobile, to the range of their mobility, and to the ability to control their motion. In order to achieve basic mission objectives, and beyond that, to maximize the return on the commitment of resources to the mission, formidable technical problems must be resolved. The major factor contributing to these problems is the round trip communications time delay between martian and earth control stations which varies from a minimum of about 9 minutes to a maximum of 25 minutes. This time delay imposes stringent requirements on the vehicle, on its control and communication systems and on those systems included on board to make the scientific measurements, in terms of their ability to function autonomously. These systems must be able to operate with a high degree of reliability and must be capable of calling for earth control under appropriate circumstances.

A number of important problems originating with these factors and relating directly the basic mission objectives of an unmanned exploration of Mars have been and are currently being investigated by a faculty-student project team at Rensselaer Polytechnic Institute with the support of NASA NGL-33-018-091.

This progress report describes the tasks which have been undertaken and documents the progress which has been achieved in the interval July 1, 1972 to December 31, 1972.

II. Definition of Tasks

The delay time in round trip communication between Mars and Earth gives rise to unique problems relevant to martian and/or other planetary explorations. All phases of the mission from landing the capsule in the neighborhood of a desired position to the systematic traversing of the surface and the attendant detection, measurement, and analytical operations must be consummated with a minimum of control and instruction by earth based units. The delay time requires that on board systems capable of making rational decisions be developed and that suitable precautions be taken against potential catastrophic failures. Four major task areas, which are in turn divided into appropriate sub-tasks, have been defined and are listed below.

A. Vehicle Configuration, Control, Dynamics, Systems and Propulsion. The objectives of this task are to investigate problems related to the design of a roving vehicle for Mars exploration with respect to configuration; motion and attitude control; obstacle avoidance; control, information and power systems; and propulsion systems. In addition, the design concepts must accommodate the equipment and instruments required to automate the vehicle and to perform the scientific objectives of the mission.

B. General Systems Analysis. The objective of this task is to develop a framework within which decisions in design involving conflicting requirements can be made rationally and in the context of the whole system and mission. Relationships between alternative mission profiles and specifications and weight, energy and space allocation and management will be sought.

C. Surface Navigation and Path Control. Once the capsule is landed and the roving vehicle is in an operational state, it is necessary that the vehicle can be directed to proceed under remote control from the landing site to specified positions on the martian surface. This task is concerned with the problems of terrain modeling, path selection and navigation between the initial and terminal sites when major terrain features precluding direct paths are to be anticipated. On board decision making capability must be designed to minimize earth control responsibility except in the most adverse circumstances.

D. Chemical Analysis of Specimens. A major objective of martian surface exploration will be to obtain chemical, biochemical or biological information. Many experiments proposed for the mission require a general duty, gas chromotograph-mass spectrometer for chemical analysis. The objective of this task is to generate fundamental data and concepts required to optimize this chemical analysis system.

III. Summary of Results

Task A. Vehicle Configuration, Control, Dynamics, Systems and Propulsion

This broad task has been divided into the following subtasks: vehicle model design, construction and evaluation, mathematical modeling of vehicle dynamics; experimental dynamics analysis; obstacle negotiation; electromechanical control systems; collapsibility and deployment; wheel testing apparatus; and wheel analysis. A brief summary of the progress achieved in the prior interval in each of these areas follows below.

A.1.a. Design, Construction and Evaluation of a 0.4 Scale Model

A 0.4 scale model of the RPI-MRV is being constructed to serve a two-fold purpose. The first objective is to permit implementation of vehicle collapsibility and serve as a test bed for vehicle components. The second objective is the comparison of computer simulation results with physical testing of the 0.4 scale vehicle.

A.1.b. Vehicle Dynamics

The work of this task is continuing in the development of a mathematical model of the RPI-MRV. The emphasis on analog simulation has been shifted to that of simulation on a digital computer. Preliminary results of the simulation have been used to determine spring rates for the 0.4 scale vehicle. In the longer range, this mathematical model as validated by experimental studies will provide the basis for optimizing the design.

A.1.c. Stability and Obstacle Negotiation

The programs developed through June 1972 for analysis of vehicle behavior over step, crevasse and slope obstacles were to be modified to include the adjustable parameter of payload height. In this effort, a force-moment approach was taken instead of the previously used geometric approach. This simplified the analysis and will permit the development of a routine to evaluate stability and torque requirements for compound straight line obstacles and obstacle fields in a plane.

A.1.d. Radio Control

With the development of a 0.4 scale model to be used as a test bed for vehicle component study, the remote control of the vehicle is desired. This task has determined the mode and manner of signal transmission to link the vehicle with a remote controller. Hardware is being designed and built to implement the scheme developed.

A.2. Collapsibility and Deployment

The vehicle has taken a new form with respect to its payload shape and location. This new form complements the collapsibility and deployment scheme which has been developed. The payload may now be located in the center of the capsule which means the placement of the center of gravity central to the capsule is only a problem of arranging payload components so the payload cg is central to the payload. This condition is desirable for vehicle operation as well as meeting capsule constraints.

A.3.a. Wheel Tester and Grouser Design

Three aspects of making the wheel tester operational and using it to test wheels have been completed. The soil which will be used to simulate the Martian surface, as it is understood, has been prepared. The instrumentation required to make the wheel tester operational has been developed. Grouser designs have been prepared as candidates for testing. These designs incorporate variations in the basic parameters of wheel tread design. The data taken from experiments with these designs will be used to determine an optimum design for the conditions used in the testing.

A.3.b. Wheel Analysis

An effort was made to correlate past wheel design programs with existing models of the wheel. Correlation was not considered acceptable, so a new approach was taken to the problem of wheel analysis for design purposes. Correlation of test data with the results of the new analysis is acceptable for small deflections. This method will be extended to include deflections which go beyond the linear range, an assumption which had been made to simplify the first stage of the analysis.

Task B. General Systems Analysis

This major task is subdivided into three subtasks: identification of optimal designs and their sensitivity; time simulation of vehicle operation;and specification of an integrated Mars Roving Vehicle controller.

B.1. Identification of Optimal Designs and Their Sensitivity

The system design optimization problem has been solved for the case of a 4-wheeled rover communicating directly with earth. The solution specifies values of the parameters of the system design, e.g., weight and power allocations to the vehicle subsystems, and subsystem performance levels (communications data rate, vehicle velocity, science time). In addition, two other cases (4-wheeled rover communicating via a Mars orbiter, 6-wheeled direct communicating rover) will be solved by July 1973.

A method has been developed which identifies the optimal readjustments of design parameters to a forced perturbation in any one parameter of the design. This procedure will be used to investigate the sensitivity of the optimal designs identified above, and promises to be of use in dealing with the effects of any design variation.

B.2. Time Simulation of Vehicle Operation

Investigation of the operation of the vehicle system in real or scaled time was initiated during the reporting period. The purpose of this subtask is to analyze the operation of the designs identified in (1) with differing mission profiles and stochastic inputs, (terrain slopes, emergencies,...). The effects of an increased amount of earth control can also be determined. A computer simulation in the Monte-Carlo mode will be prepared by May 1973. The simulation will "track" the vehicle status during its on-surface operations.

B.3. Specification of an Integrated MRV Controller

The problem of onboard computer control of the many vehicle operations is being investigated. Specifically, the demands to be placed upon the onboard computer by the vehicle subsystems and queueing and system management operations by the computer will be specified and simulated on a GE-PAC/30 which has been programmed to have the capability of "appearing" to be any of a wide range of computational machines. A working simulation which includes a section which simulates the MRV as seen by the computer will be available by July 1973.

Task C. Navigation, Terrain Modeling and Path Selection

This task deals with problems of terrain sensing, terrain modeling, obstacle detection and path selection for an autonomous roving vehicle. Specific tasks receiving active effort include: the design of a laser range-finder for terrain modeling; terrain sensor instrumentation for a laser scan system; stochastic estimation of gradients; stereo and non-stereo obstacle

detection systems; and path selection systems evaluation.

C.1.a. Design of a Laser Rangefinder for Terrain Modeling

Various methods by which a laser may be used for rangefinding purposes in the range of 3-30 meters have been analyzed and evaluated. Optical focussing, timed pulse and phase difference techniques were compared. It has been concluded that a hybrid system combining the timed pulse and phase difference concepts is most promising. The construction of a system to be used under laboratory conditions to determine reflectance of typical materials and their accuracy is currently underway.

C.1.b. Terrain Sensor Instrumentation - Laser Scan Systems

The problem of obtaining scan information in the 3-30 meter range has been considered in detail. Emphasis has been directed to electro-optical methods which would permit scanning at a sufficiently high rate to allow for vehicle motions to be neglected. Acusto-optic beam benders, piezoelectric deflectors and digital light deflectors were considered. It was concluded that a system based on digital light deflectors was the most feasible. A detailed scanning system has been outlined.

C.1.c. Stochastic Estimation of Gradients

An analysis of the effect of measurement errors, i.e., range and elevation and azimuthal angles, on the gradient of terrain in the 3-30 meter range has been undertaken. It is found that measurement errors originating with vehicle motion, (i.e. roll, pitch and heave) result in very large errors in estimating the in-path and cross-path slopes and the gradient. It is concluded that a rapid scan system should be used to eliminate these errors. Assuming a rapid scan system obviating vehicle motion effects, the relationships between the standard deviation of gradient as a function of range and of the standard deviation range and elevation and azimuthal error for a horizontal flat plain have been determined. The standard deviation of gradient varies from less than 1^{o} to about 8^{o} depending on the measurement errors. The effect of an inclined terrain has also been determined.

As this effort more completely relates the effect of measurement errors on the reliability of terrain model interpretation, specification for a terrain sensing system can be defined more rationally.

C.1.d. Stereo and Non-Stereo Obstacle Detection Systems

Stereo and non-stereo obstacle detection concepts have been evaluated with regard to their ability to identify the height and range of discrete obstacles. The three systems studied were: (a) stereo angles, (b) stereo range, and (c) non-stereo (range-angle). It is concluded that the stereo angles method which

involves only the measurement of two angles is feasible only if the range measurement error cannot be reduced below 10 cm. and if the range is less than 12 meters. The stereo range method can only be effective if range errors can be reduced significantly. The non-stereo method is almost as good as the stereo angle method at short range and is much better at ranges larger than 12 meters.

C.2. Path Selection System Simulation and Evaluation

Development of the computer program for realistically simulating the performance of various path selection systems has continued. A variety of improvements have been incorporated including the vehicle's dimensions and attitude, both vehicle and vertical-fixed sensors, improved range measurement resolution, and improved output capabilities.

A limited comparison of three related path selection systems which use single and split beam laser sensors has been carried out. Currently work is being devoted to refinement of the program and the evaluation criteria, in addition to a comparison of vehicle- and vertical-fixed sensor configurations.

Task D. Chemical Analysis of Specimens

This task is concerned with developing the fundamental concepts which will be required to optimize a gas chromatograph-mass spectrometer analysis system. Topics receiving active effort include mass spectrometer characteristics, carrier gas generation and removal, multicomponent chromatography, and chromatograph model improvement.

D.1 Gas Chromatograph/Mass Spectrometer Systems Concepts

D.1.a. Mass Spectrometer System Characteristics

The mass spectrometer studies are intended to characterize the major properties of the instrument, the resulting relations to be suitable for investigation of system power, weight, and volume requirements. Relations involving mass resolution for single and double focussing instruments have been developed. Preliminary studies showed the theoretical analysis of instrument sensitivity to be beyond the scope of this project, and empirical relations are being sought. Investigation of the effect of major design variables upon power requirements has commenced with emphasis being directed on the ionization and accelerating chambers.

D.1.b. Carrier Gas Generation and Removal

Preliminary analysis of high-pressure gas storage as a source of carrier gas has been completed. Use of filament reinforced construction will provide storage capacity for one year's operation of the chromatograph within a volume of about one or two liters and a weight of about 2 kgm. The concept appears competitive with a previously proposed electrolytic gas generator. Engineering analysis of carrier gas removal by diffusion through a palladium alloy tubing has commenced.

D.2 Chromatographic Systems Analysis

D.2.a. Multicomponent Chromatography

Prior results showing limitations on superposition of pure component data to predict multicomponent chromatograms have been verified. Additional multicomponent data are being obtained on porous and nonporous adsorbents. Improvements in the chromatographic test facility are being undertaken to permit more automatic processing of the data. This involves magnetic tape recording of the composition detector signals and preliminary data processing by minicomputer. Experimental characterization of the adsorbents (pore size distribution, etc.) has begun.

D.2.b. Chromatograph Model Improvement

Intraparticle diffusion and rates of adsorption have been incorporated into the mathematical model of the chromatograph to improve representation of the experimental data. Moment analysis of the resulting system of equations shows the model to be capable of representing more adequately the spreading of experimental data. It appears an analytical solution of the model is not realizable, and numerical solution methods are being investigated.

IV. Detailed Summaries of Progress

Task A. Vehicle Configuration, Control, Dynamics, Systems and Propulsion

This broad task is concerned with all aspects of the design of a roving vehicle for Mars exploration. Included within this major effort are the following subtasks: vehicle model design, mathematical model of the vehicle dynamics, experimental dynamic analysis, obstacle negotiation, electromechanical control systems, collapsibility and deployment, wheel testing apparatus, wheel analysis, and payload design.

Progress made in these areas during the past interval is summarized in the sections which follow.

A.1. Vehicle Design, Construction and Evaluation

Student Group Leader: J. Almstead
Faculty Advisor: Prof. G. N. Sandor

Areas of major concern to the Vehicle Group are vehicle control, component design, dynamic analysis, and vehicle evaluation with regard to mission parameters. Vehicle control pertains to the basic functions of the MRV: steering, drive speed, payload attitude, and vehicle configuration. The problems associated with the vehicle control include sensing the states, acting upon and coordinating the functions. Component design pertains to the development of what might be considered subsystems of the vehicle structure. The major emphasis in this area has been placed upon payload and wheel design. Dynamic analysis has, and will include both analytical and experimental approaches to the determination

of the dynamic behavior of the MRV. Vehicle evaluation pertains to determining the performance factors of the MRV and comparing them with the performance criteria of the mission objectives.

The Vehicle Group has developed what is considered a third generation design of the RPI-MRV. The current design includes certain payload and collapsibility aspects which the previous models did not include. The new features have changed the shape of the vehicle slightly, but retained the original concepts of a dragster vehicle with wagon steering. The vehicle design has reached a stage where evaluation with regard to the mission goals and the capabilities of other proposed vehicles is necessary. As the evaluation is conducted, areas requiring additional redesign will become apparent, and those adjustments will be made.

The construction of a 0.4 scale model of the vehicle will permit physical testing and evaluation of the design capabilities and limitations. The model, presently near completion, will be ready for testing during the spring semester. The analysis of the design and testing of the model will be directed toward establishing performance factors in the areas of dynamic behavior, stability and obstacle negotiation, maneuverability, payload fraction, flexibility, reliability, and capsule fit. The plans for remote and computer control of the model will provide the vehicle the capability of being a test bed for the analysis of vehicle control concepts.

Projects planned for the spring semester are in the areas of dynamic analysis, wheel development and testing, vehicle control and design evaluation.

A.1.a. Construction of a 0.4 Scale Model - William Embleton
Faculty Advisor: Prof. G. N. Sandor

The objective of this task is to design and construct a 0.4 model vehicle structure which would support a scaled load comparable to the full size vehicle, which would be collapsible and maneuverable without an umbilical cord. According to Ref. 1, the estimated weight of a full size vehicle is projected as 1100 pounds. A comparable scaled weight for the 0.4 model was calculated to be 70 pounds.

An area moment analysis was performed on the rigid members of the vehicle to identify a configuration of each part which would allow them to be light and strong. Assuming a maximum static deflection for the torsion bar and for each of the structural members, appropriate dimensions of each part were estimated.

While the linear wheel model was programmed, a non-powered 0.2 model was built to finalize the vehicle design to be incorporated in the 0.4 model. The 0.2 vehicle model implemented the collapsibility scheme. It also utilized the double torsion bar which allows more room in the payload by putting the levelizing and attitude motors on the main frame.

Construction is now in progress on the 0.4 model and it is

planned that the construction of the frame with the motors will be completed by the first week of February 1973. When completely finished the 0.4 vehicle model will be collapsible, radio controlled,and self-powered. During the next period, dynamic testing of the 0.4 model will be initiated.

A.1.b. Vehicle Dynamics - Mark C. Rodamaker
Faculty Advisor: Prof. G. N. Sandor

The objective of this task is the mathematical modeling and computer simulation of the vehicle to predict vehicle response to perturbations. This modeling will permit estimation of the design parameters to insure a dynamic behavior of the vehicle which is compatible with the mission objectives. The modeling is being done assuming a bicycle configuration (Figure 1), and will be extended, in the future, to a three dimensional model.

Equations of motion for the seven-degree-of-freedom planar model have been derived using a complementary virtual work method which allows the inputs to be displacements rather than forces as required in classical Newtonian methods. An analog simulation was attempted, but due to problems with the analog machines available, it was decided to discontinue the analog simulation and shift the emphasis to a digital simulation. The equations have been programmed, but at this time the program is not running correctly.

Other work the past six months has included determining desirable spring constants for the wheels and torsion bar of the 0.4 scale model. These values were based mainly on analysis of test data accumulated over the past two years on the previous 0.184 scale models.

Emphasis for the next period will be on the digital simulation of the seven-degree-of-freedom model and investigation of the development of a three-dimensional simulation. These results should provide a rational basis for improving the design of the 0.4 scale model.

A.1.c. Stability and Obstacle Negotiation - Larry Mabius
Faculty Advisor: Prof. G. N. Sandor

Previous work in the area of stability and obstacle negotiation concentrated on determining the rear-wheel torque as a function of displacement as the obstacle was negotiated. Earlier studies assumed a fixed vehicle configuration and used trigonometric analysis to calculate the torque values.

Because the vehicle is capable to adjusting its payload height, it was felt that the vehicle configuration should be made an adjustable parameter. To facilitate this, a force-moment analysis was used in calculating the torques required. With the new approach, the vehicle configuration together with the three angles indicated in Figure 2, suffice for computing torque requirements. One angle

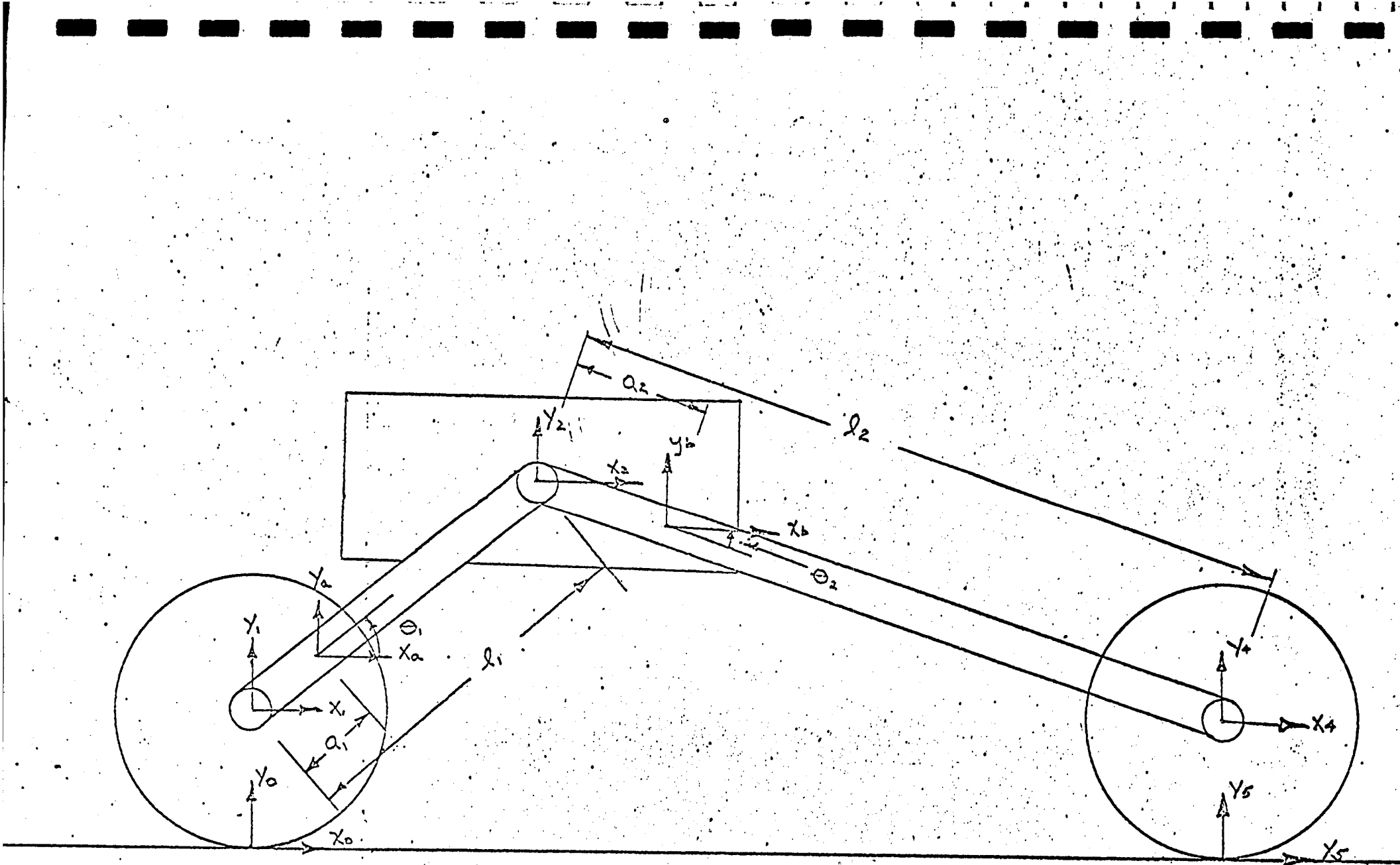

Figure 1. Mathematical Model of MRV

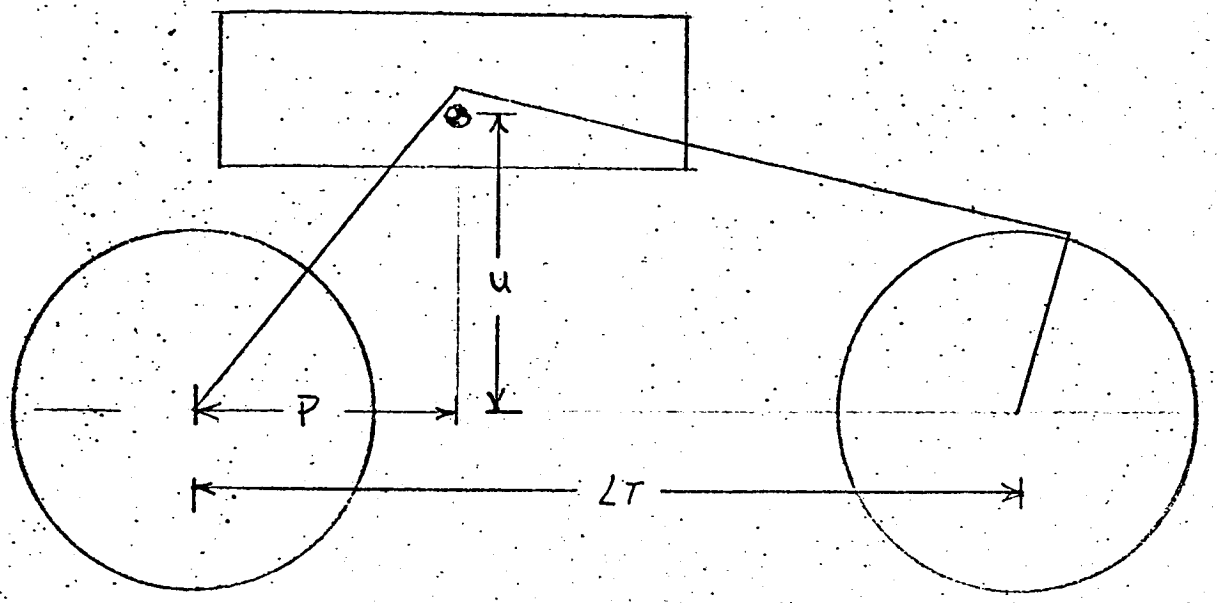

Figure 3. Model of the vehicle.

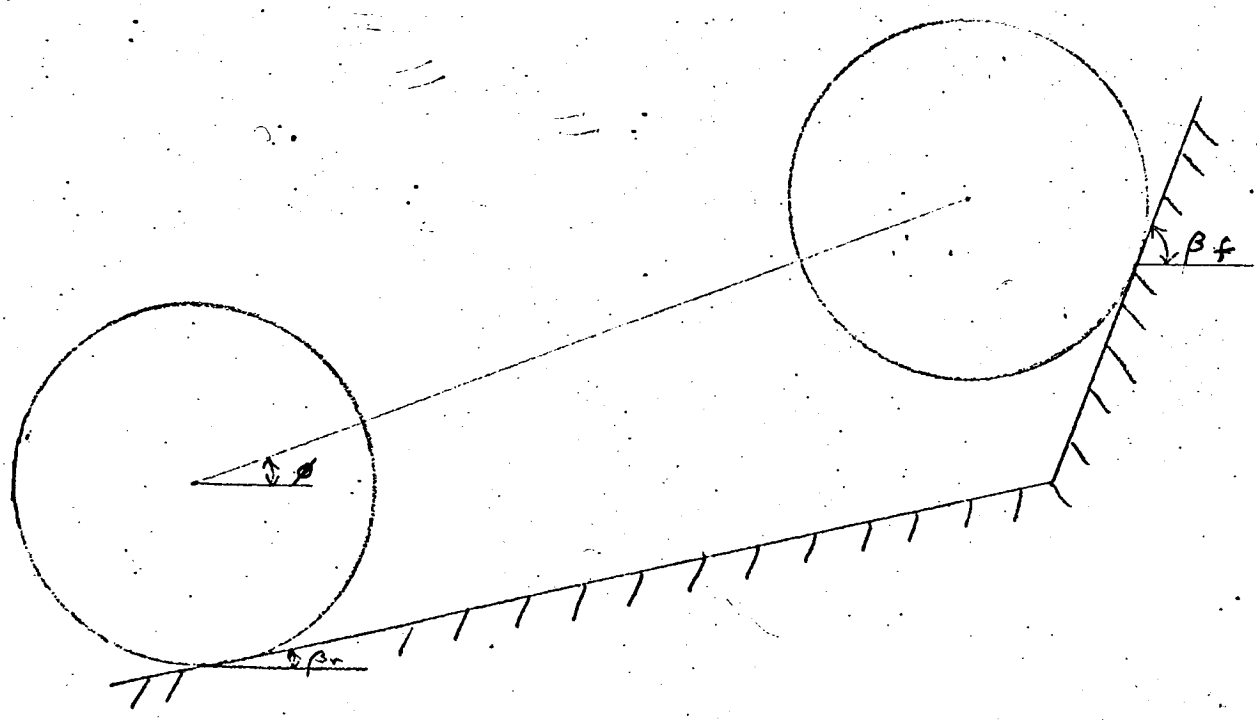

Figure 2. Angles determing the torque.

is the pitch of the vehicle and the other two reflect the slopes of the terrain on which the wheels are located. Also included was an indication when the center of gravity fell outside the wheel contact points, causing instability.

Figure 3 illustrates the relation among the dimensional parameters as the payload height is varied. The parameters of interest are the height of the center of gravity, the horizontal distance from the center of gravity to the rear wheel, and the overall vehicle length U,P and Lt respectively. Variations of these parameters have a simultaneous effect on the required torque. Analytical results indicate that, when negotiating step and crevasse obstacles, peaks in the torque demands occur when the front wheel starts over the obstacle and again when the rear wheel starts over the obstacle. In the case of slope obstacles, the analytical results, Figure 4, indicate that sharp peaks in the torque requirements do not occur.

Increasing the height of the center of gravity, which effectively shortens the rear strut length, causes a decrease in the torque requirement as the front wheel contacts the obstacle, and increases the torque demanded as the rear wheel contacts the obstacle. This may be explained by considering the vehicle as a class two lever. The wheel going up at the step applies the effort while the other acts as a fulcrum and the weight acts as the load. With the front wheel applying the effort, moving the center of gravity up and therefore rearward increases the ratio of the moment arms thereby decreasing the force applied. On the other hand, the same action with the rear wheel applying the effort, decreases the ratio of the moment arms thereby increasing the force. Since the force applied is generated by the torque on the rear wheels, the predescribed results take place. Therefore it seems the shifting of the center of gravity back and forth has a greater effect than shifting it up and down. This can be verified by observing the change in torque at U equal zero where the horizontal change in the cg is zero with respect to U and the height change is U. The change in torque is zero in all cases verifying the above effect.

Present work with the vehicle is to generalize the obstacle field. This field would consist of a series of straight lines connected together. The planar vehicle would traverse it in discrete steps. Then at each point the torque would be calculated along with an instability factor and a check for the hang-up. The instability factor would indicate where, along a line going between the two contact points on the wheels, the cg would be projected down on. In percentage terms, if this point were at the center of the line, it would be zero percent. Likewise, if it were at the end of the line (the cg would be right above the contact point), it would indicate 100% instability. The hang-up condition would test for contact between the ground and the terrain between the two wheels. This system, extended to three dimensions, will demonstrate the optimum vehicle height for negotiating any given terrain.

The generalization of the obstacle field in the plane should

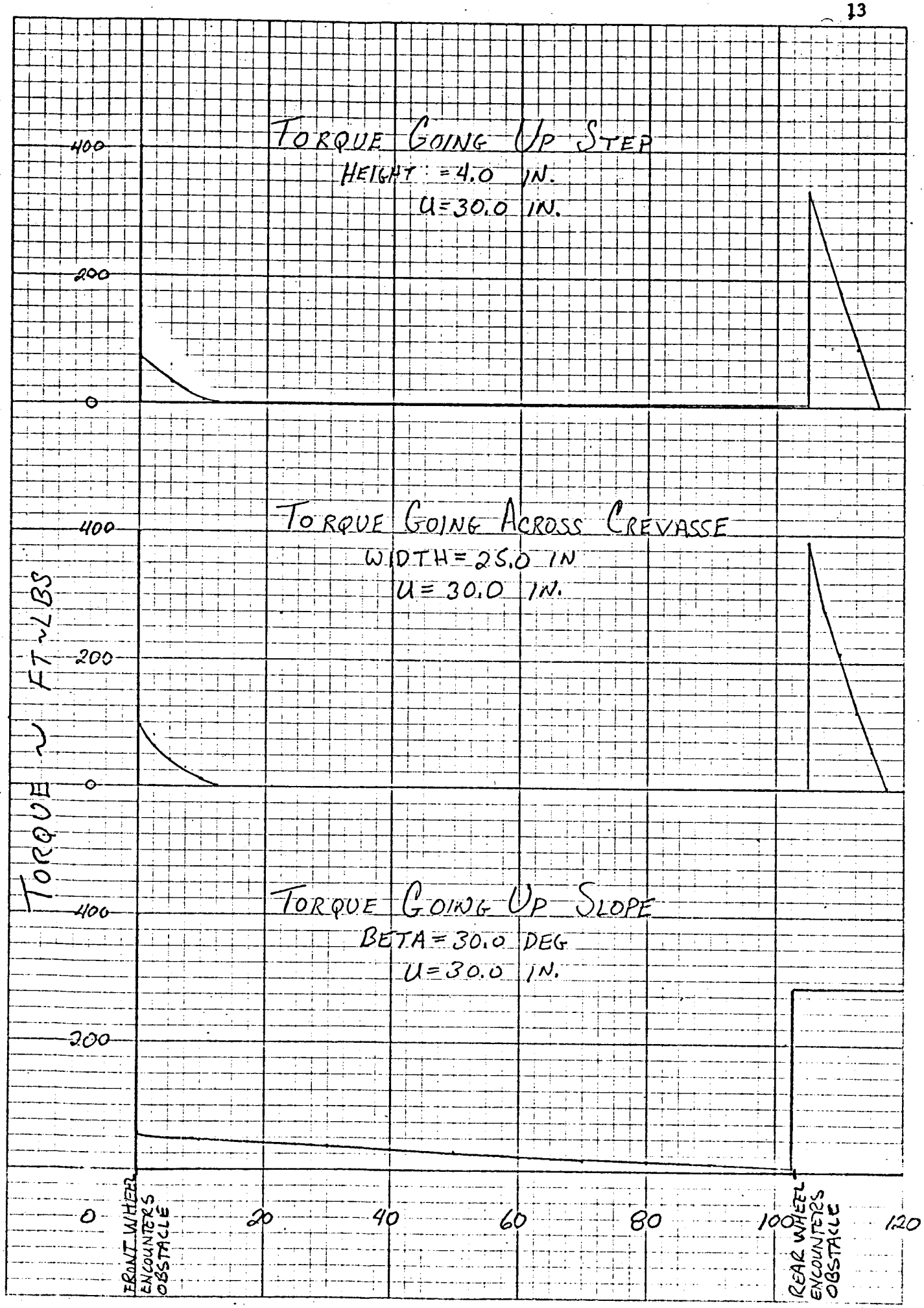
TORQUE GOING UP STEP
HEIGHT = 4.0 IN.
U = 30.0 IN.
TORQUE GOING ACROSS CREVASSE
WIDTH = 25.0 IN
U = 30.0 IN.
TORQUE GOING UP SLOPE
BETA = 30.0 DEG
U = 30.0 IN.
TORQUE ~ FT-LBS
400
200
0
400
200
0
400
200
0
20
40
60
80
100
120
FRONT WHEEL ENCOUNTERS OBSTACLE
REAR WHEEL ENCOUNTERS OBSTACLE

Figure 4.

be completed by March 15, 1973. Extension of the obstacle field to three dimensions should be concluded by May 15, 1973.

A.1.d. Radio Control - Mark Rinaldi
Faculty Advisor: Prof. G. N. Sandor

The objective of this task is the design and construction of a radio-control system for the 0.4 model of the RPI-MRV. Design of the overall system is divided into two parts:

1. The design and construction of the communications equipment that will transmit information to the vehicle.

2. The design of the accompanying vehicle control systems.

Attention was focussed primarily on the first of these two goals. Analog methods were rejected for signal transmission because of the difficulty in interfacing an analog system with the computer. The benefits of a digital transmission are primarily its large data handling capabilities and the relative ease with which it can be interconnected with the computer.

There are several ways in which digital signals can be transmitted in a serial fashion. The two which were considered are shown in Figure 5. In all serial systems, the transmitter and receiver must be synchronized so that the receiver can correctly interpret the incoming data. In the bipolar return-to-zero signal, there is a zero voltage, or "dead space" between each data bit. The appearance of a dead space indicates to the receiver that one bit has been completed and that another will soon be transmitted. The advantage of simplicity is readily apparent in such a system. Unfortunately such a bipolar signal cannot be handled by transmitters such as walkie-talkies.

Two types of transmitters were considered. The analog radio-control type, which is similar to those used for flying model airplanes, did not provide the desired system flexibility. The logical alternative was the walkie-talkie, which has the advantage of a potential for two-way, although not simultaneous, transmission.

To complement the walkie-talkie, the unipolar synchronius type signal format was chosen. With this signal, synchronization can be provided in two ways:

1. The simultaneous transmission of a synchronizing signal (also referred to as a clock) along with the data.

2. If the data rate is slow, a start pulse can be transmitted prior to the command, signaling the receiver that data is about to be transmitted. Such a pulse would activate and synchronize a clock generator at the receiver.

TYPES OF DIGITAL SIGNALS

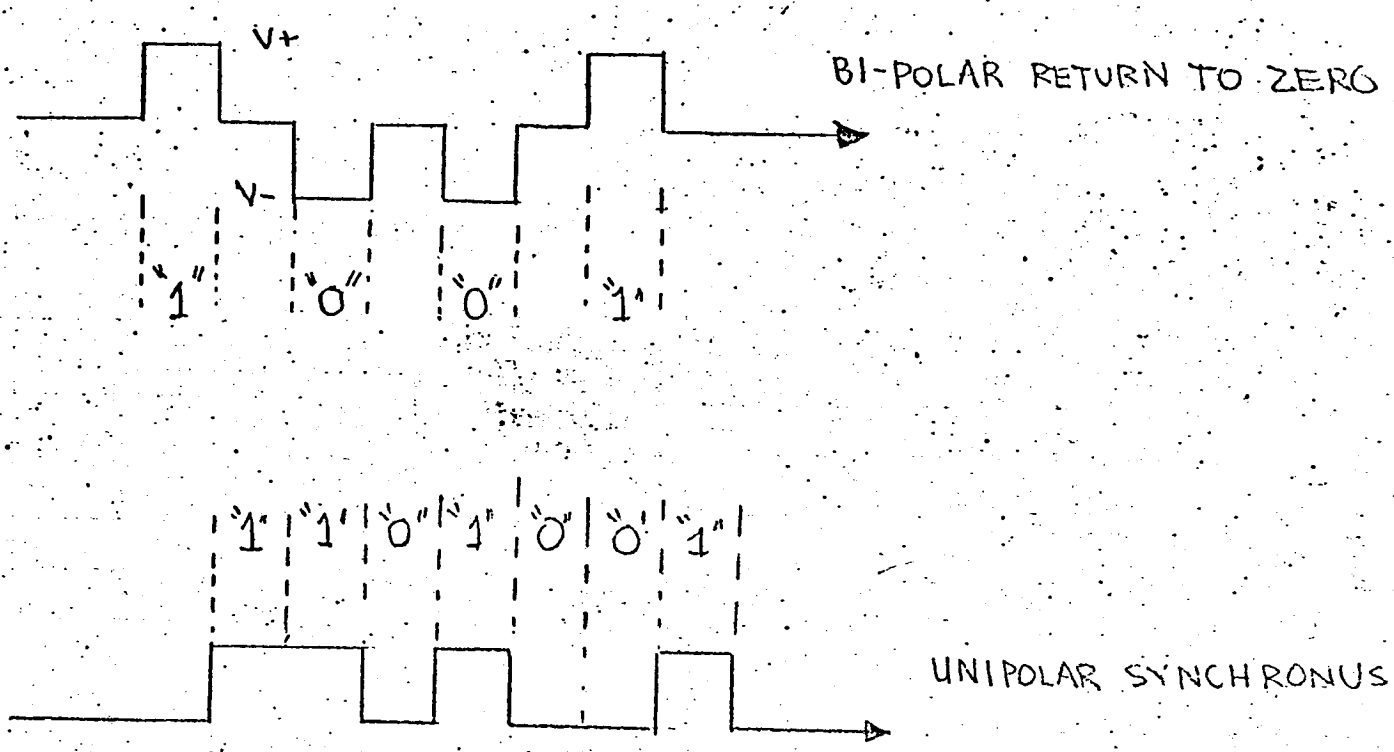

Figure 5.

SAMPLE COMMAND

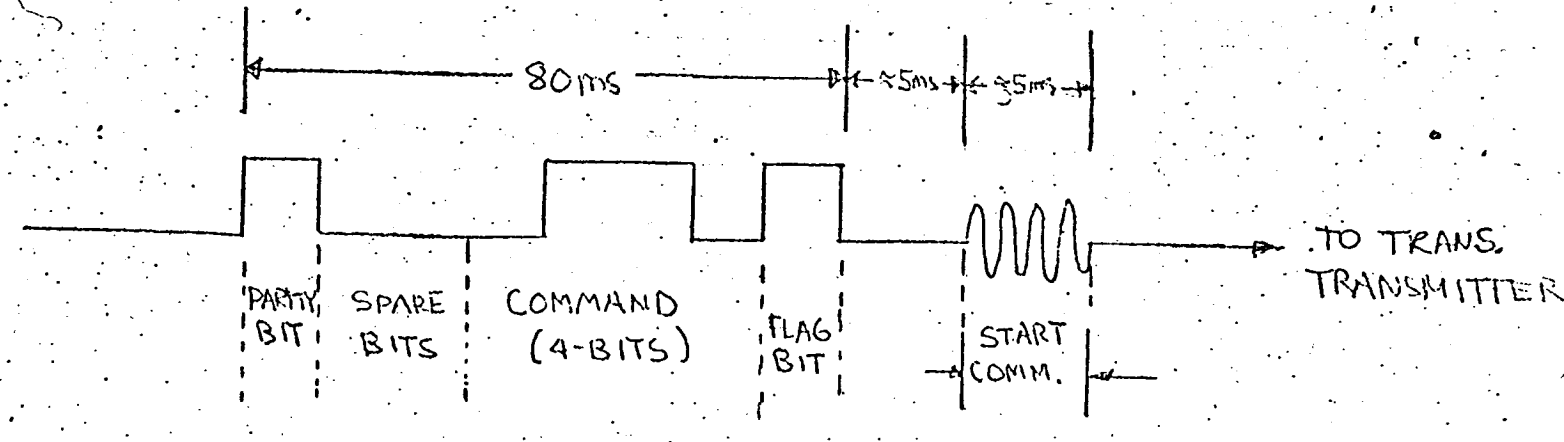

Figure 6.

The first case mentioned above would require two transmitting channels or multiplexing of the data line and the clock. Because of this difficulty the second method was chosen.

The next decision was the word length. For the actual data, a word of only four bits yielding 15 possible commands was deemed necessary. However in addition to the four data bits, one parity bit, one flag bit and two spare bits (for possible expansion of the system) were added. This brings the total bit count per command to eight. A sample command is shown in Figure 6.

The parity bit is used as a possible means of error detection. The first seven bits of the command are examined at the transmitter for even parity (an even number of "1"s). If even parity is detected then the parity bit is a "0"; if odd parity is detected the parity bit is a "1". The addition of this bit causes the now eight bit command to have even parity. When the command is received at the vehicle, it is examined for even parity. If this condition is met, the word is accepted as a valid command, if not (if odd parity exists) then the command is rejected, and a signal is sent back to re-transmit. Obviously an even number of errors will go undetected at the receiver.

Work has been concentrated on designing the Command Encoder. A schematic of this encoder is shown in Figure 7. As of this date, no concrete design work has been done on the various blocks at the receiving end. The most important unit here is the Command Decoder, which translates all binary commands into control signals for the various vehicle subsystems. The Command Decoder will operate in two modes as listed below:

1. Real Time Command Mode (RTC): In this mode commands that are sent to the vehicle are decoded and executed immediately by the Command Decoder. This work is now in progress.

2. Stored Command Mode: Here commands that are transmitted are not executed immediately. Instead the Command Decoder acts as a processor, routing the information to the Command Programmer (merely a memory unit). At some pre-determined time, these commands are fed to the Command Decoder which then decodes them and executes the necessary functions. This mode would simulate those times when an actual vehicle would be out of radio contact with Earth. (This mode will be implemented in the future).

A brief description of the RTC mode is as follows:

When the vehicle received the START (ST) pulse, it is told that data should follow at approximately 5 ms (microseconds) later.

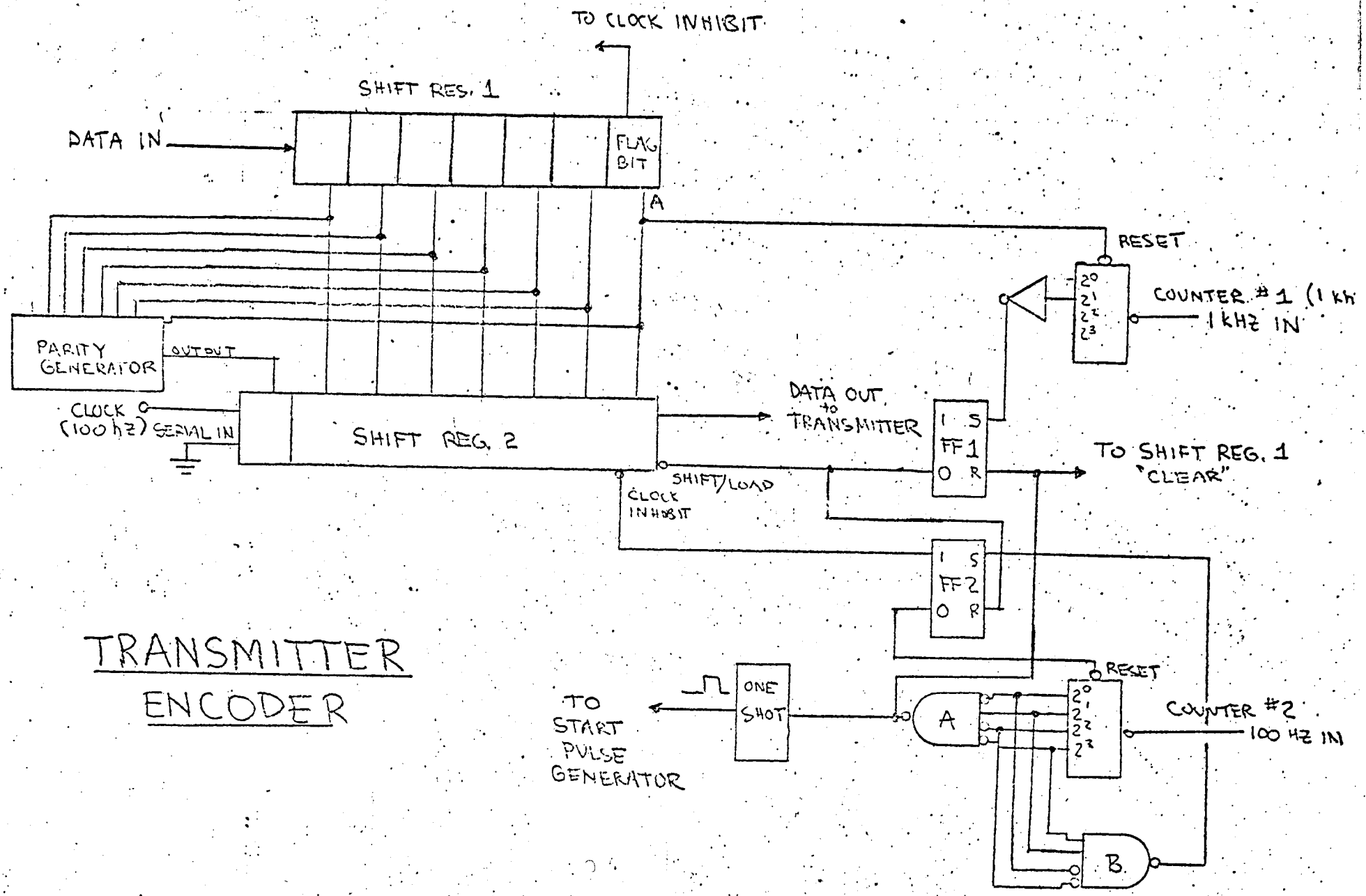
TO CLOCK INHIBIT
SHIFT RES. 1
DATA IN
FLAG BIT
A
RESET
PARITY GENERATOR
OUTPUT
CLOCK (100 hz)
SERIAL IN
SHIFT REG. 2
DATA OUT to TRANSMITTER
I S
FF 1
O R
COUNTER #1 (1 kH
1 kHz IN
TO SHIFT REG. 1 "CLEAR"
SHIFT/LOAD
CLOCK INHIBIT
I S
FF 2
O R
TRANSMITTER ENCODER
RESET
ONE SHOT
TO START PULSE GENERATOR
A
COUNTER #2
100 HZ IN
B

Figure 7.

This gives the receiver time to enable the inputs to the Decoder storage register and also to synchronize the onboard clock with that of the transmitter. After 5 ms the data starts coming in at a rate of 100 bits/sec. The first bit is the FLAG bit, and after 8 clock pulses the data completely shifts into the Decoder, and the FLAG is detected in the last register space (shown on the preceding page) the clock and data inputs are inhibited (to prevent further shifting of the data). The parity detector then samples the word, and accepts it if the parity is even. If odd parity is detected the command is rejected and a RETRANSMIT command is sent back to the transmitter (assuming two-way communication). Once the word has been accepted, bits 2-5 are decoded, executing the command. Of the 15 commands available, at least one will be reserved for addressing the Command Programmer.

The project objectives for the reat of the year are:

1. Construction of the proposed Command Encoder, March 15, 1973.

2. Design and construction of the Command Decoder, March 15, 1973.

3. Linking of the above units by radio communication, April 15,1973.

4. Interfacing the Command Decoder with the actual vehicle sub-systems, May 15, 1973.

A.2. Collapsibility and Deployment - J. Almstead
Faculty Advisor: Prof. G. N. Sandor

In the design of the RPI-MRV it is necessary that the aspects of collapsibiility and deployment be incorporated and analyzed as a functional part of the vehicle to insure a study of the complete vehicle system. The major objective of collapsibility-deployment is to permit the vehicle to fit within the Viking capsule. The secondary objectives are to utilize the collapsibility-deployment functions to further the flexibility of the operating vehicle, and to provide for collapsibility and deployment with reliability and minimum weight.

A collapsibility-deployment scheme was developed which provides for the vehicle to fit within the Viking capsule, Ref. 2. The scheme requires that the vehicle be "folded" in three areas. Figure 8 indicates these areas of concern to be: 1) the front frame pivot, 2) the folding and lengthening of the rear struts, and 3) the required flexibility of the front axle-vehicle frame connection.

The front frame pivot is to be used for collapsibility-deployment only. Once the vehicle has landed on the Martian surface

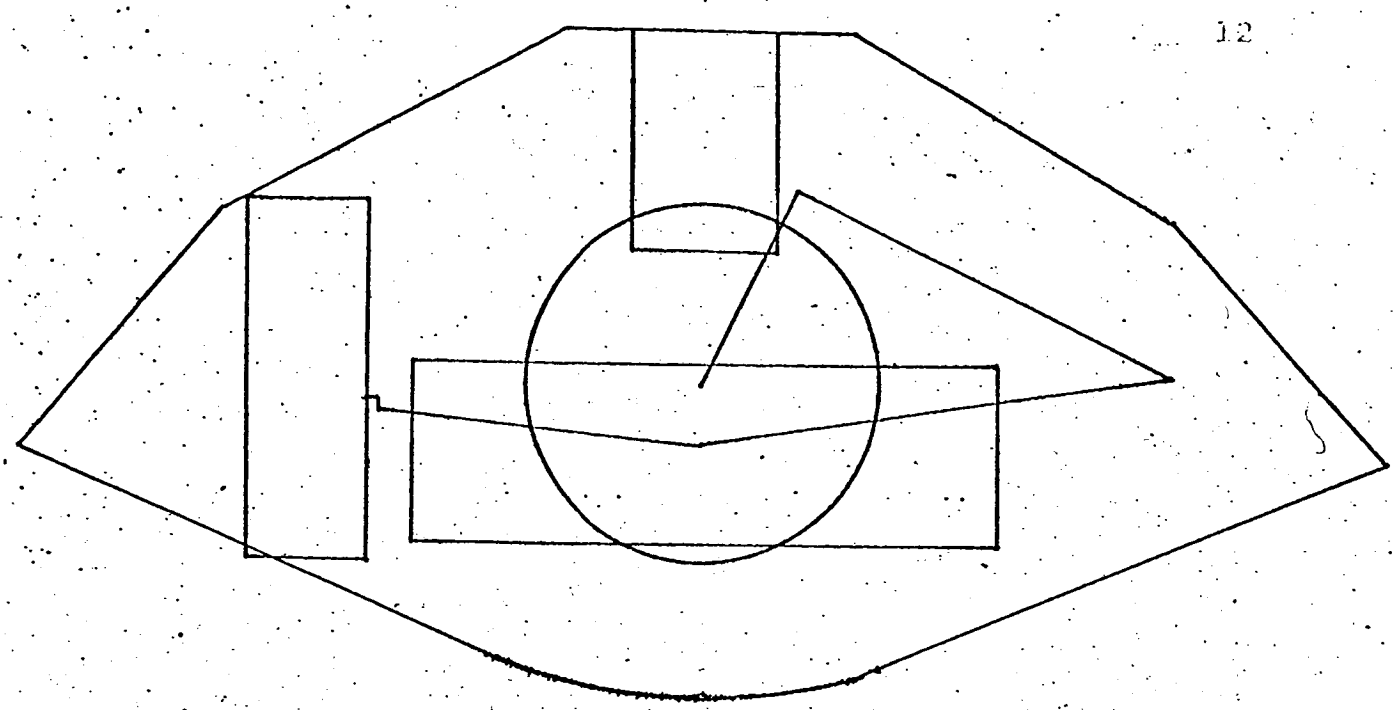

A. Side View

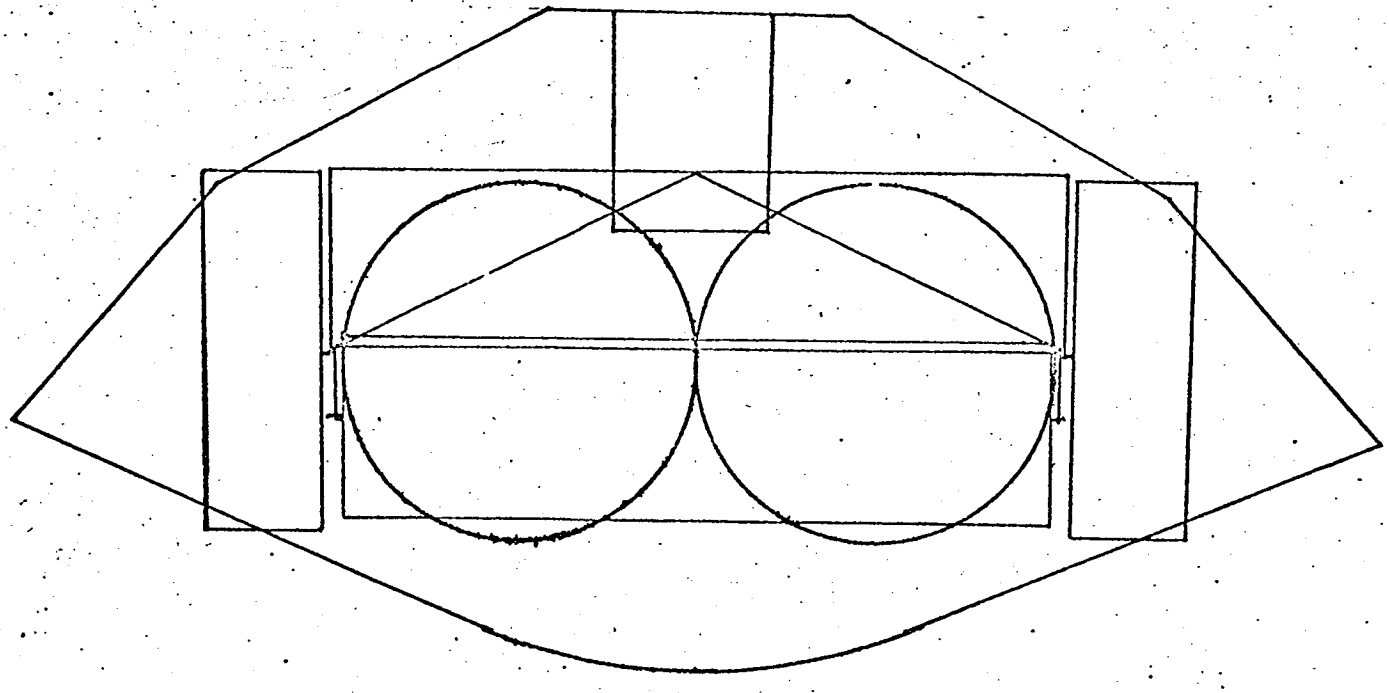

B. Front View

Figure 8 Collapsed Configuration of the RPI-MRV in the Viking Capsule

and has been deployed to its operational configuration, the front frame pivot will be fixed. Collars placed over the pivoting fore-section will attach it rigidly to the rest of the frame.

The rear strut pivot and lengthening will be accomplished by a four bar linkage. The linkage was developed through the use of the complex-number technique of linkage synthesis for three precision points and specified fixed pivot positions. A new computer program was written using this technique and used interactively on a graphic time sharing terminal to synthesize and analyze the four-bar mechanism that can be used to deploy the rear wheels. Once the rear wheels have been deployed, they will remain in the operational configuration for the rest of the vehicle life.

The front axle-frame connection has been designed to permit collapsibility-deployment, minimize weight, and provide for vehicle symmetry. The front axle and wheels may be rotated at the front axle-frame connection about an axis parallel to the torsion bar. This maneuver is accomplished by the same motor used to steer the vehicle, and permits vehicle symmetry about the plane of the vehicle frame. This allows the vehicle to perform an "emergency maneuver" without moving the vehicle body, swing the front wheels over the vehicle to the rear, and vice-versa. Thus reversed, the vehicle can drive away from a condition from which it could not have backed away.

These three mechanisms required for collapsibility-deployment are being implemented and tested on both the 0.2 scale model and 0.4 scale model.

Work during the second semester will be directed toward making operational and utilizing the Integrated Mechanisms Program (IMP) from Dr. J. J. Uicker of the University of Wisconsin, Ref. 3, and which is to be modified for our purpose. IMP is designed to analyze two or three dimensional mechanisms having single or multiple degrees of freedom. Kinematic, static or dynamic analyses are performed resulting in the calculation of positions, velocities, accelerations, forces, natural frequencies and damping ratios for a given mechanism. It is hoped that the vehicle "mechanism" and its component mechanisms may be analyzed with IMP. Once operational, this tool, it is expected, will aid the design as well as the analysis aspects of the mechanical design associated with the vehicle.

IMP is not complete. It will require writing several routines to adapt it to the RPI computer system. The program as received is not operational and will require debugging of some of its subroutines. An exact timetable is impossible to establish because the magnitude of the work is yet unknown. Much of the work depends on how similar or dissimilar the computer systems are.

A.3.a. Wheel Tester and Grouser Design - J. Ozimek and P. Marino
Faculty Advisor: Prof. G. N. Sandor

The purpose of this project is to determine the performance

aspects of wheels for a martian roving vehicle. The program was separated into six different segments, each of which had a specific goal. The first three segments were expected to be completed by January 1973 and the remaining three are expected to be finished by June 1973. The progress of the first three, i.e. sand preparation, instrumentation, and Grouser design, as well as an overall summary is as follows.

SAND PREPARATION: It was desirable to simulate the soil conditions the wheels would encounter over a year's span on Mars. Of course, this meant that all possible combinations of soil conditions could exist, from fine loose sand to hard bedrock. From a traction standpoint, loose sand represents the worst of possible conditions. For this condition,sand between two and sixty microns was obtained from a local creek bed. The sand was dried to zero percent moisture content. The moisture can be varied by the addition of water in a controlled manner. The density of soil condition can be varied by compaction as well as the addition of rocks.

There are few published results against which our findings can be compared. However, as long as soil conditions are kept consistent, valid differences can be determined between various tests and relative difference can be evaluated.

The environmental conditions at the test site are not optimal. Since most testing will take place during the colder months, heating will tend to evaporate the moisture content of the soil. This necessitates continual testing of the soil in order to maintain acceptable levels of accuracy. The test conditions will be duplicated, if necessary, by comparison with original recorded levels of parameters. Moisture content can be measured by comparison of wet and dry weights of soil. This involves a simple process of evaporating moisture content by means of a dryer.

INSTRUMENTATION: There were three different types of instruments needed for measurement. One was needed to measure speed, one to measure draw bar pull and one to measure delivered torque. The speed of both wheel and test cart will be measured electrically and recorded on a strip chart recorder. A device for measuring speed has been built and will give readings that are recordable on a strip chart. There will not be a great variation in speed and this device will be accurate enough within the range desired.

The measurement of draw bar pull can also be accomplished electrically and a device for doing this has been made. The results will be fed into a strip chart recorder with speed being recorded on a second channel.

There were problems with measuring the torque delivered to the wheel. Originally it was planned to measure the electrical power delivered to the motor driving the wheel. If the wheel is always traveling slower than the car (negative slip) this is an acceptable situation. However, if the wheel travels faster than the cart (positive slip) then power is being delivered to the motor

by the wheel. In this situation it is necessary to measure mechanical power directly, since the motor (or generator) current is no longer readily correlated with the power input.

The system chosen includes the use of four mechanical transducers which will yield constant outputs. Two solid state tachometers will record cart speed and rotational speed of the wheel under test. The tachometers were designed to facilitate recording of data during testing (see Figure 9). Two strain gauge systems will yield draw bar pull on the cart and applied torque to the wheel. One objective of this system is to enable all four parameters to be observed and recorded continually.

Several values will be kept constant for each run. These include cant angle of the wheel, load on the wheel, climbing angle, and sand conditions. Using these values and the four values being plotted, the characteristics of the wheel can be determined. The characteristics of most interest are the tractive coefficient and drive efficiency. Both of these values are typically functions of slip speed and vehicle speed, slip speed having the major effect. The tractive coefficient is the ratio of effective frictional force of the wheel on the sand to the normal load on the wheel. The tractive coefficient improves with more severe Grouser design. The efficiency, however, is highest with less severe Grousers as a rule. Therefore, the final Grouser design will involve a trade-off with respect to maximum power available from the vehicle and required performance characteristics.

Calibration of the instruments will be necessary before and during testing. This is not difficult because all conditions before actual testing are known or can be easily determined. The instruments can be kept within the same scale range and remain linear within the range of testing results.

Consistency of performance will have to be determined from the test results. The number of test runs necessary to obtain reliable data is important. Without any advance knowledge of how the device will perform, the number of individual tests remains unknown. When testing begins a large sampling will be taken and compared against itself to determine deviation. This should give some indication of how many tests for each condition is necessary and also determine the number of different conditions that can be tested within the allotted time frame.

GROUSER DESIGN: The design of Grousers is a conceptual engineering problem. Few actual formulas exist for design of Grousers, most design has been accomplished by use of empirical formulas or off the shelf designs. These formulas give only qualitative ideas of how Grousers will perform under various conditions. Three separate designs have been suggested and will be compared against each other. Trade-offs can be made among the three in order to

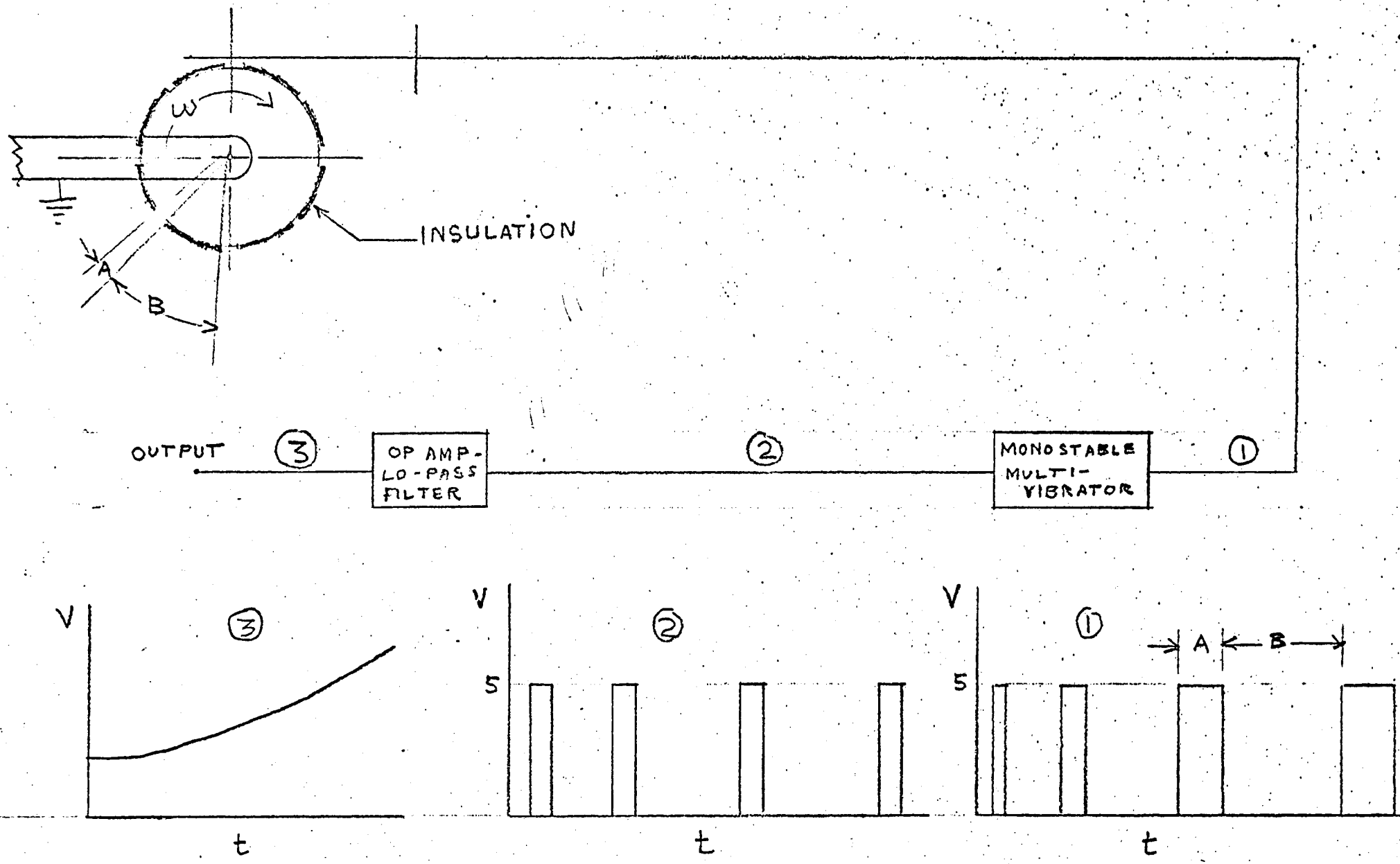

TACHOMETER

Figure 9

gain an optimally functioning Grouser.

The actual material used for the implements will be old tire rubber, because it is easily cut and shaped to desired forms. It will be glued on the rim in the present application but may be bolted on if necessary.

Selection of the best design will be made by comparison of data and observations from level and slope tests. Of course, in this application only three designs are being tested and compared. Ideally, tests should be conducted over a larger variety of Grouser designs as well as trade-offs among them.

FUTURE WORK: Three things remain to be accomplished: slope testing, level testing and lateral stiffness tests. It is expected that level testing and slope testing will take up one month each. A lateral stiffness test is necessary for three-dimensional mathematical modeling. This will be the last part of actual testing. A written summary of results and conclusions will complete the project.

A.3.b. Wheel Analysis - W. Embleton
Faculty Advisor: Prof. G. N. Sandor

The task of developing reliable methods for analyzing wheels for the Mars mission has been pursued for several years and a number of computer programs have been developed. However, none of the programs correlate effectively the experimental data for the 0.184 scale, 0.4 scale or full-size models of the RPI toroidal wheel. The objective of this task is to obtain an effective analysis method which can represent accurately the behavior of the wheel. An effective method will provide a rational basis for the design of wheels for defined specifications.

A linearized math model of the wheel was made with the help of Dr. C. A. Broniarek using methods outlined in Ref. 4. Programmed on the computer, the math model gave the deflection of the wheel due to a static load applied at the hub of the wheel. In this math model, the inner hoops which are attached to the hub and to a rigid rim are linearized. A load applied at the hub causes the springs to deflect yielding a system of forces along the rigid rim. Assuming a flexible rim and applying the system of forces a little at a time to the rim causes the rim to deform. After each deformation of the rim is accomplished, the deformed rim is regarded as rigid with the new deformation of the springs causing a new system of forces. When the sum of the forces of the springs caused by the deformed rim and the initial load is zero, an equilibrium is found for the wheel and a deflection of the wheel is found for a given load.

The results from the computer program compared satisfactorily to the experimental results previously observed. The graph of the

full scale model wheel showing the comparison of the computer results and the experimental results is shown in Figure 10. An effort is now being made to provide for Grouser design in the linearized math model program and to design a non-linear math model to be programmed which would give dynamic responses of the wheel due to external loads which might be applied. This math model will divide external loads into incremented parts and apply them to a linearized math model which will have material properties and spring coefficients changed after each deformation so that each incremented load will use the properties at the previous deflection to get an approximation for a deflection at the larger load thus giving a deflection curve for loads greater than those permitted by the linearized analysis.

During the next period a non-linear math model of the wheel will be designed and programmed. This will give a better design tool for the wheel giving fairly accurate displacement-versus-load graphs for the dynamic modeling of the vehicle.

Task B. Systems Analysis

The objective of this task is to develop a framework within which vehicle design decisions involving conflicting requirements can be made. Work previous to this report period established the method of optimal system design for the Mars roving vehicle to consist of: developing a static system model, measuring the system performance as a function of model variables, and imbedding the optimization problem in a nonlinear programming (NLP) format and so locating the optimal design. In addition, study of the computer requirements of such a system were initiated.

The progress of the work during this period will be summarized as follows:

B.1. Identification of optimal designs for several possible system configurations, namely

a. 4-wheeled vehicle, direct Mars-Earth communication
b. 4-wheeled vehicle, communication via a Mars orbiter
c. 6-wheeled vehicle, direct communication

B.2. Analysis of the performance of the optimal designs obtained in B.1 by Monte-Carlo scaled-time simulation.

B.3. Specification of an integrated Mars roving vehicle (MRV) controller.

B.1. Identification of Optimal Designs

Design of a vehicle intended to semi-autonomously rove the Mars surface while gathering scientific data, involves the incorporation of the ability to perform eight rather distinct functions. These functional divisions, or subsystems are:

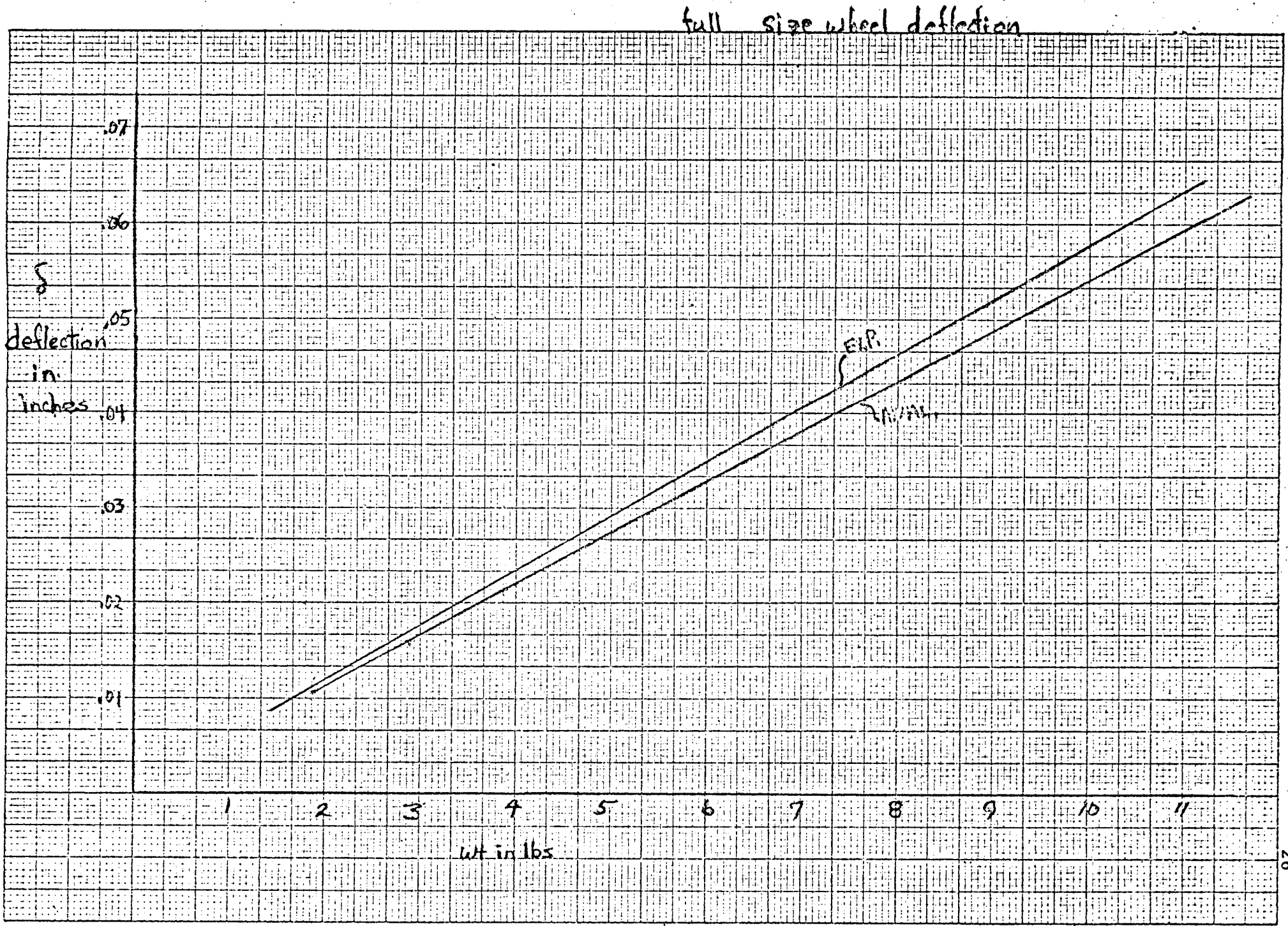

Figure 10

Science - collecting data and samples and performing experiments

Communications - transmitting science and engineering (vehicle status) data to earth and receiving earth commands

Power - generation and storage of energy required by vehicle subsystems

Thermal control - maintaining acceptable internal temperatures onboard

Navigation - locating the vehicle in Mars-centered coordinates

Obstacle avoidance - identifying terrain hazards and choosing a safe path for vehicle travel

Computation and data-handling - performing onboard computational operations

Vehicle structure - frame, motors, and suspension

The requirement that the vehicle system be deliverable to the Mars surface imposes weight, volume, and size limitations. The design problem then becomes an allocation problem. The operation of each subsystem will improve with increased power, weight, and volume allotted to it. The technique of this approach is to use a system model to measure these improvements and arrive at optimum allocations on the basis of a specified measure of system performance (the system evaluation or objective function).

B.1.a. Optimal Design of a Four-Wheeled Vehicle with Direct Mars-Earth Communication - C. Pavarini
Faculty Advisor: Prof. E. J. Smith

The system model equations (see pages 34-36) do not include volume considerations, for the sake of simplicity. It was found that a simple constraint (eqn. 49) could be used to guarantee adequate volume for the onboard equipment.

Based upon a list of equipment priorities determined in light of mission goals, approximate relations established for the science package are given in equations 1 through 3.

Analysis of the communications problem revealed that downlink (Mars-to-earth) considerations were far dominant. For a pulse-code modulated, X-band system assuming worst case link distance, equations 4 and 5 relate the important parameters.

The source of energy for the rover will be radioisotope thermoelectric generators (RTGs). Energy storage will be by nickel-cadmium

batteries. Equations 6 - 13 describe the subsystem. Because battery recharge can occur at the end of a Mars day, eqn. 13 constrains total roving time before a recharge to less than or equal to this time period. The square-bracketed term in eqn. 11 is a probabilistic measure of the percentage of roving time the vehicle will be using battery energy. It is based upon exponential slope distributions for the Mars surface.

Temperature control will be achieved through the use of an active cooling system with two radiators, on opposite sides of the rectangularly-solid equipment package, and an electrical heater. Assuming worst case radiation and surface degradation effects, eqns. 14 - 30 hold in the steady state. Note that a radiator exposed to direct solar radiation will be shut off.

Based upon analysis of the accuracy of several candidate navigation schemes, and relative insensitivity of other subsystem operations to navigation error, allocations to the navigation subsystem were fixed prior to optimization (eqns. 31 -33).

The obstacle avoidance subsystem uses a laser rangefinder to sense terrain at a distance r_a in front of the vehicle, and uses this information to calculate approximations of slopes. The term $\frac{2\, r_a \Delta\beta}{w_b}$ refers to the worst case error in slope detection. The equation for path length ratio (PLR) was established via Monte Carlo simulation. Eqns. 34 - 38 describe the subsystem.

Computation and data-handling will be accomplished as per NASA recommendation, by the use of the Thermoelectric Outer Planet Spacecraft (TOPS) computer subsystem, which is described by eqns. 39 and 40.

Based on the RPI MRV proposal for a four-wheeled rover, and using the fact that the vehicle will be dynamically scaled, vehicle structure dimensions and weight can be found by eqns. 41 - 43.

Finally, equation 44 simply places a limit on the total weight of the system to be delivered to Mars. The launch weight used is that for a Titan III-C launch vehicle, with allowances left for the equipment necessary to achieve a soft landing.

System Evaluation Function

When the expression that measures system performance is written as a function of the design parameters, the optimal design problem becomes one of choosing the design parameters to extremize that value of the objective function subject to the equality and inequality relations of the system model. Since the Mars rover has two responsibilities, to rove the surface and perform scientific

estigation, a reasonable objective might be to maximize the uct of distance roved and experimental science time. Of rse, there are other possible objective functions. On a Marsly basis, in terms of the model parameters, the chosen expression is written:

$$PLR \left[\frac{T_{esci}\, S_{sci}\, v_f^2\, T_{rov}^2\, V^2}{T_{sci}\, S_{sci}\, v_f\, T_{rov} + T_{rov} + T_r} \right]^2 \qquad (45)$$

Results of Optimization

The nonlinear programming problem (NLP) is:

$$\max_{F} \quad f(x)$$

$$F : g_i(x) \geq 0 \qquad i=1,2,\ldots,m \; ; \quad x \geq 0$$

where x is an n-dimensional vector and the f and g functions are general nonlinear functions of the elements of x. For solution of this problem, a program implementing Fiacco and McCormick's Sequential Unconstrained Minimization Technique was utilized. For NLP problem, only local maxima can be computationally located, several diverse starting points were used to achieve some degree of confidence in the solution. In all cases, convergence was the same point.

Letting the elements of x be W_{sci}, D_{com}^2, P_{com}, s*, v_f, A, E_{batt}, $_{sci}$ and L_i, and using the equality relations of the model to nate variables, the system design optimization problem reduces NLP problem in ten variables (n=10) with thirty-two inequality raints (m=32). The large number of inequalities results from act that many of the eliminated variables must be constrained ive since they represent real physical quantities.

A first solution of this problem indicated that there were incient constraints on several system variables due to factors considered in the model. D_{com}^2, s*, and v_f were too large, while and A were too small. Adding constraints on these variables:

$$s^* \leq 20 \text{ degrees} \qquad (46)$$

$$v_g \leq 1.5 \text{ m/sec} \qquad (47)$$

$$D_{com}^2 \leq 2.0 \text{ m} \qquad (48)$$

$$A \geq 7.35 \text{ m}^2 \qquad (49)$$

inal solution was:

W_{sci} = 66.3 kg

D_{com}^2 = 2 m^2

P_{com} = 180.0 watts

s^* = 20 degrees

v_f = 1.5 m/sec

A = 7.44 m^2

E_{batt} = 9.36 watt-hrs

w_b = 3.10 m

L_i = 0.0260 m

S_{sci} = 0.27 x 10^{-3}/m

from which all other system parameters can be calculated. The constraints of equations 39, 43 - 49 were equalities at the solution point.

B.1.b. Optimal Design of a Four-wheeled Vehicle Communicating via a Mars Orbiter - F. Stulen
Faculty Advisor: Prof. E. J. Smith

Analysis of this problem in the past established that the availability of an orbiter would effectively remove all constraints on data rate given a 10 kg weight allocation for the communications subsystem. Identification of the optimal design in this case then requires only that certain modifications are made in the system model presented in B.1.a and the NLP problem is resolved for this new model.

Modifications

The following changes can be made in the system model (new equation numbers relate to the unprimed numbers in B.1.a.):

a. The time required to transmit science data becomes negligible so that (2) becomes

$$T_{sci} = T_{esci} \qquad (2')$$

b. Weight allocation to communications is now constant

$$W_{com} = 10 \text{ kg} \qquad (4')$$

c. (5) can be eliminated.

d. The new optimal design problem reduces to a 9 variable problem (as opposed to 10 in B.1.b.) because P_{com} can be dropped as an independent variable and instead P_{com} is set to 40 watts.

Notation (values of constants are given in parentheses)

A	equipment package surface area, m^2
a	radiometric albedo of Mars, (0.295)
$A_{alb(r)}$	radiator surface area illuminated by albedo radiation, m^2
$A_{alb(s)}$	equipment package " " " " " "
A_r	total radiator surface area, m^2
A_T	surface area of the top and two sides of equipment package, m^2
A_{TR}	A_T plus area of one radiator, m^2
$A_{sun(r)}$	radiator surface area illuminated by direct solar radiation, m^2
$A_{sun(s)}$	equipment package " " " " " " "
a_1	ratio of radiator length to height, (3.33)
a_2	ratio of length of open side of equipment package to its height, (4.0)
a_{12}	$a_1 + a_2 + a_1 a_2$, (20.65)
D_{com}	communications antenna diameter (parabolic dish), m
E_{batt}	battery energy, watt-hrs
E_f	depth of battery discharge divided by efficiency of recharge process, (0.5
E_{fd}	depth of battery discharge, (0.40)
g_m	Mars gravitational constant, (3.75 m/sec^2)
h_c	Mars forced convection transfer coefficient, (1.30 watts/m^2-^oK)
k_i	heat transfer coefficient of insulation, (0.0216 watts/m-^oK)
K_q	cooling capacity, watts/^oK
L_i	insulation thickness, m
L_w	maximum launch weight, (570 kg)
M_r	mass of total vehicle system, kg-mass
P_{com}	power required by communications subsystem, watts
P_{cp}	" " " computation and data-handling subsystem, (90 watts)
PLR	path length ratio, ratio of actual to straight-line distance roved
P_{mv}	power required by onboard subsystems during roving periods, watts
P_{nav}	power required by navigation subsystem, (6 watts)
P_{oa}	" " " obstacle avoidance subsystem, (15 watts)
P_{prop}	power required to propel vehicle, watts
P_{RTG}	constant power output of RTGs, watts
P_{scia}	average power required by science package, (26 watts)
P_{str}	power required by onboard subsystems during recharge mode, watts
P_θ	" " " thermal control subsystem, watts
Q_h	heater power required at night, watts
Q_{id}	internal heat dissipation during the day, watts

Q_{in} internal heat dissipation at night, watts

r_a horizontal distance from vehicle to terrain being sensed, (30 m)

R_{com} communications data rate, bits/sec

S_c Mars solar constant, (720 watts/m^2)

s* maximum slope for allowable vehicle traverse, degrees

S_{sci} science stops per meter of travel, ___

T percentage of terrain vehicle will consider impassable

t vehicle track, side-to-side distance between wheels, m

T_{bd} temperature of equipment package external skin during day, ^oK

T_{bn} " " " " " " at night, ^oK

T_{esci} time required for experimental science during one science stop, sec

T_{hi} worst case (high) Mars ambient temperature, (275^oK)

T_{intd} required internal temperature during day, (310^oK)

T_{intn} " " " " night, (290^oK)

T_{low} worst case (low) Mars ambient temperature, (175^oK)

T_r time required to recharge batteries, hr

T_{rd} radiator surface temperature during day, ^oK

T_{rn} " " " " night, ^oK

T_{rov} maximum roving time between battery recharges, hr

T_{sci} time required to obtain and transmit science data per science stop, sec

V time during Mars day when earth is visible from rover, (10 hrs)

v_f roving velocity, m/sec

w_b wheelbase, front-to-back distance between wheels, m

W_{com} earth weight of communications subsystem, kg

W_{cp} " " " computation and data-handling subsystem, (46.8 kg)

W_{nav} " " " navigation subsystem, (15 kg)

W_{oa} " " " obstacle avoidance subsystem, (5 kg)

W_p " " " power subsystem, kg

W_{sci} " " " science package, kg

W_v " " " vehicle structure, kg

W_θ " " " thermal control subsystem, kg

α_r absorbtivity of radiator to solar radiation, (0.5)

α_{ri} " " " "infrared " , (0.8)

α_s " " equipment package to solar radiation, (0.5)

α_{si} " " " " "infrared " , (0.8)

$\Delta\beta$	error in detection of local vertical by navigation subsystem, (0.25 deg)
ϵ_r	emissivity of radiator, (0.8)
ϵ_s	emissivity of equipment package skin, (0.8)
μ_k	coefficient of kinetic friction of vehicle, (0.10)
σ	Stephan-Boltzman constant, (5.67×10^{-8} watts/m^2-$^oK^4$)

System Model Equations

Science

$$T_{esci} = 35.75\ W_{sci} - 135.0 \quad (1)$$

$$T_{sci} = T_{esci} + \frac{n \times 10^6}{R_{com}} \quad n = \#\text{ pictures/sci. stop } (n = 3) \quad (2)$$

$$P_{scia} = 26 \quad (3)$$

Communications

$$W_{com} = 0.418\ P_{com} + 2.0\ D_{com}^{\ 2} + 61.8 \quad (4)$$

$$R_{com} = 42.0\ D_{com}^{\ 2}\ P_{com} \quad (5)$$

Power

$$P_{RTG} = P_{prop} + P_{mv} \quad (6)$$

$$P_{prop} = M_r g_m v_f \left[\mu_k + \sin(s^* + 2^o) \right] \quad (7)$$

$$P_{mv} = P_{nav} + P_{cp} + P_{oa} + 0.2\ P_{scia} + 0.1\ P_{com} + P_\theta \quad (8)$$

$$T_r = \frac{E_f\ E_{batt}}{P_{RTG} - P_{str}} \quad (9)$$

$$P_{str} = P_{nav} + P_{cp} + 0.2\ P_{scia} + 0.1\ P_{com} + P_\theta \quad (10)$$

$$T_{rov} = \frac{\left[\dfrac{1 - e^{-.17\left(s^* + \frac{2\ r_a\ \Delta\beta}{w_b} \right)}}{e^{-.17\ s^*} - e^{-.17\left(s^* + \frac{2\ r_a\ \Delta\beta}{w_b}\right)}} \right] E_{fd}\ E_{batt}}{M_r g_m v_f \left| \sin\left(\frac{2\ r_a\ \Delta\beta}{w_b} + 2^o \right) \right|} \quad (11)$$

$$W_p = 0.168\ P_{RTG} + 0.037\ E_{batt} + 14.0 \quad (12)$$

$$T_{cy} \leq V, \text{ where } T_{cy} = T_{sci} S_{sci} V_f T_{rov} + T_{rov} + T_r \quad (13)$$

Thermal Control

$$(14)\quad A_T = \left(1 - \frac{a_1 a_2}{2\ a_{12}} \right) A - A_r \quad , \quad (15)\quad A_{TR} = A_T + \frac{A_r}{2}$$

$$(16)\quad A_{sun(s)} = \frac{\sqrt{a_1^{\ 2} + a_2^{\ 2} + a_1^{\ 2} a_2^{\ 2}}}{2\ a_{12}}\ A \quad ; \quad (17)\quad A_{alb(s)} = \frac{2\ a_1 + a_2}{2\ a_{12}}\ A$$

$$(18)\quad A_{sun(r)} = 0 \quad , \quad (19)\quad A_{alb(r)} = \frac{A_r}{2}$$

(20) $$A_T \epsilon_s \sigma T_{bn}^4 + (A - A_r) h_c (T_{bn} - T_{low}) = A_T \alpha_{si} \sigma T_{low}^4 + (A - A_r) \frac{k_i}{L_i} (T_{intn} - T_{bn})$$

(21) $$A_r \epsilon_r \sigma T_{rn}^4 + A_r h_c (T_{rn} - T_{low}) = A_r \alpha_{ri} \sigma T_{low}^4 + A_r \frac{k_i}{L_i} (T_{intn} - T_{rn})$$

(22) $$Q_h + Q_{in} = A_r \frac{k_i}{L_i} (T_{intn} - T_{rn}) + (A - A_r) \frac{k_i}{L_i} (T_{intn} - T_{bn})$$

(23) $$A_{TR} \epsilon_r \sigma T_{bd}^4 + (A - \frac{A_r}{2}) \frac{k_i}{L_i} (T_{bd} - T_{intd}) + (A - \frac{A_r}{2}) h_c (T_{bd} - T_{hi}) =$$

$$A_{TR} \alpha_{si} \sigma T_{hi}^4 + \alpha_s (A_{sun(s)} + a A_{alb(s)}) S_c$$

(24) $$\frac{A_r}{2} \epsilon_r T_{rd}^4 + \frac{A_r}{2} h_c (T_{rd} - T_{hi}) = \frac{A_r}{2} \alpha_{ri} \sigma T_{hi}^4 + \alpha_r (A_{sun(r)} + a A_{alb(r)}) S_c$$

$$+ \frac{1}{e} K_q (T_{intd} - T_{rd}) + \frac{A_r}{2} \frac{k_i}{L_i} (T_{intd} - T_{rd})$$

(25) $$Q_{id} + (A - \frac{A_r}{2}) \frac{k_i}{L_i} (T_{bd} - T_{intd}) = K_q (T_{intd} - T_{rd}) + \frac{A_r}{2} \frac{k_i}{L_i} (T_{intd} - T_{rd})$$

(26) $$W_\theta = 55.5 A L_i + 3.64 (\frac{a_1 a_2}{a_{12}}) A + 0.1 A_r K_q + 7.28 A_r$$

(27) $$Q_{id} = P_{cp} + P_{nav} + 0.2 P_{scia} + 0.05 P_{com} + 0.25 P_{oa}$$

(28) $$Q_{in} = P_{cp} + 0.5 P_{nav} + 0.2 P_{scia}$$

(29) $$P_{RTG} \geq Q_h + Q_{in}$$

(30) $$P_\theta = \frac{1}{e} K_q (T_{intd} - T_{rd}) \qquad \text{where } e = 0.8$$

Navigation

$$W_{nav} = 15 \text{ kg} \quad (31)$$

$$P_{nav} = 6 \text{ watts} \quad (32)$$

$$\Delta\beta = 0.25 \text{ degrees} \quad (33)$$

Obstacle Avoidance

$$W_{oa} = 5 \text{ kg} \quad (34)$$

$$P_{oa} = 15 \text{ watts} \quad (35)$$

$$r_a = 30 \text{ m} \quad (36)$$

$$T = e^{-.17 (s^* - \frac{2 r_a \Delta\beta}{w_b})} \quad (37)$$

$$PLR = 2 (1 + 0.05 T + 0.167 T^2) / (1-T) \quad (38)$$

Computation and Data-handling

$$W_{cp} = 46.8 \text{ kg} \tag{39}$$

$$P_{cp} = 90 \text{ watts} \tag{40}$$

Vehicle Structure

$$w_b = t \tag{41}$$

$$W_v = 182 \left(\frac{w_b}{3.04} \right)^3 \tag{42}$$

$$\frac{W_{sci} + W_{com} + W_p + W_\theta + W_{nav} + W_{oa} + W_{cp}}{W_v} \leq 2.0 \tag{43}$$

Launch Weight Constraint

$$W_{sci} + W_{com} + W_p + W_\theta + W_{nav} + W_{oa} + W_{cp} + W_v \leq L_w \tag{44}$$

Optimization

The changes noted above will obviously lead to an optimal design quite different than that identified in B.1.a. This new design will indicate the gains in system performance to be derived from servicing the MRV with a Mars-orbiter which has the capability of relaying data from the vehicle to earth.

Identification of the optimal design has not been completed, but is in the programming stage. Results are expected by March 15, 1973.

B.1.c. Optimal Design of a Six-Wheeled Vehicle with Direct Mars-Earth Communication - M. O'Callaghan
Faculty Advisor: - Prof. E. J. Smith

Modifications

Use of a 6-wheeled vehicle (e.g. Bendix or McDonnell Astronautics prototypes) requires considerable modification to the original system model. Major differences appear in the thermal control, obstacle avoidance, (and obviously) vehicle structure subsystems.

The six-wheeled vehicle consists of three segments, each with two wheels, coupled together. The thermal control problem is much different from the 4-wheeled case where there is only one equipment package to control. For the 6-wheeled configuration, there are two separate volumes requiring temperature control, each with different internal heat dissipation. Thus, the magnitude of the thermal control problem doubles, and in addition the two new problems are coupled.

The mobility of the 6-wheeled vehicle is quite different from the 4-wheeled version. Thus, (38) no longer holds, and a new expression is necessary.

Finally, the equations of the vehicle structure itself must change. The most important modification occurs in (43), which represents the payload fraction consideration. While for a 4-wheeled vehicle it is expected that the ratio of equipment weight to structure weight can be as high as 2:1, the 6-wheeled case should decrease this to 1.75:1.

All of the required modifications to the system model have been completed.

Optimization

As in B.1.b., the identification of the optimal design has proceeded to the programming stage. However, since this problem is more complex than that of B.1.4., more problems can be expected in obtaining the NLP solution, and so the projection for completion in this category is April 15, 1973.

B.2 Time Simulation of Vehicle Performance - R. Gallerie and T. Mans
Faculty Advisor: Prof. E. J. Smith

This is a new task area developed for the purpose of investigating the time performance of the vehicle. There are two motivations:

1. The optimal designs were established from static models which accounted for dynamic processes by averaging and/or worst-case approaches. It is important to check the validity of these approaches by finding out exactly what will occur onboard the vehicle during its operational life.

2. Dr. Garrett Paine of JPL has indicated interest in how the vehicle would perform under less autonomous operation, i.e. if earth commands were more frequent and specific. A time simulation will allow just that kind of analysis.

The goal in this area is to develop a working simulation of the vehicle by 1 June 1973. Major considerations will be flexibility of the simulation package, complete description of the vehicle time-state, and capability to simulate a comprehensive set of stochastic inputs and mission profiles.

B.3. Mars Roving Vehicle Computer - C. Boroughs and F. Samuel
Faculty Advisor: Prof. E. J. Smith

The objective of this task is to determine the onboard computer requirements for the Mars Roving Vehicle and to translate these requirements into a practical device that can be built and tested with the interfacing vehicle subsystems.

The onboard computer must be a very sophisticated device. Because of the communication delay time between earth and Mars and the nature of the mission profile, the computer must have the ability to make decisions concerning path selection, obstacle avoidance and navigation. It must also monitor, sequence and record the results of the MRV's scientific investigations as well as monitoring and controlling its own internal housekeeping functions which include power and temperature control and earth communication.

A study of the subsystem functions with respect to computer design has been initiated. Mathematical models of subsystems are being revised to be adaptable to the computer design. The computer will be modeled on a queing theory basis. The machine queing will be dictated by the subsystem functions. Then various computer architecture can be compared using the queing theory pattern developed.

In addition to definition and evaluation of parameters for the subsystems, preliminary design work was done in support of the vehicle group, Task A. The control program and hardware interface for the GEPAC-30 have been designed. This will be used to control

the 0.4 scale model under development. Effort has been directed at the design of an interface between the proposed hand held radio control unit and the existing hardware on the GEPAC computer.

In the next period, the complete subsystem parameter evaluation with the queing model will be completed. The design, writing and debugging of this simulation program will be effected.

Work on the 0.4 scale model and its associated electronics will be completed. It is anticipated that a certain amount of instructional effort will be required to acquaint the vehicle group with the operation of the GEPAC-30 computer. It is anticipated that computer programming will be required to support this effort.

Task C. Navigation, Terrain Modeling and Path Selection

The mission plan to undertake a systematic exploration of Mars requires that the roving vehicle can be instructed to proceed under remote control from its landing site to a succession of desired locations. This objective requires that the vehicle possess the capabilities: of sensing and interpreting the terrain to provide the information required by a path selection system, of selecting paths with due regard to safety and other considerations, and of knowing its location and that of its destination. Emphasis has been directed to the subtasks of: range measurement using lasers, obstacle detection systems, terrain modeling, and path selection systems evaluation. Details of the progress made are provided below.

C.1.a. Design of a Laser Rangefinder for Terrain Modeling - D. Palumbo
Faculty Advisor: Prof. C. N. Shen

The objective of this task is to investigate alternative methods by which range may be determined using a laser system. Included in the study were: optical focussing, timed pulse and phase difference methods. A hybrid scheme combining the timed pulse and phase difference concepts has been defined.

Optical Focussing

This method was investigated primarily for use with the "Stereo Angle" scheme being investigated under Task C.1.c. and involves the following basic features:

1. Laser light is used to illuminate a point.
2. A detector scans the field, "looking" for the point of laser light.
3. As the detector approaches the point, the intensity the detector "sees" will begin to rise until a maximum is reached and passed at detector angle .

If data was stored during the scan concerning intensity vs θ, the value θ' at maximum intensity can be determined through computer methods. Once θ' is known, geometry yields

$$\tan \theta' = R/B$$

where R is the range and B the laser-detector separation.

The accuracy of this method depends on how well θ can be resolved. Calculations made under Task C.1.c. indicate that accuracies on the order of five arc seconds are necessary to determine R within five centimeters. Although this may at first seem formidable, encoders are available at this accuracy. Gurley-Teledyne of Troy, New York, produces such a mechanism. It consists of an encoder wheel divided with 16,384 slots per revolution. The slots are sensed by a LED-photodiode combination. Using electronic extrapolations, accuracies of 4-5 arcseconds are available. The encoder is cylindrical, 6 inches long with a 3 inch diameter; electronics are rectangular with dimensions, 3x4.5x2 inches. The entire system weighs 5.5 lbs. and can be bought for 4-5 thousand dollars. Output from the encoder is in the form of a digital up-down counter.

Although the system seems feasible at this point, many factors weigh against it. The one dominating flaw is a resulting slow scan rate. A fast scan rate would eliminate error in data acquisition due to vehicle rock and roll. The necessity of the system to scan for a point, plus added encoder inertia would limit performance beyond fast scan assumptions.

Timed Pulse

In the Timed Pulse method, the laser is pulsed and split into two beams. One represents the leaving beam, the other the returning beam. The leaving beam is used to start a counter, which records elapsed time of flight, dt, when stopped by the returning beam. This time is related to the range through the speed of light.

In a previous investigation of the Timed Pulse method at Rensselaer, it was found that in order to achieve a 5 cm. accuracy a time resolution of .25 nanoseconds must be available for dt. Obtaining this resolution is a formidable task. For example, Reference 6, in 1969 investigated obstacle detection for the lunar rover, and reported accuracies of 30 cms. In 1971, W. Kuriger, Reference states that under laboratory conditions, accuracies of 10 cms. were available. Further investigation showed that a counter is commercially available through Nanofast corporation. The counter has .25 nanosecond resolution, but comes in large modular form, is heavy and lists from 4-5 thousand dollars.

Phase Difference

The basics are as follows. If the laser beam is modulated at a frequency f, the resulting wavelength, L, will be given by

$$L = c/f$$

where c is the speed of light. The rangefinder is to have a depth of field R in meters such that,

$$10 \leq R \leq 50.$$

The maximum distance the wave will travel will then be 100m. So L must be greater than 100 meters to insure a unique relation between the phase and the range. At L = 100 m the frequency of modulation will be given by

$$f = c/100 \quad 3\text{Mhz}$$

A pulse generator will be used to turn the laser on and off. When "on", a pulse modulator will superimpose the megahertz signal on the pulse. The modulating amplitude should not be large enough to turn the laser on or off. If the threshold voltage of the laser is given by Vt, then the modulating amplitude should be approximately equal Vt at most, so that the pulse amplitude must be twice Vt. This allows maximum modulation without disturbing laser operation. The laser pulse will contain several cycles of modulation. The phase difference between the reference, Vr, and the detector voltage, Vd can be determined through a heterodyning technique, explained below, (see Figure 11).

When two signals of different frequencies (w1, w2) are combined, side band frequencies are generated at the sum and difference frequences. If

$$Vd = \sin(w_1 t + \theta)$$
$$Vm = \sin(w_2 t)$$

where Vm is the modulating voltage, then,

$$V = \sin(w_i t + \theta) - 1/2 \cos(w_1 + w_2 + \theta)$$

If Vd and Vm are cosine functions then

$$V = \cos(w_1 t + \theta) + 1/2 \cos(w_1 t + w_2 t + \theta)$$
$$1/2 \cos(w_1 t + w_2 t + \theta)$$

These relations can be proved through Euler's equations

$$\exp(iy) = \cos(y) + i\sin(y)$$
$$\exp(iy) + \exp(-iy) = \cos(y) + i\sin(y) + \cos(y) - i\sin(y)$$
$$\cos y = (\exp(iy) + \exp(-iy))/2$$
$$\cos(x)\cos(y) = 1/4(\exp(i(x+y)) + \exp(i(y-x)) \exp(-i(y+x)) + \exp(-i(y-x)))$$
$$= 1/2\cos(y+x) + 1/2\cos(y-x)$$

If we let $y = w_1 t + \theta$
$x = w_2 t$

the relation is proved.

Using proper modulation frequency and band pass filtering, Vd may be reduced from 3Mhz to 3Khz and compared with Vr at 3Khz.

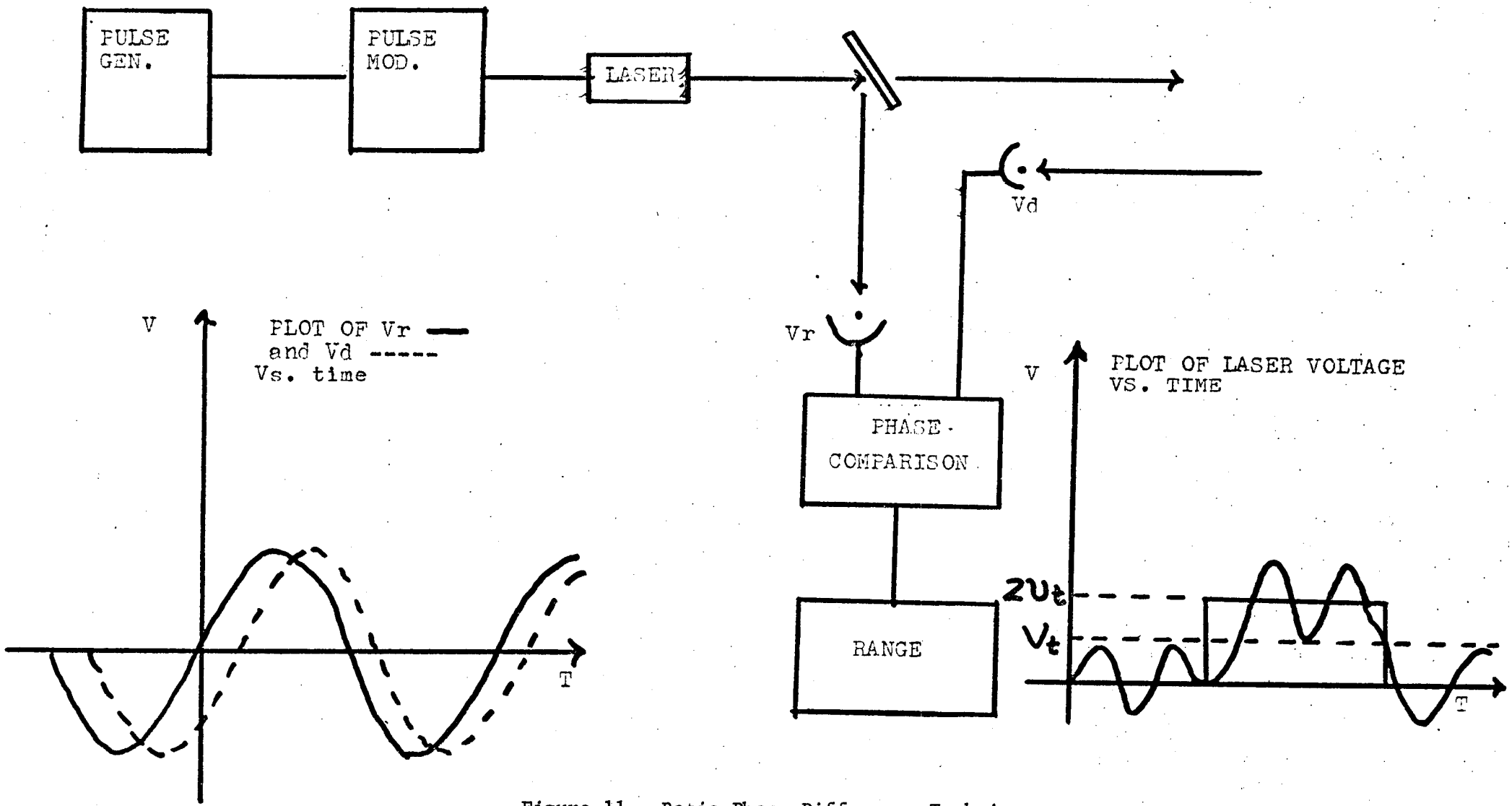

Figure 11. Basic Phase Difference Technique

If for example $\theta = \pi/2$, this corresponds to one quarter of the wave's period at 3Mhz or 83.3nsec. A phase delay of $\pi/2$ corresponds to a range of 25 meters. The resolution needed for 5cm. accuracy is

$$.05/25(83.3\text{nsec}) = .16\text{nsec}.$$

At 3Khz., after heterodyning, the period will be one thousand times greater, 83.3 microsec. and .16 microsecond resolution will be needed to resolve five centimers.

Conceptual Design Based on Hybrid Method

The Hybrid Method combines the Timed Pulse and Phase Difference methods to achieve accuracies within the requirements necessary. This type of design is used in surveying equipment with accuracies reported at 1 cm.

If a range calculation has just been completed and a new range is to be determined at a different point, the pulse generator is signaled. The pulse turns on the laser allowing modulation by the frequency generator. The returning wave is reduced by mixing with appropriate frequencies produced by the frequency generator until a 3Khz wave results. Zero detectors are used for controlling the counter by sensing the reference and reflected signals. The time displayed on the counter will represent the elapsed time of flight. Since many zero crossings can be obtained per pulse, the range may be averaged to further improve resolution. At the end of the calculation the rangefinder is ready for another pulse, (see Figure 12) for details.

Another design consideration is if the reflected beam will have enough power. Although the device will be operated primarily in the laboratory, some insight might be gained from looking at W. Kuriger's calculations for a Martian Rangefinder, Ref. 6

Pr = received power
Pt = transmitted power = 15 watts
E = optics efficiency = .4
Z = Martian surface reflectivity = .3
Ar = area of receiver = $.49\text{x}10^{-2}\text{m}^2$

then,

$$Pr = PtEZAr/2\text{pi}R^2$$

For a range of R = 30 meters, Pr equals .137 microwatts. At 5 meters, Pr equals 5 microwatts. With this in mind the following components were chosen for the prototype.

GaAs single diode laser

RCS TA 7609 @ 15 watts

photodiode - UDT Pin-5

Active area - .037 cm.^2

NEP - $6.5\text{x}10^{-3}$ w/Khz

Risetime - $5\text{x}10^{-9}$ sec.

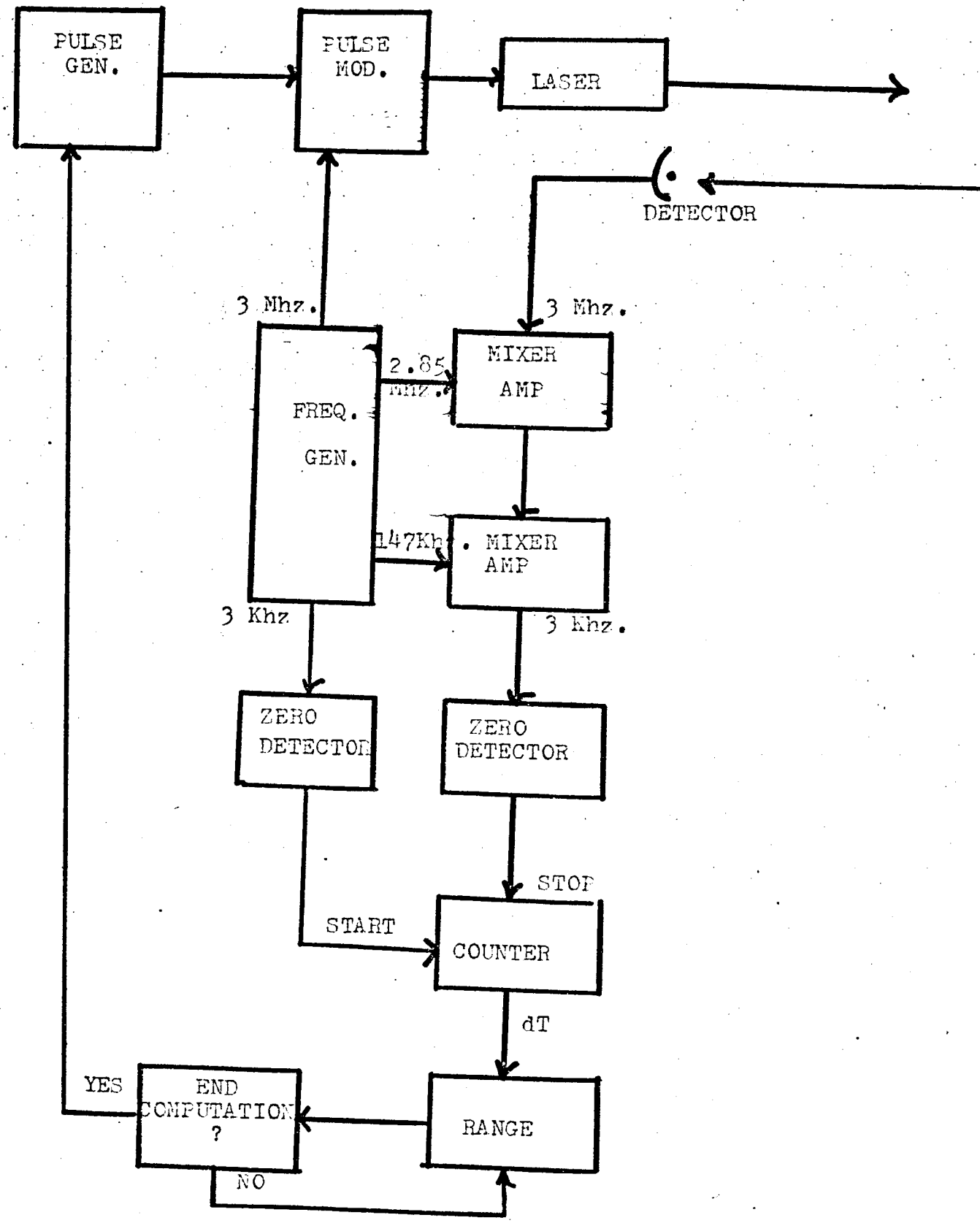

Figure 12. Final Design

Timetable for Future Investigation

	FEBRUARY	MARCH	APRIL	MAY
laser operation	----------			
analysis of terrain reflectance		----------		
incorporation of heterodyning			----------	
conclusion				----------

C.1.b. Terrain Sensor Instrumentation- Laser Scan Methods - G. Herb
Faculty Advisor: Prof. C. N. Shen

It is assumed that a laser range finder type of sensor will be used to supply the terrain data used by the Mars roving vehicle during its autonomous navigation. If this data is to be collected as the vehicle is moving, the rocking and rolling of the vehicle as it travels the uneven terrain can be a large source of error. The objective of this task is to reduce this error. Accordingly, the laser scan methods considered here are of a block scanning nature. That is, the entire field of view of the rover is scanned out very rapidly so that the rock and roll error between points is negligible and all points in the field may be considered to have been obtained simultaneously.

The criterion for a system worked under were:

1. No or few moving parts
2. A minimum of 10 data points per horizontal scan
3. An angle incremented scan (i.e. point spacings vary with distance from the vehicle)
4. Scan requirements: azimuthal angle 40° - 60°
   range angle - 40°

The last criterion results from the projected dimensions of the vehicle and the range of the scan (about 3 to 30 meters). The RPI vehicle is currently designed to be 10 feet wide, or about 3.1 meters. A 60° scan angle (i.e. $\pm 30^{\circ}$ from the direction of travel) is required to cover this width with a scan at 3 meters from the vehicle whereas at 5 meters a 40° scan angle is required.

The first method investigated was a system using oscillating mirrors to do the sweeping. With this system it is very easy to synchronize the transmitter and the detector since both use the same optics. The transmitted pulse is fired, and the return pulse comes back through the optics a few nano-seconds later. The mirrors have essentially not moved during this time and thus the

detector is "looking" at the same spot at which the pulse was fired.

The problem with this system is that it uses oscillating mirrors from which the angle data must be taken. At the scan frequencies of interest (> 10 KHz) angle decoders cannot be used on the oscillating mirrors because of the decoder disc's non-negligible inertia at those frequencies. Spinning poly-faced mirrors would solve the inertia problem, but synchronizing the two spinning mirrors with a high degree of accuracy and keeping them synchronized would be an extremely difficult task. It is therefore felt that this system would not be satisfactory.

Electro-Optics

In order to decrease or eliminate this necessity of detecting angle information from a mechanically oscillating mirror, it seemed that a reasonable approach would be to investigate electro-optic and other electronic scanners.

There are several types of electro-optic devices. The three considered were: (a) acusto-optic beam benders, (b) piezoelectric deflectors and (c) digital light deflectors.

Acusto-optic beam benders use the property of some crystals which causes their refractiveindex, n, to have a gradient proportional to a pressure gradient set up in the crystal. Therefore, since light is bent toward an increasing gradient in the refractive index, by changing the index gradient of the crystal the deflection of the beam is changed. In crystals which possess the acusto-optic property, the index gradient may be changed simply by changing the pressure gradient in the material. The major problem with this type of deflection, however, is that the proportionality constant between the pressure gradient and the n-gradient is extremely small, Ref. 7. Typical units provide deflection angles on the order of tenths of degrees. These angles are much too small for our purposes.

Piezoelectric deflectors use the well known piezoelectric effect of certain crystals which causes them to deform in certain ways when an electric potential is applied across them. The most common deformation used are the longitudinal and the shear deformation. A reflective surface is attached to one face of the crystal, and it is the motion of this surface as the crystal is deformed which is used to cause the deflection.

The advantages of this type of deflection is that the transmitted light pulse and return pulse may use the same optics. It thus has all the advantages of the vibrating mirror scan described earlier without the problems associated with the mirrors being mechanically scanned and synchronized. But once again maximum angle is limited. Commercially available units have maximum scans on the order of 6^{o}, Ref. 8. Also the angle data must be obtained indirectly from the analog control voltages.

Digital deflectors are sensitive to the incident light's direction of polarization. The incident beam will be laterally displaced or angularly deflected to one of two possible positions depending on its direction of polarization. These deflectors consist of a polarization modulator, such as a Pockel or Kerr cell, which either rotates the direction of polarization 90^{o} or allows it to pass unrotated, followed by a binary birefringent discriminator, i.e. a crystal with two indices of refraction depending on the direction of polarization of the incident light. Much work has been done on these deflection devices, notably by Kulcke, et al, Ref. 9 and T. J. Nelson, Ref. 10. The number of positions available at the output of a deflection system can be increased by cascading individual binary units. Properly cascading N of these units results in 2^{N} positions in the final output. Going from a one dimensional to a two dimensional scan is easily accomplished by adding an M unit scanner rotated by 90^{o} with respect to the first N units. This results in an array of 2^{N} by 2^{M} possible deflection positions.

The binary units accomplish a lateral displacement as shown in Figure 13a. An incident beam of collimated light will be deflected by an angle θ if its polarization direction is in the plane of the crystal's optical axis. If the direction of polarization is normal to the plane of the axis, the beam is not deflected at all. When the deflected beam hits the edge of the crystal, it is again deflected so that it emerges from the unit parallel to the incident beam. Therefore a two dimensional digital scanner will provide a 2^{N} by 2^{M} matrix of parallel beam positions. A method of converting these parallel beam scans into angular scans will be covered later.

The angle θ is a function of the crystal material and the angle the optic axis has with respect to the incident beam. The figure also gives maximum values of θ for three crystal materials and the value of γ needed to obtain that maximum.

Note that in each cell the control voltage is either present or absent, corresponding to either a rotated polarization in that cell or a non-rotated polarization. Therefore, each position available at the output can be associated with a unique binary code word determined by which cells are energized and which are not for that point. Thus each point in the sweep is known exactly by the particular code word being issued by the control logic at that instant.

There are several problems with these binary units. Two are mentioned here for completeness.

To rotate the polarization of light by 90^{o} in a Pockles cell, the half wave voltage must be applied to the cell in such a way as to set up an electric field in the cell parallel to the direction of light propagation. To accomplish this, electrodes must be placed in the optical path. This then creates the problem of finding the optimum compromise between the two competing requirements

of low resistance electrodes and maximum transmittance of light by the electrodes. Kulcke found highly acceptable results could be obtained using a variety of electrode-adhesive combinations, Ref. 9. It was also found that the modulator electrode transmittance was the limiting factor and hence the total system transmittance could be approximated as

$$Tsys \cong t^{2n}$$

where t is the transmittance of an electrode-adhesive combination, and n is the number of cells in the system (2n appears because there are two electrodes per modulator).

Another problem of discriminator cells is background light, that is light appearing at a point or points other than the one called for. The major cause of this is deviation of the modulators' control voltage from the required half wave voltage. As the control voltage becomes greater than or less than the half wave voltage, the polarization of the light is rotated more or less than 90^{o}. It will then have a component in the unrotated direction. The two components will be split by the discriminator crystal and the undesired component will appear as ghosting at the un-called-for position. Values of this background light have been graphed, Ref. 9, and are shown in Figure 13b. Note that the background light can be kept below the incident light by more than 40 db if the voltage deviation is kept below 10%, a tolerance which is easily obtained with a good regulator circuit.

The advantage of this system is that the positions and therefore the scan angles transmitted are known exactly. A position is called for by the scan logic and that scan angle (both horizontal and vertical angles) is produced. Therefore no indirect measurement is needed, and the associated error is thus eliminated. The disadvantages are its relative bulk, and the large voltages required (the half wave voltage of a Pockels cell is on the order of a kilovolt). Also the return beam cannot use the same optics.

An alternative to the digital deflector optics is a matrix of N by M individual laser diodes. This has all the advantages of the binary deflectors, but lacks the problem of high voltages and is somewhat less bulky. It does, however, require N times M diodes whose alignment is critical.

Converting Parallel Positions to Angles

The last two methods both provide parallel light outputs. This must be converted to scan angles if the method is to be useful in a scanning system.

This can be accomplished by placing the origin of the parallel positions on the focal plane of a small apature lens. This is shown in Figure 17 for the case of a matrix of laser diodes, i.e. uncollimated light. The case of binary deflection optics with collimated light is similar except that instead of collimating, the lens simply deflects the beam almost as if it were an ideal "ray".

Scanning Systems

One possible system, the dual vibrating mirror scan, was mentioned much earlier in this task summary. Here, two more systems will be introduced which attempt to alleviate the problems of the dual mirror approach.

Kuriger, Ref. 11, has worked on and proposed a hybrid scan system using a vibrating mirror for a vertical scan and a line of laser diodes to accomplish the horizontal scan. His range finder system is not capable of producing the necessary accuracy, but his scanning system does have some advantages. Kuriger's system is presented with some minor modifications in Figure 15. The "pulse transmitted detector" has been added to conform with the information needed in range finding schemes currently under study. In this system both the transmitter and the detector use the same vertical scan mirror. The diodes provide the horizontal scan, while the receiver looks at the entire horizontal scan area via the cylindrical lens. The use of the same scan mirror assures synchronization between transmitter and receiver, and the narrowing of the detector's field of view to only one horizontal row at a time increases the signal to noise ratio. Further advantages of this system are its compactness and small number of components. But although the horizontal transmitted angle is known exactly, the vertical angle determination relies on the same type of mirror position detection as does the dual mirror system and suffers the same problems.

An alternative system which seems to avoid all the major scan problems is now presented. Figure 16 shows the proposed system using digital deflection optics, but a matrix of laser diodes could be substituted just as well.

The detection system used is similar to Kuriger's except that the detector section is mechanically a separate entity from the transmitter. When the mirror drive starts its vertical sweep the synch (start) circuit detects this and initiates the transmitter's scan. The transmitter's vertical scan is approximately synchronized to the mirror, but the detector is given a wide enough field of view to compensate for a slight mis-match. Any mis-match which does occur does not continue to accumulate since the transmitter and detector are re-synchronized at the beginning of each vertical scan.

The advantages of this system are many-fold. First, the actual laser scanning is completely solid state. Also the transmitted angles are known exactly with each pair of horizontal and vertical scans having its own binary code lable. Finally, although a hybrid detector scheme is used, data point accuracy is extremely improved over Kuriger's scheme because the mirror position is not used to give point location but only to narrow the detector's field of view to the approximate azimuthal scan line of the transmitter. This system then seems to have the potential for extremely accurate transmitted angle information while maintaining a reasonable signal to noise ratio at the detector by narrowing its field of view.

The maximum scan angle obtainable with this system is determined

by the angle generating lens system used. For the single lens set up shown in Figure 14, maximum scans of 55^{o} can be obtained with a good lens. If a multiple lens system is used, this "viewing angle" can be greatly extended from this maximum. For example, using standard photographic lenses as a guide, a 28 mm focal length lens (6 elements) has a viewing angle of 74^{o}, a 20 mm lens (11 elements) has a viewing angle of 94^{o}. If distortion of field is allowed (an effect which can be compensated for by appropriate placement of beam sources on the matrix plane) fisheye lenses can also be used. Fisheye lenses have viewing angles from 180^{o} (10mm focal length) to 220^{o} (6mm focal length), Reference 12.

Since all lenses are circular, the angle maximum is completely symmetric with respect to the optic axis and therefore holds for both azimuthal and range angles.

Scan rate is limited only by position switching time. For the case of a matrix of laser diodes, minimum switching time is caused by the diodes' minimum pulse width and the maximum usable frequency of the driver circuits. This is on the order of magnitude of 100 KHz or 10 micro seconds per position. Thus the limiting factor for sweep rate will not be the scan unit, but rather the minimum on-time of the laser needed by the range finder system. This will be much larger than 10 micro seconds.

For a matrix of diodes system the weight of this scan mechanism will most likely be under 10 pounds.

One problem with all the angular scan methods is the incident spot distortion at the terrain. Since a collimated beam is transmitted at an angle, the actual shape and size of the spot will be distorted when it strikes all surfaces other than those to which it is normal (see Figure 17). This is most severe at the maximum ranges. As can be seen from the figure

$$W' = \frac{W}{\sin \theta}$$ for horizontal terrain (i.e. in the plane of the rover)

Therefore at 30 meters ($\theta = 5.7^{o}$) a 2.5 cm beam diameter ($\cong$ 1 inch) would produce a spot length of 25 cm. This effect worsens for negative in path slopes and improves up to a point for positive in-path slopes.

This spot distortion phenomenon will be analyzed in greater detail later with respect to its resulting phase distortion or blurring of the modulation frequency of the laser.

Shown below is the projected schedule of work to be undertaken.

	February	March	April	May
Spot Distortion-Phase "blur" prob.	----------			
Design of Rangefinder Instrumentation	----------	----------		
Building and Testing of Rangefinder		----------	----------	
Final Report			----------	----------

C.1.c. Stochastic Estimates of Gradient from Laser Measurements - P. Burger
Faculty Advisor: Prof. C. N. Shen

The objective of this task is to determine the errors in estimating gradients from laser range measuring systems as a result of measurement errors for the purpose of path selection decision making. Autonomous terrain sensing systems of high reliability will be required by an unmanned mission because of the round trip communication time delay. At this time, the investigation is focussed on determining terrain features in the 3 to 30 meter range.

The central concept of the system is the range finder, which locates a point on the terrain according to a range measurement R, azimuth angle θ, and elevation angle β. Two points along the path of the vehicle determine an in-path slope, while those across the path compute a cross path slope. However, inaccuracy in measurment can introduce very large errors in the computed slopes and heights, which are the main factors in path selections. There are some threshold values for these factors above which a change of path is required, Ref. 13.

In brief, the results which have been obtained to date relate the standard deviation of the gradient which an operating system would encounter as a function of the standard deviations in the range, deviation and azimuthal measurements of a scanning system. Accordingly, the consequences of accepting hardware laser systems with specified accuracy limits can be assessed in terms of the uncertainty in the calculated gradient and ultimately in the probability that an improper path selection will be made. These results also provide a basis for specifying optimum data spacing.

Method of Approach

From the measurement data it is desirable to obtain the maximum slopes and the elevations of the terrain in front of the vehicle.

a. Transformation of Coordinate Systems

The quantities R, θ, and β are measured with respect to the coordinate system h", a", and b", fixed to the vehicle, Figure 18. With laser height fixed at

Fig. 13-a. Properties of Digital Light Deflectors

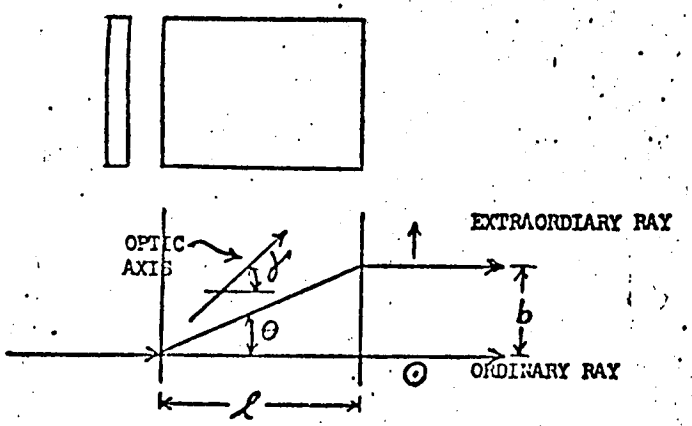

MATERIAL	θ IN DEG.	γ IN DEG.	
$NaNO_3$	9.17	49.34	for λ=6328 A
$CaCO_3$	5.90	51.27	(He-Ne)
KH_2PO_4	1.48	53.87	

From [3] pp 1420

Figure 13-b. Background Light vs. Modulator Voltage Deviation

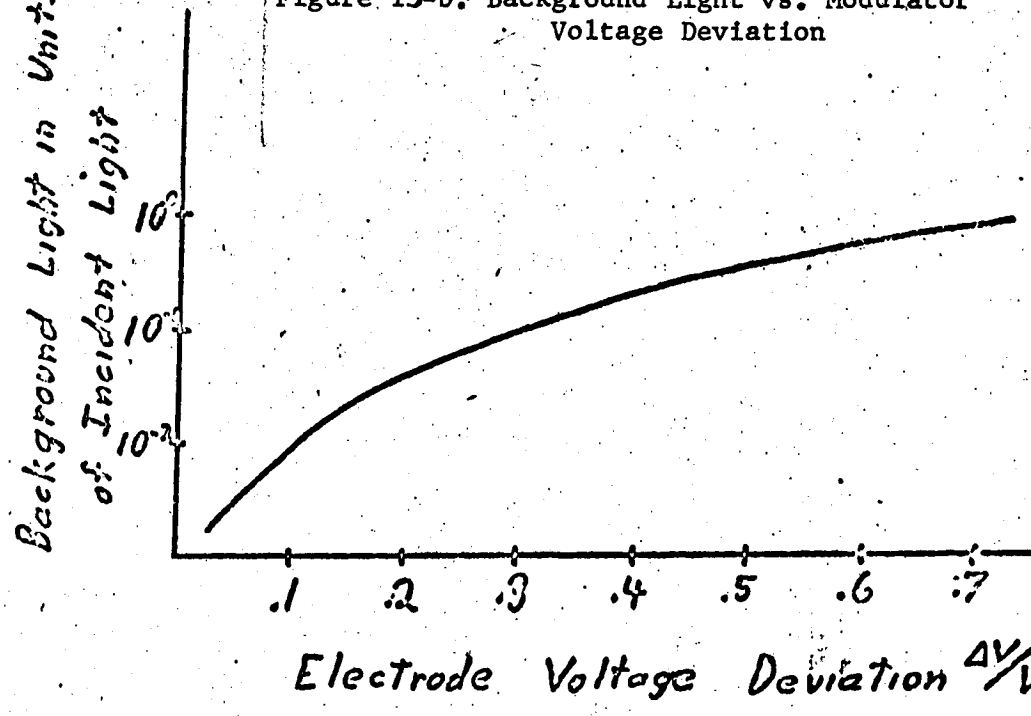

Figure 14
Optical Generation of Beam Angle from a Matrix of Light Sources

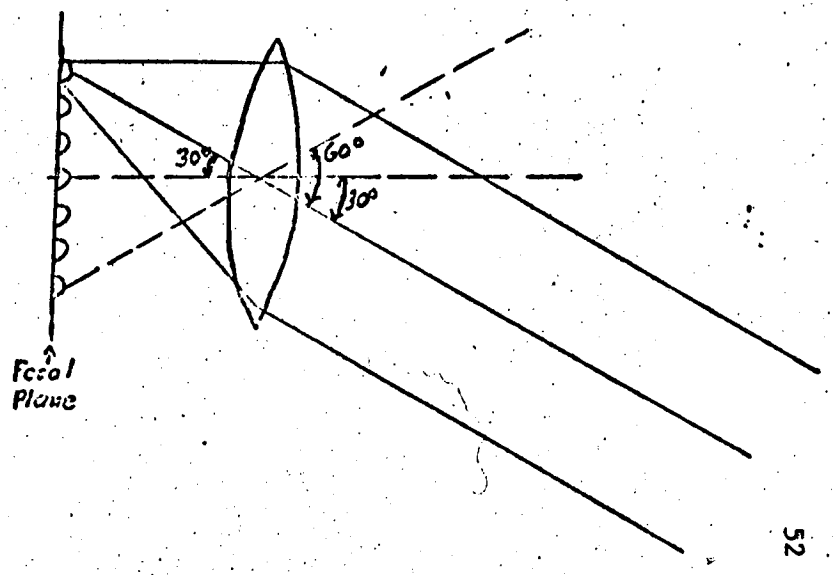

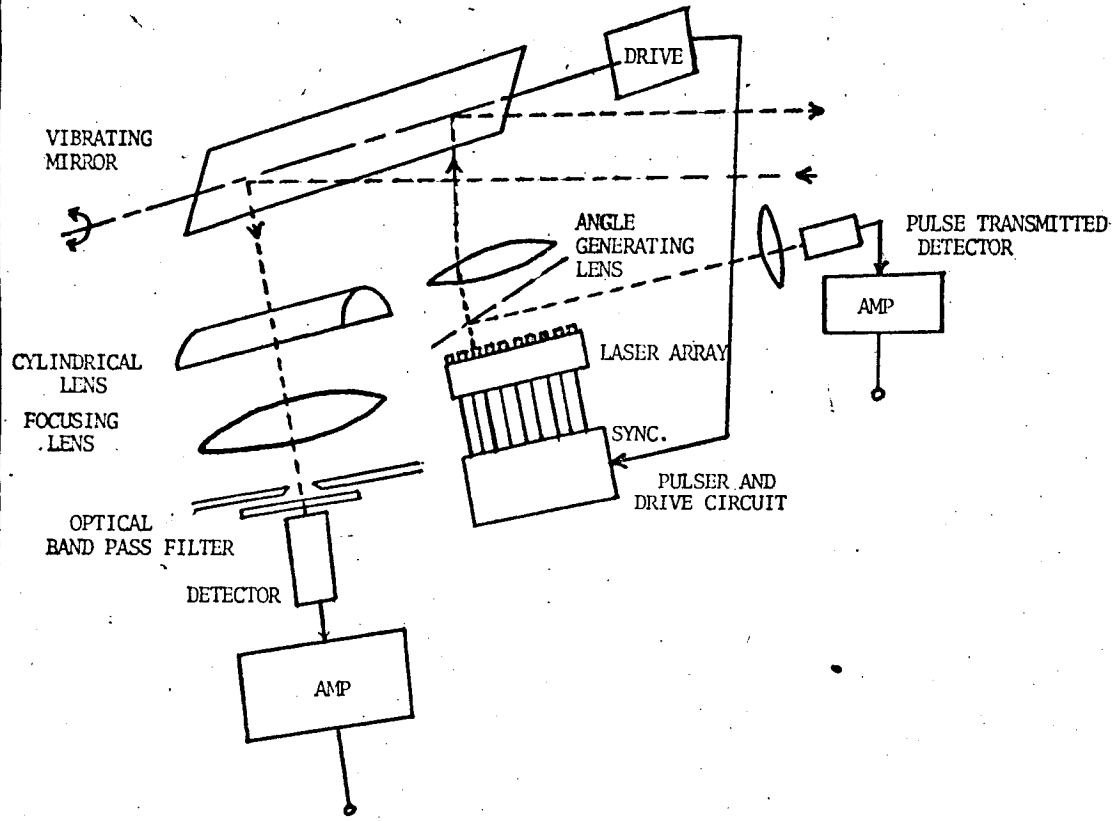

Fig. 15. Kuriger Scan System

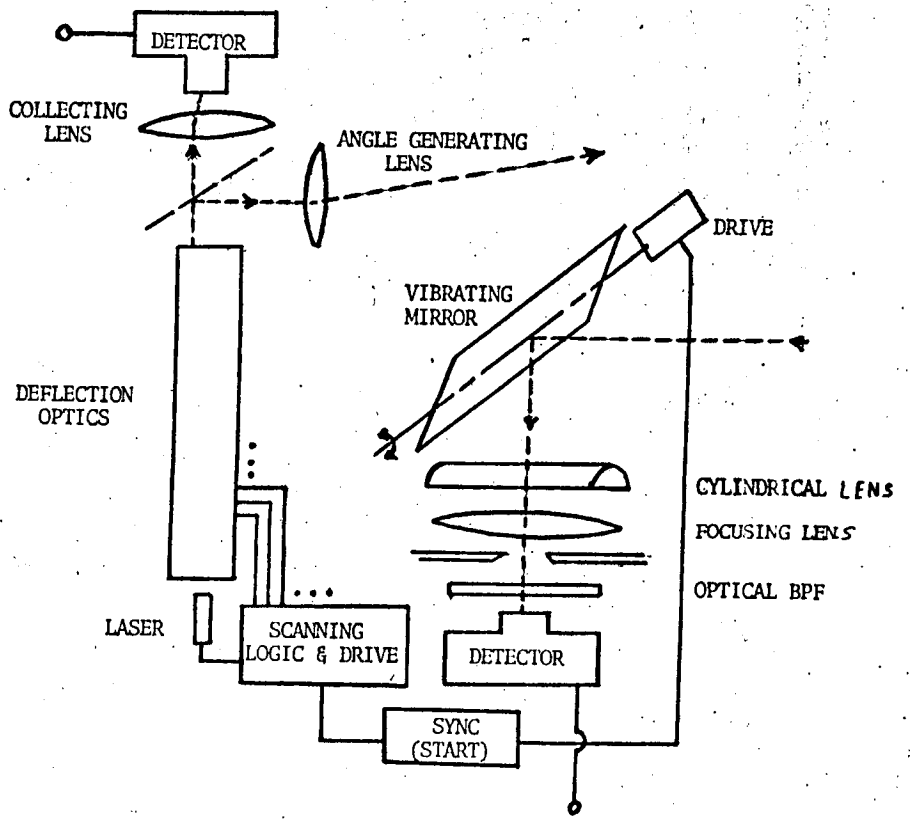

Fig. 16. Proposed Scan System

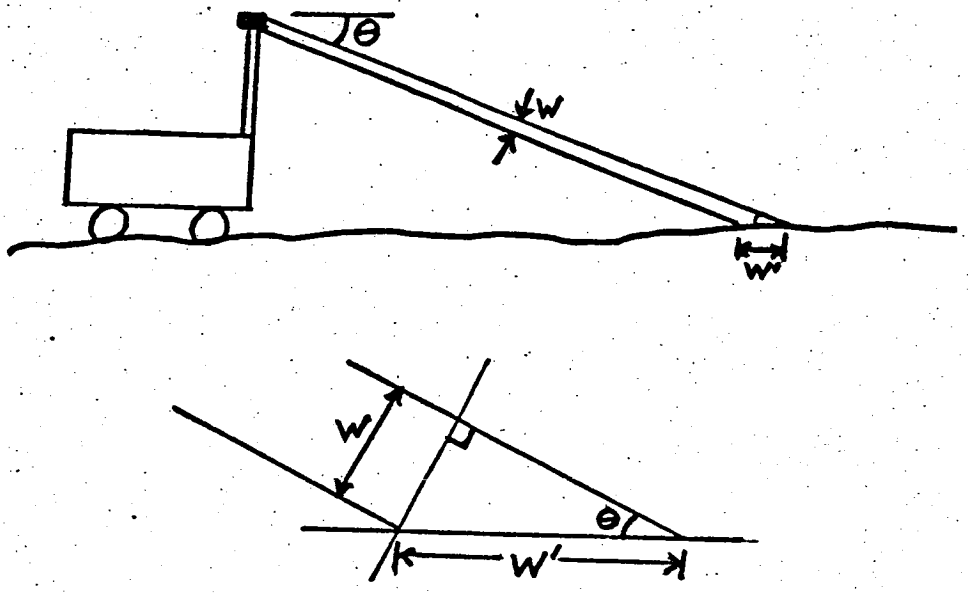

Fig. 17 Incident Spot Distortion

3 meters:

$$h'' = 3 - R\sin\beta \tag{1a}$$
$$a'' = R\cos\beta\sin\theta \tag{1b}$$
$$b' = R\cos\beta\cos\theta \tag{1c}$$

The body-bound axis rolls with the angle ϕ and pitches through an angle ξ about a reference frame h, a, and b formed by the local vertical and an axis in a plane containing the heading and the local vertical. The coordinate transformation, Ref. 14, is:

$$\begin{vmatrix} h \\ a \\ b \end{vmatrix} = C(\phi) \quad B(\xi) \quad \begin{vmatrix} h'' \\ a'' \\ b'' \end{vmatrix} \tag{2}$$

where $C(\phi)$ and $B(\xi)$ are the roll and pitch transformation matrices respectively.

b. Determination of Slopes and Gradient

A number of measurement points within a certain small area of surface can be used to determine a plane in space, which may be written as:

$$h = ax_1 + bx_2 + x_3 \tag{3}$$

where x_1 is the cross path slope and x_2 is the in-path slope, which are the two constant parameters to be determined, Ref. 15 and 16. The corresponding gradient of the plane, which is defined as the gradient of the terrain is

$$Sg = (x_1^2 + x_2^2)^{\frac{1}{2}} \tag{4}$$

If the slope is less than a predetermined criterion, it is considered to be safe for the vehicle to travel ahead.

In order to locate the plane by a number of measurement points, one may rewrite Eq. (3) as

$$h_i = a_i x_i + b_i x_2 + x_3 \tag{5}$$

where h_i, a_i, and b_i are found from R_i, Θ_i, and β_i in Eqs. (1) and (2) for each ith point. Theoretically, three points determine a plane (i=1,2,3). For greater accuracy however, more than three measurements (i=1,2,3,..,n) (probably n=4 or 6) are needed to determine the slopes. A complete picture of the terrain in front of the vehicle can be constructed by modeling numerous adjacent planes, each covering a small area of surface.

Analytic Solutions for Parameter Estimation

In this section are listed the solutions of the least square

estimate, the covariance matrices when $n > 3$.

a. Least Square Estimate of Slopes

If $a_i = \bar{a}_i$ and $b_i = \bar{b}_i$ are assumed to be true in Eq. (5), a least square error estimate can be performed which minimizes

$$\sum_{i=1}^{n} (\hat{h}_i - \bar{h}_i)^2 \tag{6}$$

where $\bar{h}_i$ is the actual measured height and $\hat{h}_i$ is the corresponding height in the modeled plane.

In matrix-vector notation, Eq. (5) is:

$$\bar{h} = \bar{A}x \tag{7}$$

where $\bar{h} = (\bar{h}_1, \bar{h}_2, \ldots \bar{h}_n)^T$, $x = (x_1, x_2, x_3)^T$

and

$$\bar{A} = \begin{bmatrix} \bar{a}_1 & \bar{b}_1 & 1 \\ \bar{a}_2 & \bar{b}_2 & 1 \\ \vdots & \vdots & \vdots \\ \bar{a}_n & \bar{b}_n & 1 \end{bmatrix} \quad n = 4 \text{ or } 6$$

The least square estimate of the parameter x becomes, Ref. 17:

$$\hat{x} = (\bar{A}^T\bar{A})^{-1}\bar{A}^T\bar{h} \tag{8}$$

b. Perturbation of the Variables

The least square estimate in the previous section assumes the matrix A to be completely deterministic, Ref. 18. In reality, however, there is error involved in the determination of a, b, and h, due to the errors in the measured values of ϕ, ξ, R, β, and θ.

If the symbol δ denotes a perturbation, then δh, δa, and δb in terms of $\delta\phi$, $\delta\xi$, δR, $\delta\beta$, and $\delta\theta$ are:

$$\begin{bmatrix} \delta h \\ \delta a \\ \delta b \end{bmatrix} = D(h'', a'', b'', \phi, \xi) \begin{bmatrix} \delta\phi \\ \delta\xi \end{bmatrix} + C(\phi)B(\xi)G(R, \beta, \theta) \begin{bmatrix} \delta R \\ \delta\beta \\ \delta\theta \end{bmatrix} \tag{9}$$

c. Covariance Matrix of the Variables

The covariance matrix of the variables can be defined as

$$M = E\left\{ \begin{bmatrix} \delta h \\ \delta a \\ \delta b \end{bmatrix} \begin{bmatrix} \delta h & \delta a & \delta b \end{bmatrix} \right\} \tag{10}$$

where E denotes expected value.

If $\delta\phi$, $\delta\xi$, δR, $\delta\beta$ and $\delta\theta$ are not correlated, then with the aid of Eq. (9)

$$M = D\begin{bmatrix} E(\delta\phi)^2 & 0 \\ 0 & E(\delta\xi)^2 \end{bmatrix} D^T + CBG \begin{bmatrix} E(\delta R)^2 & 0 & 0 \\ 0 & E(\delta\beta)^2 & 0 \\ 0 & 0 & E(\delta\theta)^2 \end{bmatrix} G^T B^T C^T \qquad (11)$$

From Eqs. (10) and (11) the standard deviations of h, a, and b, can be computed in terms of those of ϕ, ξ, R, β, and θ for each point. These are known quantities that depend upon the accuracy of the measuring devices.

d. Covariance Matrix of the Slopes

Eq. (5) can be written as

$$h = Ax \qquad (12a)$$

$$\text{If } h = \bar{h} + \delta h,\ A = \bar{A} + \delta A, \text{ and } x = \bar{x} + \delta x, \qquad (12b)$$

then with the aid of Eq. (7) the covariance matrix of the slopes is found as:

$$E\left[\delta\hat{x}\,\delta\hat{x}^T\right] = F\left\{E\left[\delta h \delta h^T\right] - E\left[\delta A x \delta h^T\right] - E\left[\delta h (\delta S x)^T\right] + E\left[\delta A x (\delta A x)^T\right]\right\} F^T \qquad (15)$$

where $$\delta\hat{x} = \begin{bmatrix} \delta\hat{x}_1 \\ \delta\hat{x}_2 \\ \delta\hat{x}_3 \end{bmatrix} \quad \delta h = \begin{bmatrix} \delta h_1 \\ \vdots \\ \delta h_n \end{bmatrix} \quad \delta A\bar{x} = \begin{bmatrix} (\delta a_1 \bar{x}_1 + \delta b_1 \bar{x}_2 \\ \vdots \\ (\delta a_n \bar{x}_1 + \delta b_n \bar{x}_2 \end{bmatrix} \qquad (16)$$

This equation utilizes the least square estimate of the parameter x from Eq. (8) and the elements of the covariance matrix of the variables for each point, which are determined from Eq. (11).

e. Variance of the Gradient

If the symbol σ_{Sg} denotes the standard deviation of the gradient, Sg, then from Eq. (4)

$$dSg = (x_1^2 + x_2^2)^{-\frac{1}{2}} x_1 dx_1 + (x_1^2 + x_2^2)^{-\frac{1}{2}} x_2 dx_2$$

The variance of the gradient is

$$\sigma_{Sg}^2 = \frac{\bar{x}_2^2}{\bar{x}_1^2 + \bar{x}_2^2}\sigma_{x_1}^2 + \frac{\bar{x}_1^2}{\bar{x}_1^2 + \bar{x}_2^2}\sigma_{x_2}^2 + 2\frac{\bar{x}_1 \bar{x}_2}{\bar{x}_1^2 + \bar{x}_2^2}\sigma_{x_1 x_2} \qquad (17)$$

where $\sigma_{x_1}^2 = E(\delta\hat{x}_1)^2$, $\sigma_{x_2}^2 = E(\delta\hat{x}_2)^2$ and $\sigma_{x_1 x_2} = E(\delta\hat{x}_1 \delta\hat{x}_2)$

The covariances $\sigma_{x_1}^2$, $\sigma_{x_2}^2$, and $\sigma_{x_1 x_2}$ can be found from Eq. (15).

The value of σ_{Sg} gives a rough estimate of the accuracy in the estimation of the gradient. If the estimated gradient, Sg, is 20° with $\sigma_{Sg} = 2^\circ$, then there is a 68% probability that the actual slope is between 18° and 22° and a 95% probability, Ref. 19, that it is between

16° and 24°. In general, there is a 68% probability that the actual gradient lies between the values of $Sg + \sigma_{sg}$ and $Sg - \sigma_{sg}$ and a 95% probability that the actual gradient lies between the values of $SG + 2\sigma_{sg}$ and $Sg - 2\sigma_{sg}$. This is important when the estimation is close to the maximum permissible value.

Numerical Results

It is assumed the rover will use a split beam where $\Delta\beta$ is the difference in the elevation angle between the two beams and $\Delta\theta$ is the difference in azimuth angle between any two laser pulses as shown in Figure 19.

The values of β and θ for each data point, along with the magnitude of the cross-path and in-path slopes of the terrain, determine the data point spacing and the distance of the data points from the vehicle. After a number of data points are measured, they are transformed to the non-rotating reference system by Eqs. (1a to 2c). Then a least square estimate of the slopes is performed which is given by Eq. (8). This least square estimate depends directly on the values of h, a, and b for each measurement point. Utilizing the value of the vector $\hat{x}$ found in Eq. (8), the values of ϕ, ξ, R, β, and θ for each data point, and the standard deviations of these quantities, the magnitude of the gradient and its variance can be determined.

The standard deviation in gradient, σ_{sg} is calculated by utilizing Eqs. (11), (14), (15), and (17). From Eq. (15) and (17) it can be noted that the variance of the gradient depends in part upon the cross path and in path slopes of the terrain. Eqs. (11) - (15) depend ultimately upon the measured values of ϕ, ξ, R, β, and θ for each point, and the standard deviations in these quantities. That is to say, the variance of the gradient depends additionally upon the roll and pitch angle of the vehicle, the data point spacing, the distance of the data points from the vehicle, and the accuracy of the measuring devices. How much each of these factors affects σ_{sg} is to be investigated.

For simplicity, the roll and pitch of the vehicle are first set equal to 0, and the reference gradient of the measured plane is assumed to be 0° wherever it may be located. By setting $\sigma_{\beta} = \sigma_{\theta} = 0.1^{\circ}$ and $\sigma_{\phi} = \sigma_{\xi} = 1^{\circ}$ it is determined that for any reasonable data point spacing at 20-30 meters from the vehicle, σ_{sg} was on the order of 30°-60°. On the other hand, if $\sigma_{\phi} = \sigma_{\xi} = 0^{\circ}$, σ_{sg} decreased to only 2°-3° at that distance. Since we can expect that σ_{ϕ} and σ_{ξ} are really in the neighborhood of 1° (due to the constant rock and roll of the vehicle as it traverses the surface), the rover will have to be provided with a "rapid scan" laser. If the scan rate is on the order of milliseconds, which is perfectly feasible with electronic scanning, then each set of 4 adjacent data points is measured practically instantaneously, since the rover motion is on the order of seconds. Each of the 4 data points will have the same value for ϕ and ξ and therefore all 4 points will retain the same relative position to each other when they are

transformed from the vehicle coordinate system to the fixed system. Consequently, the rover can model the planes in the vehicle coordinate system and then transform the planes to the non-rotating frame. Since the maximum positive or negative slope that the vehicle can navigate is $\pm 25^{o}$, relative slopes might be as high as $\pm 50^{o}$ and still be navigable, as shown in Figure 20. Therefore, a range of slope changes from $+50^{o}$ to -50^{o} have been considered.

Also due to rapid scan, the error introduced by setting $\sigma_{\phi} = \sigma_{\xi} = 1^{o}$ will be consistently between 1^{o} and 2^{o} because it only involves the error in transforming the already modeled plane from the vehicle system of reference to the fixed system. Consequently, the effect of σ_{ϕ} and σ_{ξ} is not considered in this analysis.

On the basis of a flat terrain, with $\sigma_{\theta} = \sigma_{\beta} = 1'$ and $\sigma_{R} = 5$ cm, and vary $\Delta\beta$ and $\Delta\theta$ (and consequently the data point spacing) for each set of 4 points, the graphs shown in Figure 21 are obtained. Each solid line represents constant values for $\Delta\theta$ and $\Delta\beta$. Δb and Δa are the data point spacings along the in-path and cross path directions respectively. It is noted that for any constant value of $\Delta\theta$ and $\Delta\beta$, the data point spacing decreases very rapidly as the scan approaches to the vehicle and consequently the error in gradient rises very rapidly.

In choosing an "optimum" data point spacing it must be kept in mind that by increasing the spacing the error in gradient is decreased. However, this renders the data less meaningful, as more terrain has been overlooked. At the 30 meter range, a general picture of the terrain with a spacing of 2-3 meters is sufficient. At close range, (4-7 meters) the points should be at least as close as 0.66 meters because this is the width of the widest navigable crevice. In Figure 21, the dotted line represents σ_{sg} vs distance from the vehicle for such a scheme, where the data point spacing varies from about 0.5 meters at a distance of 4 meters from the vehicle to about 3 meters at a distance of 30 meters from the vehicle.

Each of the plots in Figures 22 and 23 utilize the same optimum scheme as the dotted line in Figure 21. Once again flat terrain is assumed for all the data points. In Figure 22, σ_{R} is kept at 5 cm and σ_{β} and σ_{θ} are set to 0, .017 (1'), and .1 (6'). The error in gradient is markedly reduced by decreasing σ_{β} and σ_{θ} from 6' to 1' but any further increases in accuracy will result in bulkier and heavier equipment which is not very beneficial. By comparing the plots for $\sigma_{\beta} = \sigma_{\theta} = 1'$ and $\sigma_{\beta} = \sigma_{\theta} = 0^{o}$ it is seen that a standard deviation in σ_{β} and σ_{θ} of 1' has very little effect on the error in gradient.

In Figure 23, σ_{R} is varied from 1 cm to 10 cm while σ_{β} and σ_{θ} are kept constant at 1' (.017). The error in gradient increases rapidly at close range for each value of σ_{R}.

Figure 24 plots σ_{sg} vs relative in-path slopes of from -30^{o} to $+ 50^{o}$ at 4 meters from the vehicle. In all cases, the cross path slope of the measured plane is 0^{o} and there is at least 1 data

point with a height h of 0 meters in each group of 4 points. The graph only extends to -30° because the laser beam cannot "see" over a negative in-path slope greater than this value at 4 meters distance. σ_R is varied from 1 cm to 5 cm with $\sigma_\beta = \sigma_\theta = 1'$. A data point spacing of .6 meters is assumed. Figure 25 plots σ_{s_γ} vs relative in-path slopes of from -6° to $+50^{\circ}$ at 20 meters from the vehicle. All the other conditions are the same as in Figure 24 except that the data point spacing is 1.2 meters instead of 0.6 meters. Finally, Figure 26 shows graphs of σ_{s_γ} vs relative cross-path slopes of from 0° to 50° for distances of 4 meters and 20 meters from the vehicle. This time the in-path slopes are set to 0°. Once again $\sigma_\beta = \sigma_\theta = 1'$ and σ_R is varied from 2 to 10 cm. The data point spacing at 20 meters from the vehicle is 1.2 meters and the spacing at 4 meters from the vehicle is 0.6 meters.

From Figures 24 - 26 it is noted that the higher the relative in-path or cross path slope, and the closer the data points are to the vehicle, the larger the error in gradient. All other factors considered equal, the error in gradient is larger for a given in-path slope than for a cross path slope of the same magnitude. It is obvious in Figure 24 that σ_R should be as close to 1 cm as possible in order that σ_{s_γ} will be within 2° at 4 meters distance and high values of relative in-path slopes.

This analysis leads to 3 very important conclusions. First, the very large error due to the motion of the vehicle is eliminated by utilizing a rapid scan laser. Secondly, if σ_β and σ_θ are reduced below 1 arcminute, bulkier and heavier equipment would result. In fact, with $\sigma_\beta = \sigma_\theta$ of 1 arcminute, very little error is introduced into the calculations. Finally, most of the error is due to σ_R. The variance of the gradient should be as low as possible, but if an upper bound of 2° is set, then σ_R must be as low as 1 cm.

Projected Work Schedule

Due to surface irregularity, data points will not fall at regular intervals as they would on a flat plane, but will be scattered about unevenly. A procedure must be developed to determine how each group of 4 points is to be chosen prior to the modeling procedure. Another question that should be investigated is whether the modeling procedures should be modified for terrain at the 20-30 meter range so that the rover can model hills and craters as well as flat planes. More generally the problem is one of determining a complete picture of the terrain from an array of different sized and shaped planes, each of whose gradients have a different magnitude.

	February	March	April	May
Choosing data points	----------			
Complete picture of terrain		----------		
Writeup			----------	

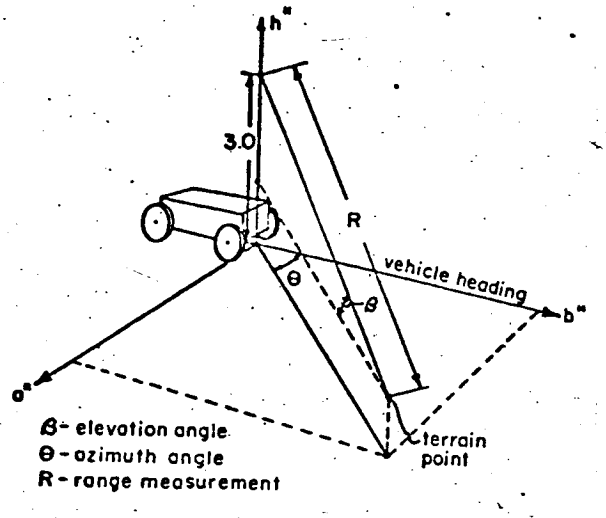

Fig. 18 Vehicle Coordinate System

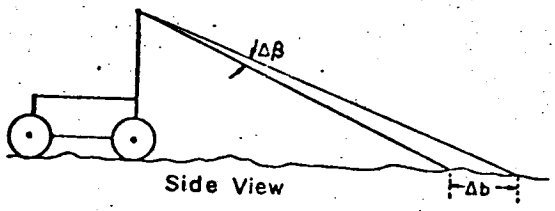

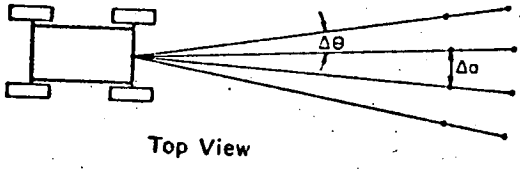

Fig. 19. Split Beam Laser

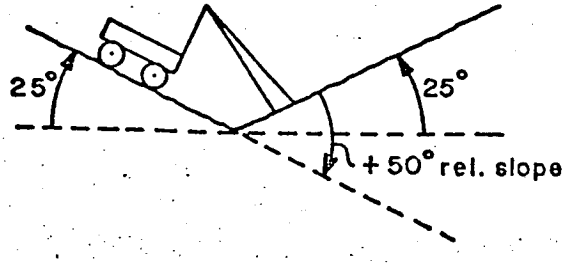

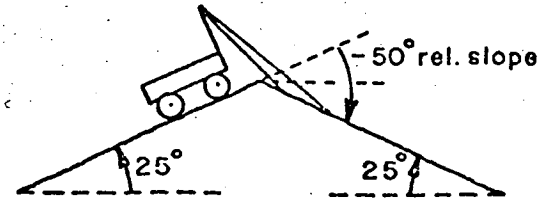

Fig. 20. Relative In-Path Slopes

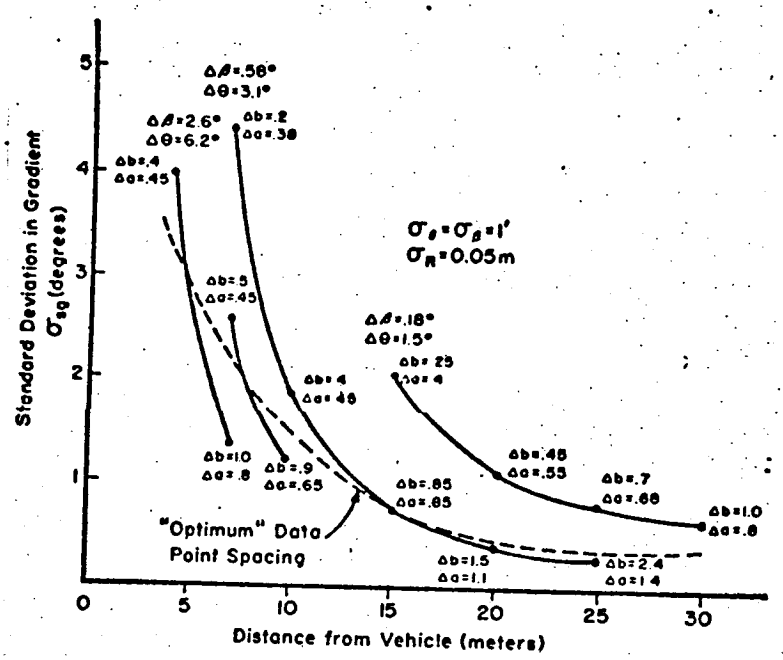

Fig. 21. Standard Deviation in Gradient vs. Distance from Vehicle on Flat Plate

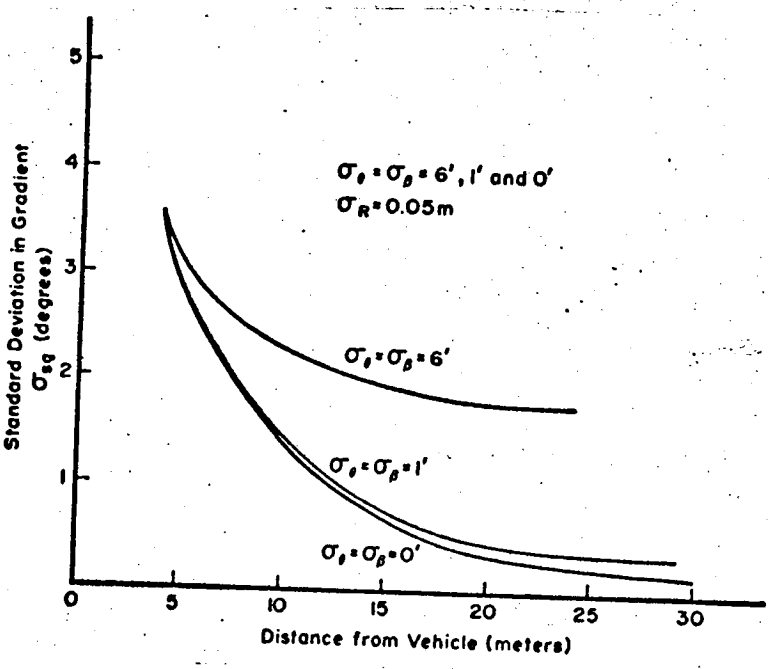

Fig. 22. Standard Deviation in Gradient vs. Distance from Vehicle for "Optimum" Data Point Spacing on Flat Surface

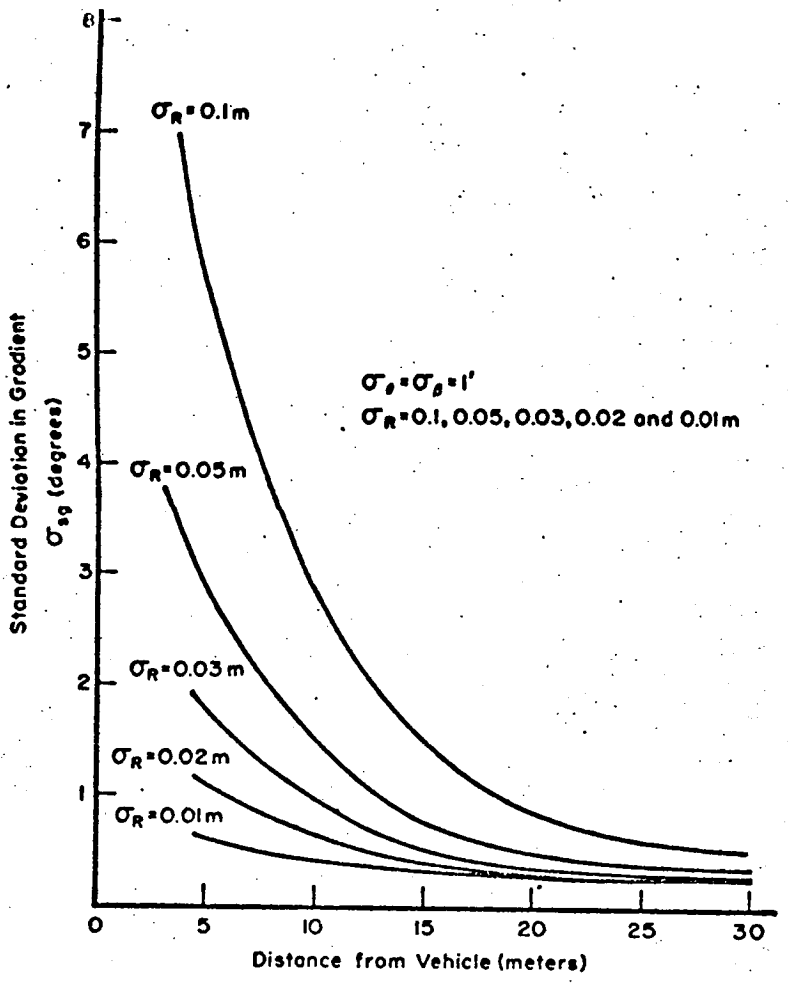

Fig. 23. Standard Deviation in Gradient vs. Distance from Vehicle for "Optimum" Data Point Space on Flat Surf.

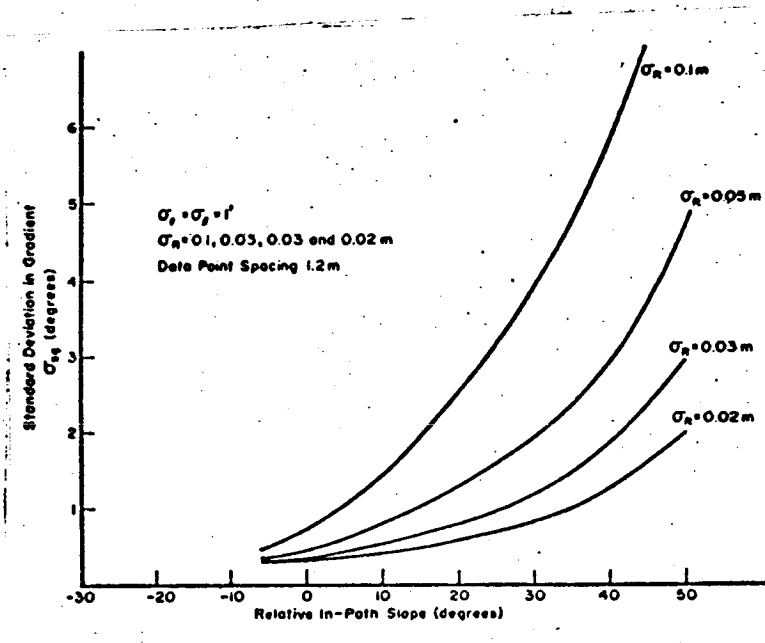

Fig. 25. Standard Deviation in Gradient Relation In-Path Slope at 20m from the Vehicle

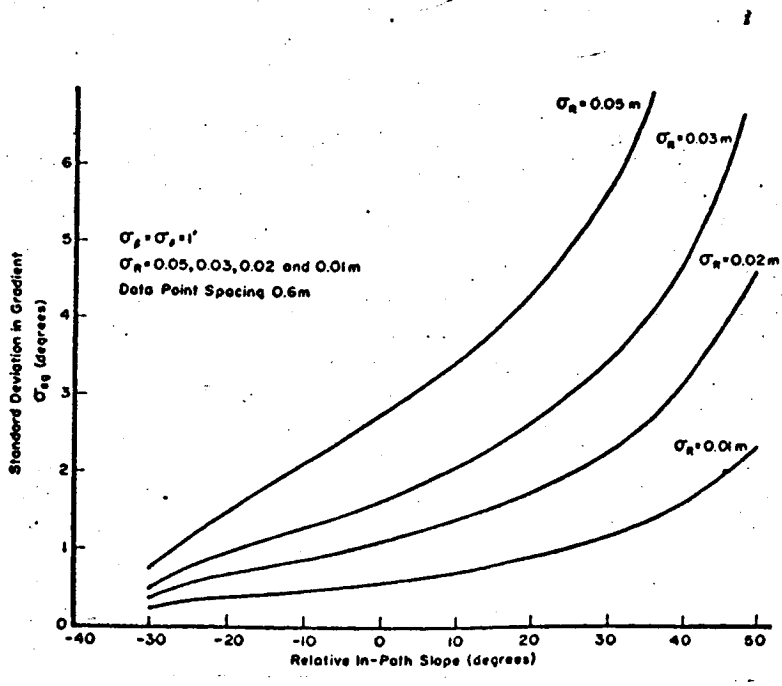

Fig. 24. Standard Deviation in Gradient vs. Relative In-Path Slope at 4m from the Vehicle

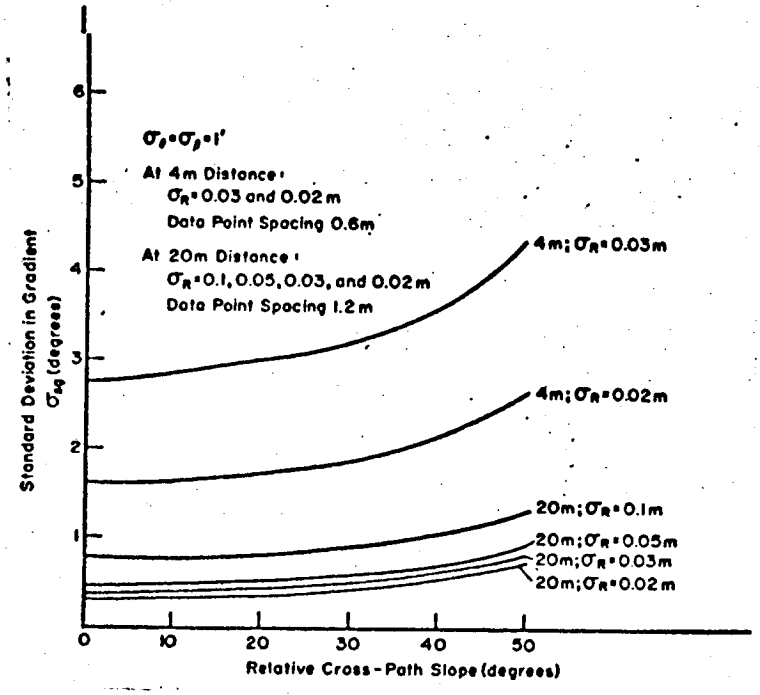

Fig. 26. Standard Deviation in Gradient vs. Relative Cross-Path Slope at 20m and 4m from the Vehicle

C.1.d. Stereo and Non-Stereo Obstacle Detection Systems - W. Pfeifer
Faculty Advisor: Prof. C. N. Shen

The objective of this task is to evaluate obstacle detection systems based on alternative combinations of range and angle measurements. Both stereo and non-stereo concepts are being investigated to determine the relation between measurement errors and the conclusions regarding the terrain feature.

The concept is based on the assumption that a laser rangefinder or its equivalent will be able to measure ranges and angles to terrain points on the Martian surface. The location of these points may be determined by several combinations of range and/or angular measurements.

The Martian terrain has been modeled as a plane with discrete obstacles extending above and below it. Obstacles are defined as points on the surface with a height greater than .45 meters above or below the plane, Ref. 20. In addition, slopes between successive points must be considered because a change of height greater than .45 meters spread out over a distance of several meters may be safely traversed by the vehicle. Both in-path and cross-path slopes must be determined since the vehicle has maximum limits of both pitch and roll from the local vertical. These limits are expected to be about twenty to twenty-five degrees. A method of fitting planes to data points and estimating the gradient of local surfaces is being developed under Task C.1.c.

The coordinate system used in the investigations has the sensor mast as its vertical axis and a plane perpendicular to this axis at the surface. This plane may be referred to as a "vehicle base plane".

Stereo Angles Method

Preliminary investigation started with a two dimensional configuration which then can be generalized to three dimensions by the addition of one more measurement. A data point may be located by measuring the elevation angles from two known points on the vehicle to the point on the surface. This can be accomplished by using a transmitter (laser) at one location and a receiver at a second location on the vehicle. The transmitter and receiver are separated by a known distance L. As shown in Figure 27, by measuring the transmission and reception elevation angles, α and β, and the known vehicle dimensions, the location (height above the vehicle plane and distance from the vehicle) of a point on the surface may be measured. Some type of scanning apparatus would aim the laser beam at a predetermined pattern of points on the surface.

The transmitter should be located at the lower point A as shown in Figure 28 and the receiver at the upper point (B). With the transmitter at B, some data points will be lost since obstacles may intersect the reflected beam.

The values of h and b may be easily calculated once α, β and L and the remaining vehicle parameters are known from geometric considerations,

$$h = 3 - \frac{L \tan \beta}{\tan \beta - \tan \alpha} \tag{1}$$

$$b = \frac{L}{\tan \beta - \tan \alpha} \tag{2}$$

The variances of h and b are computed from the variances of the angular measurements. It is believed that angular measurements with standard deviations of several arc seconds may be possible and that a standard deviation of one minute of arc is likely. Standard deviations of h and b have been calculated using the values of 6 arc seconds, 1 minute, and 10 minutes for the standard deviations of both α and β. The value used for the standard deviation of L is .01 meters.

The equations for variances are as follows:

$$\text{Var } h = \frac{\tan^2\beta}{(\tan\beta - \tan\alpha)^2} \text{Var } L + \frac{L^2 \tan^2\beta \sec^4\alpha}{(\tan\beta - \tan\alpha)^4} \text{Var } \alpha + \frac{L^2 \tan^2\alpha \sec^4\beta}{(\tan\beta - \tan\alpha)^4} \text{Var } \beta \tag{3}$$

$$\text{Var } b = \frac{1}{(\tan\beta - \tan\alpha)^2} \text{Var } L + \frac{L^2 \sec^4\alpha}{(\tan\beta - \tan\alpha)^4} \text{Var } \alpha + \frac{L^2 \sec^4\beta}{(\tan\beta - \tan\alpha)^4} \text{Var } \beta \tag{4}$$

Figure 29 shows the height standard deviation, σ_h, versus the distance from the vehicle, b, for h=0 and L=1.0 meters. Clearly the reduction of angular uncertainty from 10 minutes to 1 minute results in a significant improvement in accuracy. Also, further reduction from 1 min. to 6 seconds results in slight improvement. Angle uncertainty should be reduced to 1 minute if possible, but further reduction is not very useful. Note that this stereo angles system determines heights very accurately over the entire 3 to 30 meter range when σ_α = 1 min. with σ_h being less than 4 cm.

Varying the value of the distance L between the transmitter and receiver also affects the accuracy of height determinations. Larger L gives better results, i.e. smaller σ_h. The percentage change in L results in about the same percentage change in σ_h. The 1 meter value for L has been used in most calculations because the length L is limited by the vehicle design. Moreover, if point A moves too close to the surface the rangefinder loses some of its ability to see craters.

The distance measurement is not as accurate as the height. The distance standard deviation, σ_b, versus distance, b, is shown in Figure 30 for h=0 and L=1.0 m. Sigma b is 1 meter for b greater than 16m and sigma angle = 10 min. With σ_ϕ = 1 min., reasonable values of less than 12 cm are obtained for σ_b at close range, i.e. less than 10m.

It appears that the stereo angles method will be most useful at close range. At longer range, problems will be encountered because of the inaccuracy in the determination of b. The distance determinations will be very important in the calculation of in-path and cross-path slopes.

Stereo Rand Method

Instead of measuring two angles, two ranges can be used to determine the coordinates of terrain points. To obtain two range measurements for a single terrain point a transmitter and receiver are located at one point on the vehicle and a separate receiver at a second point, Figure 31. Another possibility is to locate a transmitter between two receivers.

The transmitter-receiver combination measures twice the distance from the combination to the terrain point. The second receiver measures the sum of the distance from the transmitter to the terrain point and the distance from the point back to the second receiver.

L, h and b are the same as in the stereo angles case.

From the geometry in Figure 31:

$$R^2 = (3-h)^2 + b^2 \tag{5}$$

$$P^2 = (3-h-L)^2 + b^2 \tag{6}$$

Which can be solved for:

$$h = 3 - \frac{L}{2} + \frac{P^2 - R^2}{2L} \tag{7}$$

$$b = \left[\frac{R^2 + P^2}{2} - \frac{L^2}{4} - \left(\frac{P^2 - R^2}{2L}\right)^2\right]^{\frac{1}{2}} \tag{8}$$

The actual quantities measured are defined as follows:

$$M = 2R \tag{9}$$

$$N = R + P \tag{10}$$

If the range standard deviation is defined as σ_R, it follows that:

$$\text{Var } M = 4 \text{ Var } R$$
$$\sigma_M = 2\sigma_R \tag{11}$$

$$\text{Var } N = 4 \text{ Var } R$$
$$\sigma_N = 2\sigma_R \tag{12}$$

The variance of height and distance are then determined as

$$\text{Var } h = \left(\frac{MN - N^2 - L^2}{2L^2}\right)^2 \text{ Var } L + \left(\frac{N}{2L}\right)^2 \text{ Var } M + \left(\frac{2N-M}{2L}\right)^2 \text{ Var } N \quad (13)$$

$$\text{Var } b = \left(\frac{1}{2b}\right)^2 \left[-\frac{L}{2} - \frac{(N^4 - 2N^3M + N^2M^2)}{2L^2}\right]^2 \text{ Var } L$$

$$+\left(\frac{1}{2b}\right)^2 \left[\frac{M - N}{2} + \frac{(N^2M-N^3)}{2L^2}\right]^2 \text{ Var } M \quad (14)$$

$$+ \left(\frac{1}{2b}\right)^2 \left[\frac{N - M}{2} + \frac{(2N^3-3N^2M+NM^2)}{2L^2}\right]^2 \text{ Var } N$$

The range standard deviation values used were 10, 6, 2, 1, 0.6, and 0.2 cm. Figure 32 shows height standard deviation versus distance when h=0 and L=1.0 m. The height uncertainty is very large if range uncertainty is greater than 1 cm. To get σ_h less than 10 cm at b = 7 meters σ_R will have to be less than .5 cm. This type of range accuracy is not expected from present technology.

The distance standard deviation, σ_b, versus distance is shown in Figure 33. The distance measurement has good accuracy when the range uncertainy isl centimeter or less. The distance uncertainty decreases slightly as b is increased from 7 to 28 meters.

At present the stereo range system doesn't appear to be useful because range accuracy is expected to be on the order of 5 to 10 centimeters which leads to extremely large uncertainties in height determinations. However, if range standard deviation can be reduced to 0.5 centimeter or less this method would be acceptable.

Non-Stereo (Range-Angle) Method

This system,shown in Figure 34, uses a transmitter and receiver located at the top of the sensor mast. The rangefinder measures the range R to the terrain point at the elevation angle β to the point.

From the geometry:

$$h = 3 - R \sin\beta \quad (15)$$

$$b = R \cos\beta \quad (16)$$

Estimating the uncertainties in h and b using equations 19 and 20 leads to

$$\text{Var } h = \sin^2\beta \text{ Var } R + R^2 \cos^2\beta \text{ Var } \beta \quad (17)$$

$$\text{Var } b = \cos^2\beta \text{ Var } R + R^2 \sin^2\beta \text{ Var } \beta \quad (18)$$

σ_h and σ_b were calculated by assuming values for h, b, σ_R and σ_β. Height standard deviation as a function of distance is shown in Figure 35 for range uncertainties of 10 cm, 6 cm, and 2 cm with angle uncertainties of 10 min., 1 min., and 6 seconds of arc. At close range, (less than 14 meters), range error seems to

dominate. If angle uncertainty is less than some threshold value between 1 and 10 minutes, height error actually decreases with distance at longer range. With σ_R = 10 cm and σ_β = 10 minutes, σ_h is less than 9 centimeters over the entire 3 to 30 meter range. With angle accuracy of 1 min., height uncertainty is less than 4 cm even if σ_R = 10 cm.

In the non-stereo system σ_b was approximately equal to the range standard deviation over the 3 to 30 meter range.

The non-stereo system is the most accurate method at ranges greater than 10 meters. If range error is 10 cm. and angle is 1 min. then the non-stereo system is slightly less accurate than the stereo angles system for distances of less than 10 meters.

The conclusion is that the non-stereo system is probably optimum because it has reasonable accuracy over the entire 3 to 30 meter range.

Three Dimensional Systems

The most logical way to extend the two dimensional systems to three dimensions is to measure an azimuthal angle Θ as shown in Figure 36. Coordinates a_1 and b_1 are defined in the figure.

$$a_1 = R \cos\beta \sin\Theta = b \sin\Theta \tag{19}$$

$$b_1 = R \cos\beta \cos\Theta = b \cos\Theta \tag{20}$$

$$\text{Var } a_1 = \sin^2\Theta \text{ Var } b + b^2 \cos^2\Theta \text{ Var } \Theta \tag{21}$$

$$\text{Var } b_1 = \cos^2\Theta \text{ Var } b + b^2 \sin^2\Theta \text{ Var } \Theta \tag{22}$$

Equations 4, 14 or 18 may be substituted into equations 25 and 26 to find Var a_1 and Var b_1 in terms of actual measured parameters. The variances of a_1 and b_1 are expressed in terms of the variances of b and Θ. This means that the system which has the smallest variance of b will have the smallest variances of a_1 and b_1. If σ_Θ = 1 minute of arc, simple calculations show:

if $\Theta = 0^\circ$ σ_{a_1} 1 cm 7 m < b < 28 m all σ_b

$\Theta = 12^\circ$ σ_{a_1} 2.3 cm 7 m < b < 28 m σ_b = 10 cm

In general σ_{b_1} is approximately equal to σ_b.

Effects of Heights Above or Below the Plane

The stereo angle system is more accurate for positive heights than for negative ones as shown in Figure 37. For example, when

σ_ϕ = 1 min. at a distance of 7 meters, σ_h = 2 cm if h = + 1 meter, σ_h = 3 cm if h = 0 m, and σ_h = 4 cm if h = - 1 m. This effect is certainly tolerable. Varying h has a negligible effect on in the stereo angles system.

Non-stereo height accuracy is also better for positive heights than for negative ones. When angle standard deviation was 1 minute, the effect of heights between plus 1 and minus 1 meter was similar to the effect on the stereo angles system and as range increased the effect decreased substantially as can be seen in Figure 38. Again this effect is tolerable. Varying h has a slight effect on σ_b at close range and almost no effect at ranges greater than 15 meters.

In-Path and Cross-Path Slopes

The in-path slope S_I and cross-path slope S_c could be calculated between successive data points, Ref. 21.

$$S = \frac{\Delta h}{\Delta b} = \frac{h_2 - h_1}{b_2 - b_1} \tag{23}$$

$$\text{Var } S_I = \frac{\text{Var } h_2 - \text{Var } h_1}{(\Delta b)^2} + \left[\frac{(h_2 - h_1)}{(\Delta b)^4}\right]^2 \left[\text{Var } b_1 + \text{Var } b_2\right] \tag{24}$$

For cross path slopes the following substitution was included:

$$\Delta b = \left[(a_2 - a_1)^2 + (b_2 - b_1)^2\right]^{\frac{1}{2}}$$

$$\text{Var } S_c = \frac{\text{Var } h_1 + \text{Var } h_2}{(\Delta b)^2} + \left[\frac{(h_2 - h_1)^2}{(\Delta b)^4}\right]\left[\frac{(a_2 - a_1)^2(\text{Var } a_1 + \text{Var } a_2)}{(\Delta b)^2} + \frac{(b_2 - b_1)^2(\text{Var } b_1 + \text{Var } b_2)}{(\Delta b)^2}\right] \tag{25}$$

Figure 39a shows the in-path slope standard deviations for the stereo angles system with σ_ϕ equal to one minute of arc. The data point spacing, Δb, is 0.5 meter and 1.5 meters. The lines labeled S = 0° were determined from two points on the plane ($h_1 = h_2 = 0$). The lines labeled S = 25° were determined from point 1 on the plane and point 2 a distance above the plane.

$$h_2 = (\Delta b)(\tan 25^\circ) \tag{26}$$

The slope of a theoretical line between the two points is 25 degrees.

When the two points are at the same height, the second term of the variance equation (24) is equal to zero which makes standard deviation of the slope smaller. The stereo angles system yields its lowest in-path slope accuracies at close range.

Non-stereo in-path slope standard deviation is shown in Figure 39b

with σ_R of 10 cm and σ_ϕ of 1 min. Again two points at different heights give greater uncertainty in the in-path slope. With this system accuracy improves with increasing range. Non-stereo is more accurate than stereo angles for ranges greater than 10 meters.

Cross-path slope uncertainties are nearly the same as the in-path slope uncertainties when the height difference is zero. Cross-path slopes do not appear to be very sensitive to the difference in height between the two points used in the calculation.

Data point spacing should be increased as distance from the vehicle is increased. A larger number of points can be used in an averaging or plane fitting slope or gradient estimating scheme, Ref. 21.

A rapid scan has been assumed so there is virtually no vehicle motion between the measurement of adjacent data points. The actual slope of the vehicle could be added afterward to the slope of the terrain measured to obtain the slope in relation to the local vertical.

Conclusions

Stereo angles may be a useful method, especially if range standard deviations are greater than 10 centimeters. The stereo angles method will be effective only at close range, i.e. within about 12 meters. The non-stereo method is almost as good at close range and is much better at ranges in excess of 12 meters. The stereo range method will not be accurate enough unless range uncertainty can be reduced drastically. The schedule for future work during the next period is shown below.

	February	March	April	May
Investigation of data point spacing	----------			
Application of plane fitting to stereo systems		----------		
System evaluations and comparisons			----------	
Final report			----------	

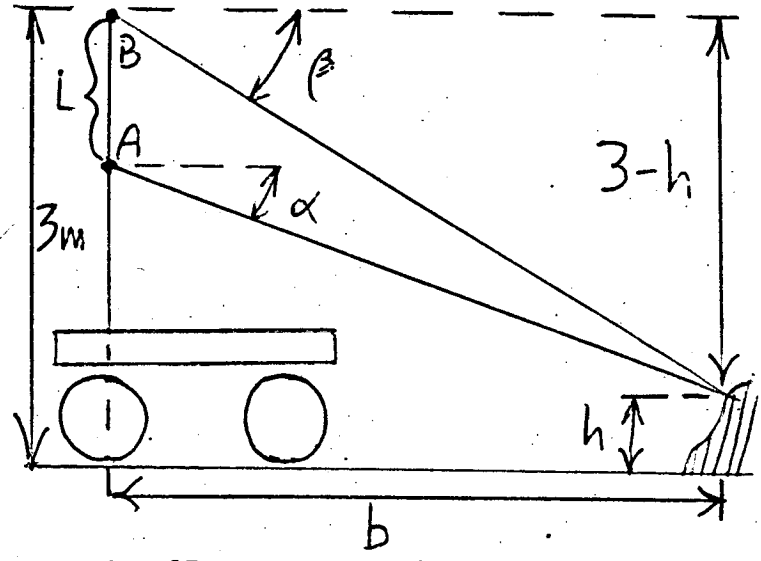

Fig. 27. Stereo Angles Method Geometry

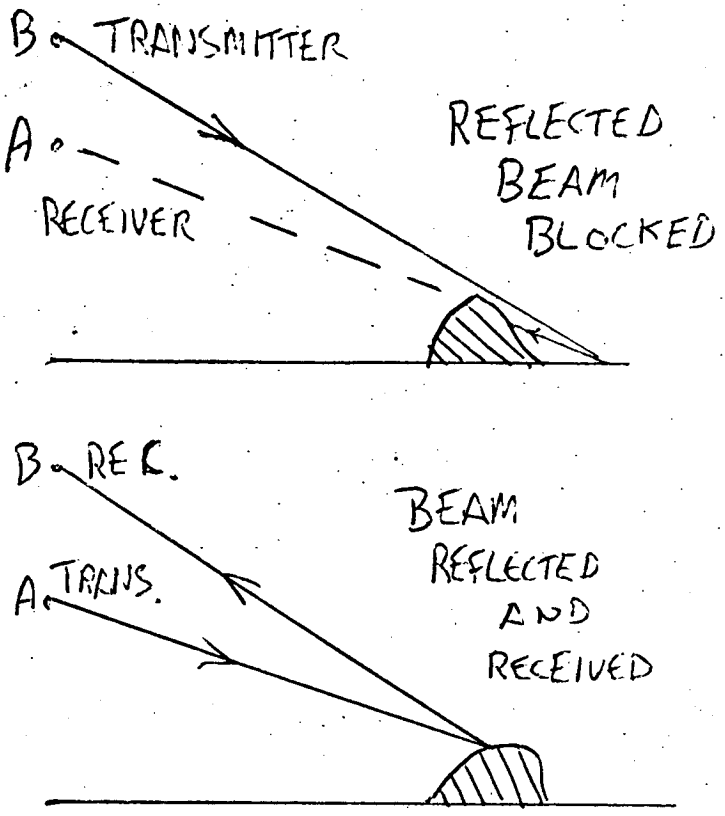

Fig. 28. Data Loss Resulting from Transmitter and Receiver Locations

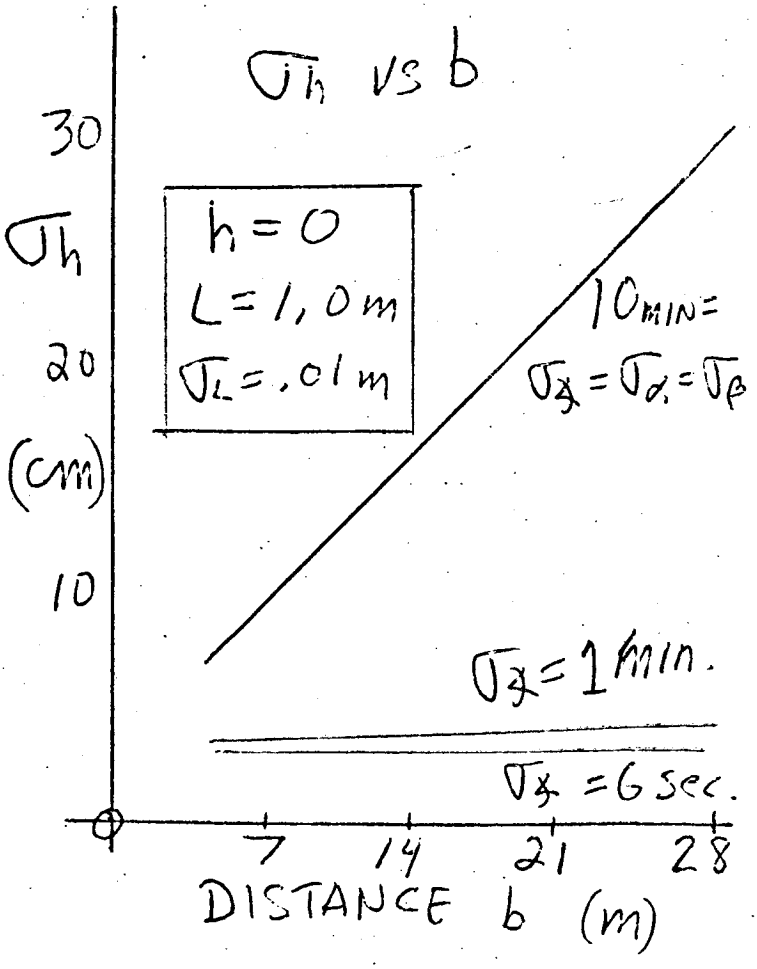

Fig. 29. Stereo Angles System Height Standard Deviation vs. Distance from the Vehicle

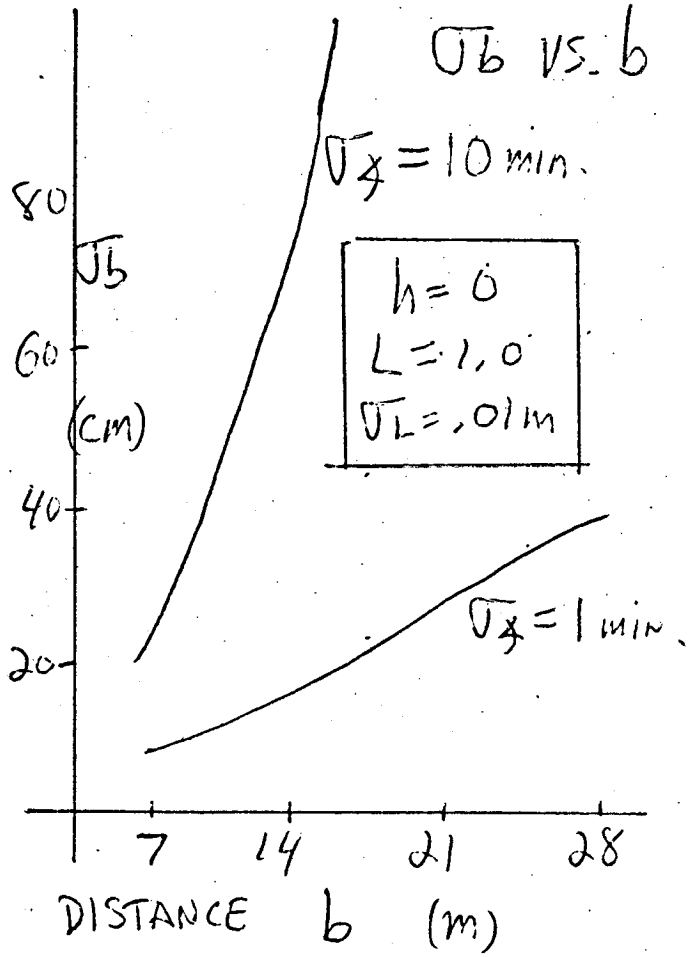

Fig. 20. Stereo Angles System Distance Standard Deviation vs.

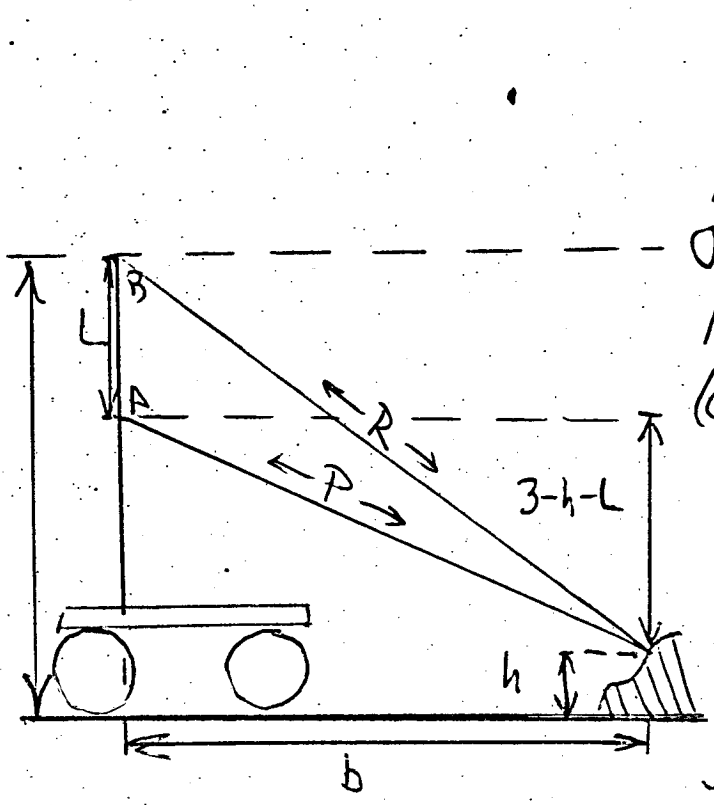

Fig. 31. Stereo Range Method Geometry

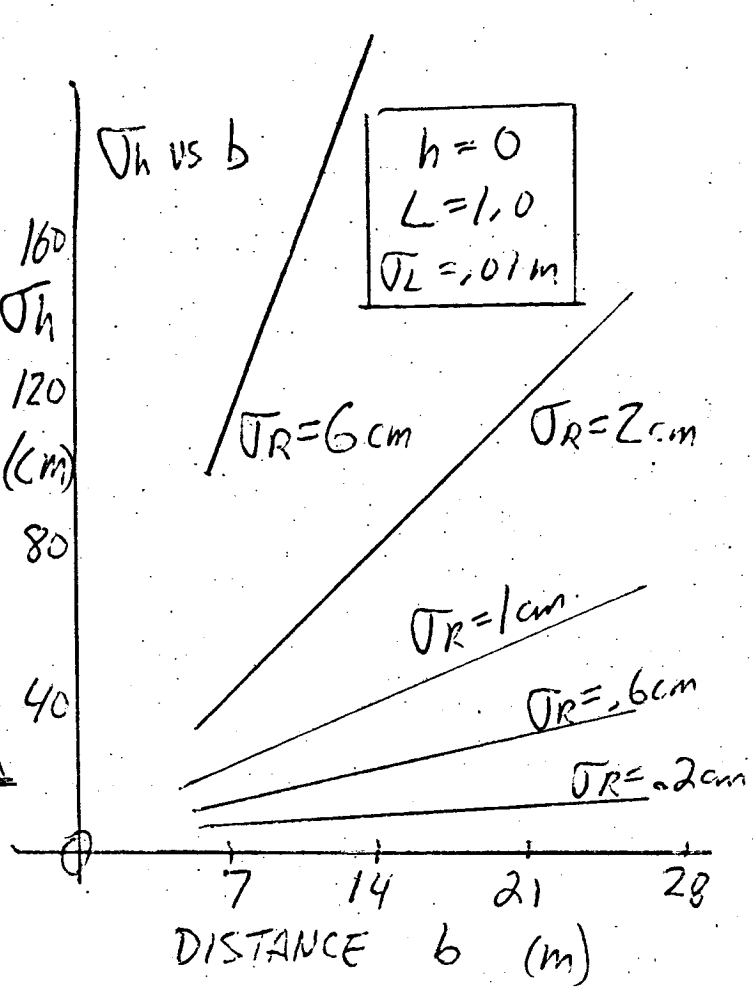

Fig. 32. Stereo Range System Height Standard Deviation vs Distance from the Vehicle

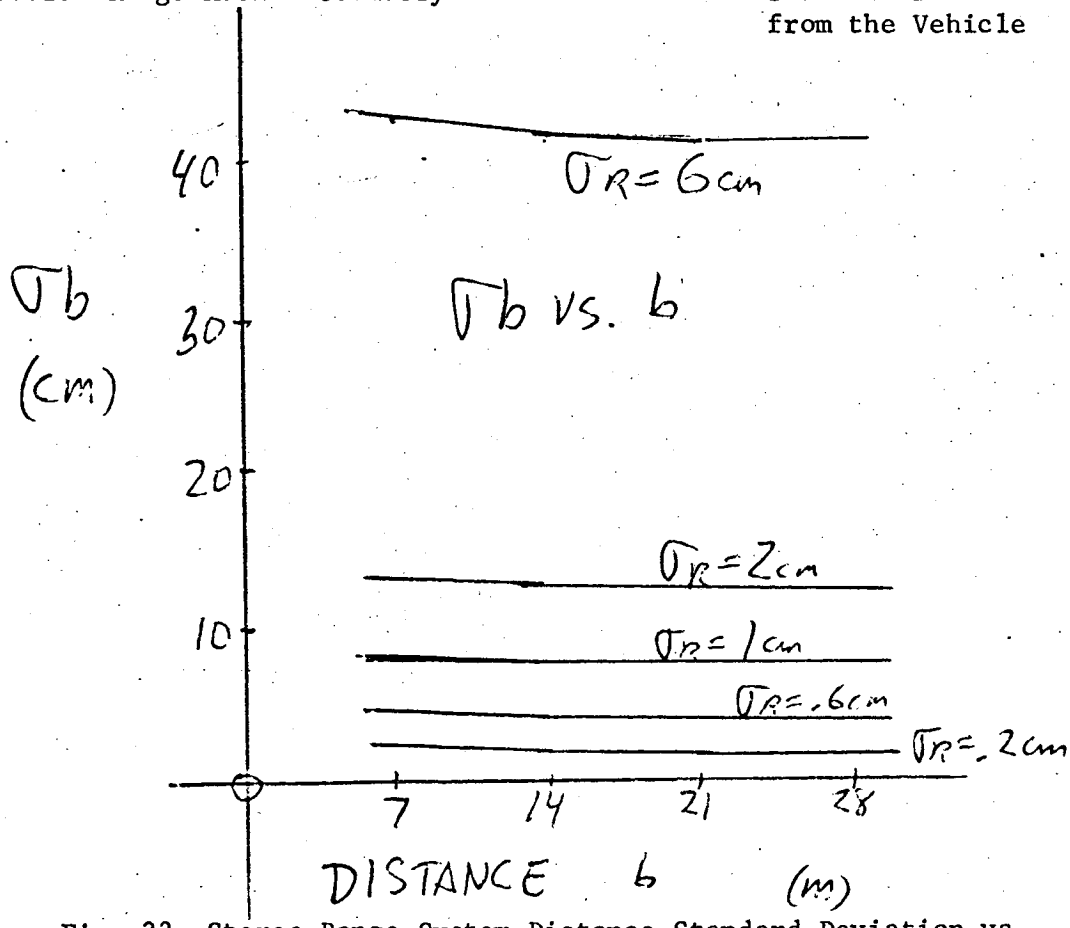

Fig. 33. Stereo Range System Distance Standard Deviation vs Distance from the Vehicle

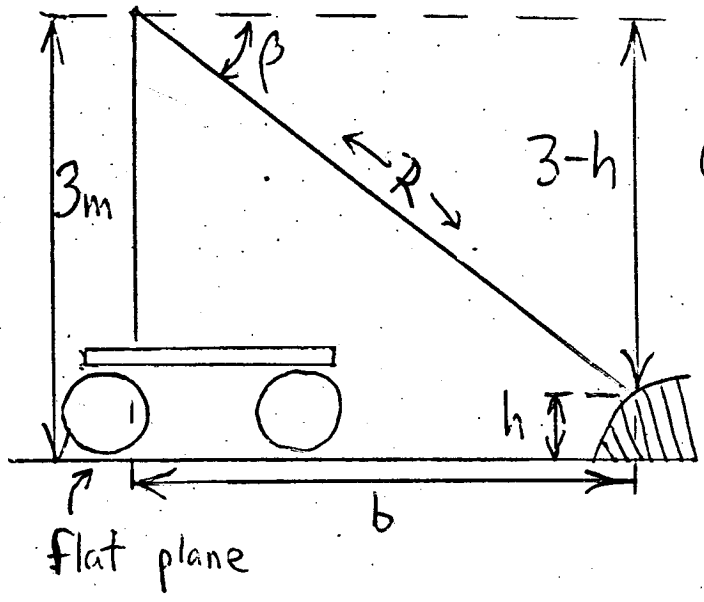

Fig. 34. Non-Stereo Method (Range-Angle Method) Geometry

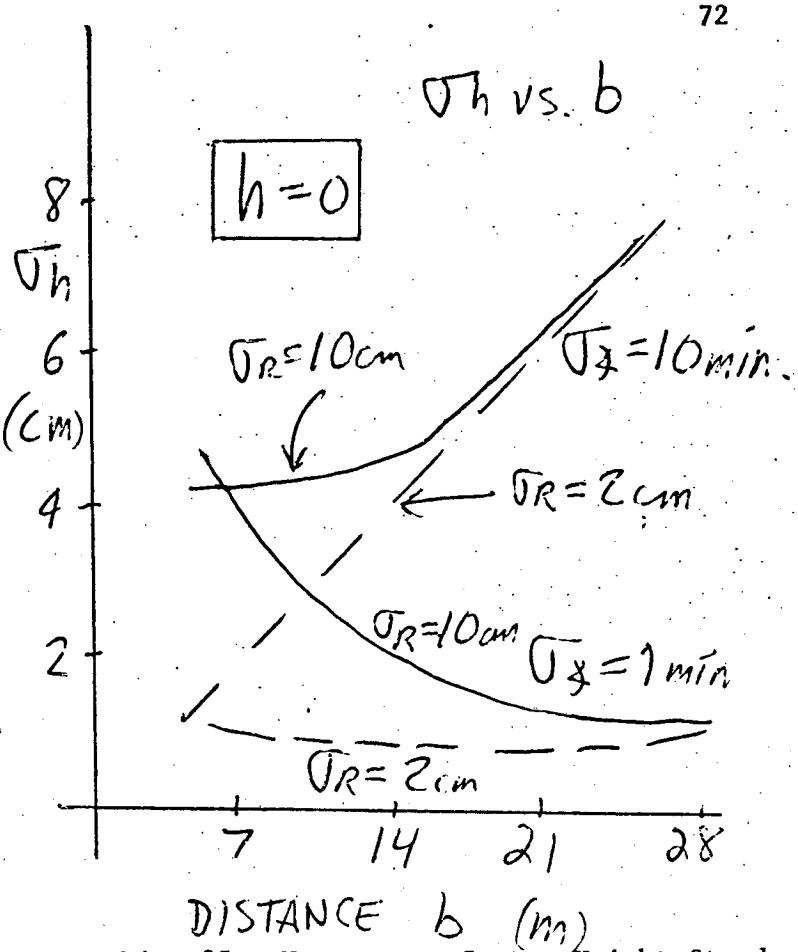

Fig. 35. Non-stereo System Height Standar Deviation vs Distance from the Vehicle

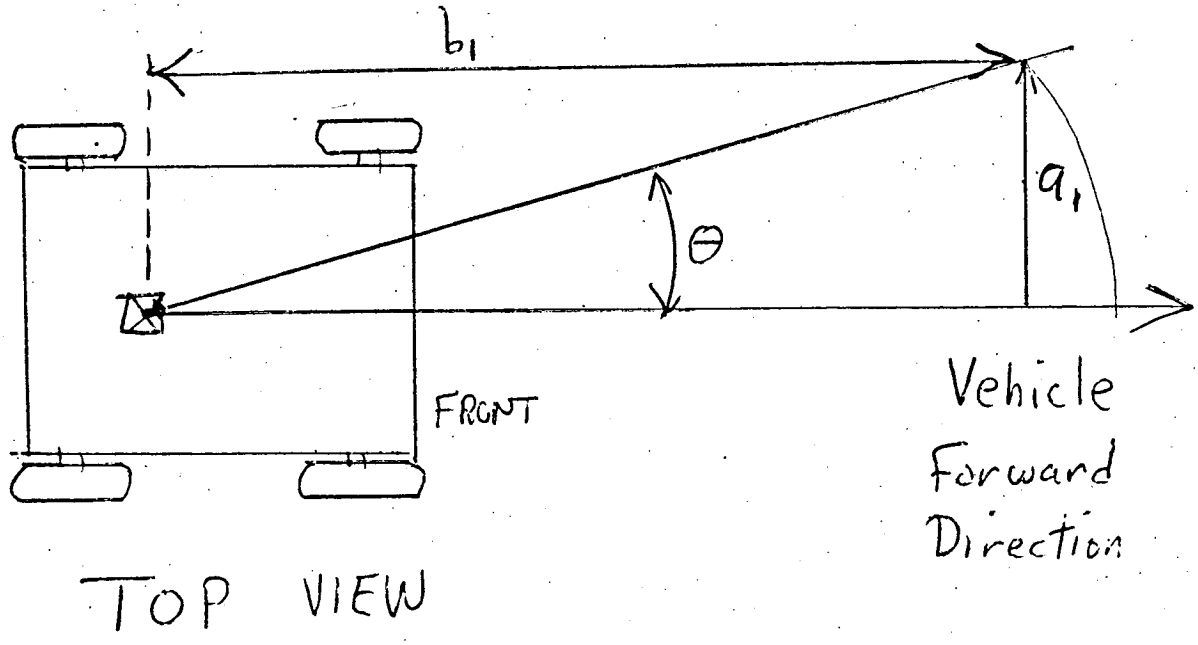

Fig. 36. Three Dimensional Measurement Horizontal Plane Geometry

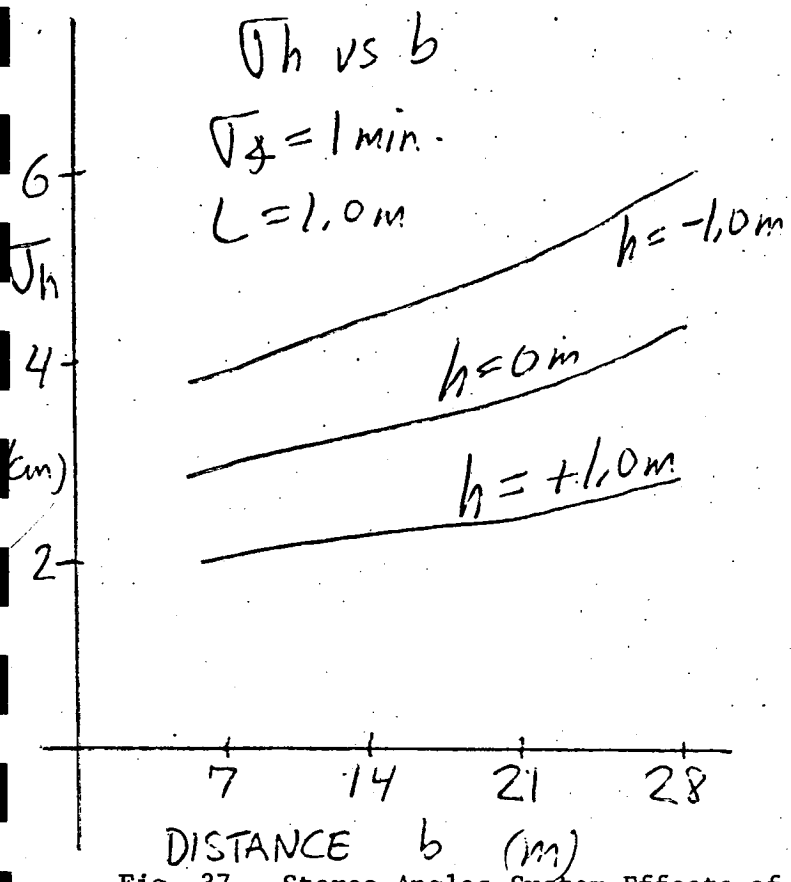

Fig. 37. Stereo Angles System Effects of Heights Other than Zero on Height Standard Deviation

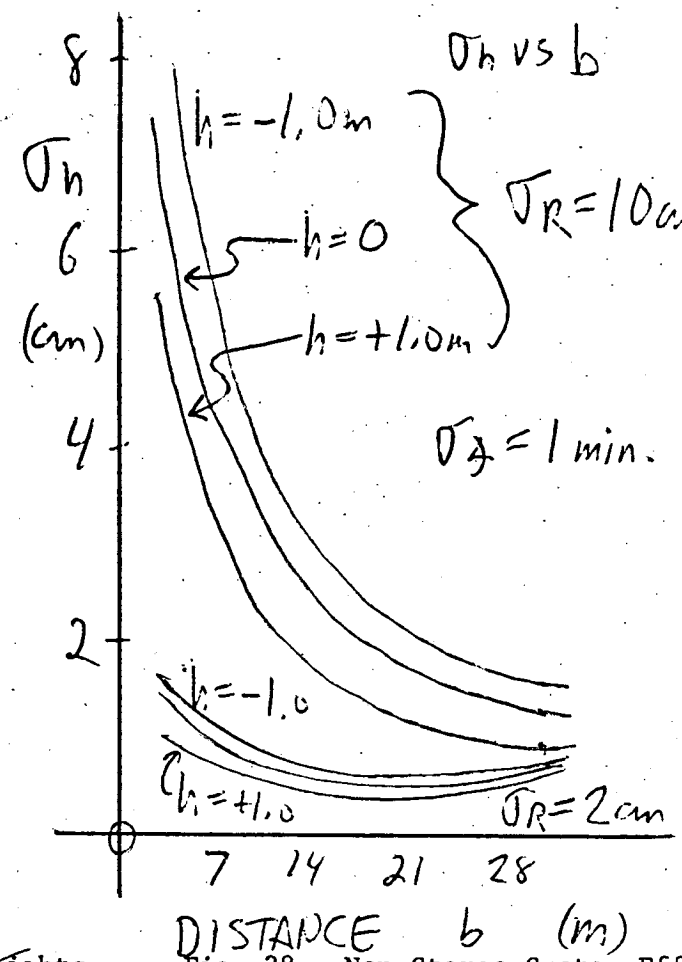

Fig. 38. Non-Stereo System Effects of Heights Other than Zer on Height Standard Deviat

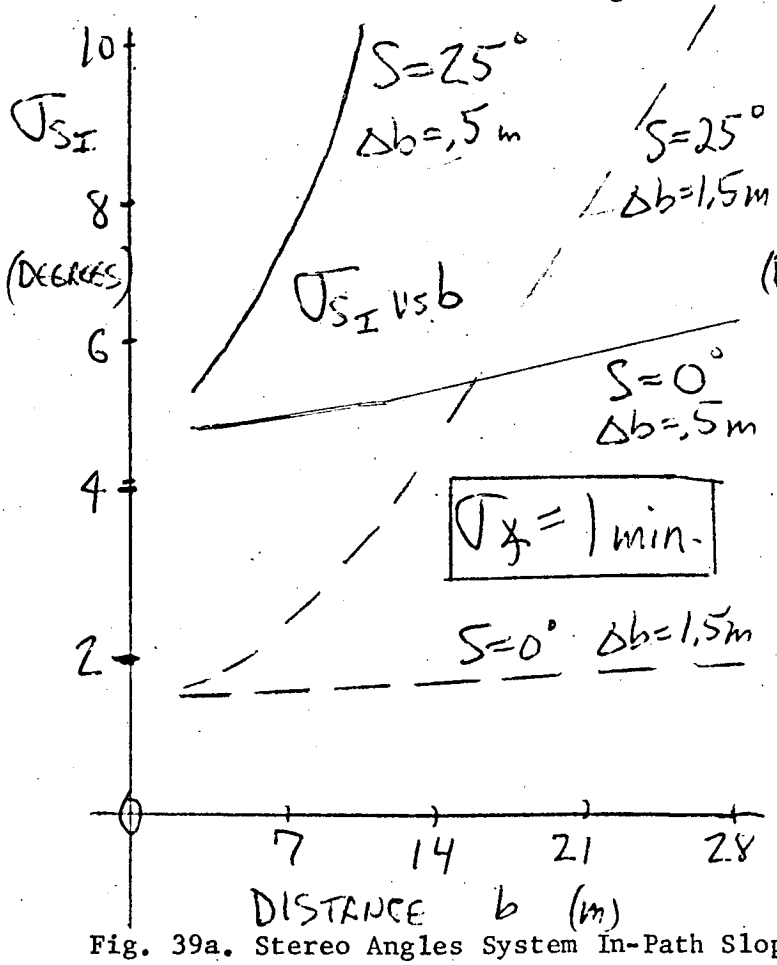

Fig. 39a. Stereo Angles System In-Path Slope Standard Deviation vs Distance

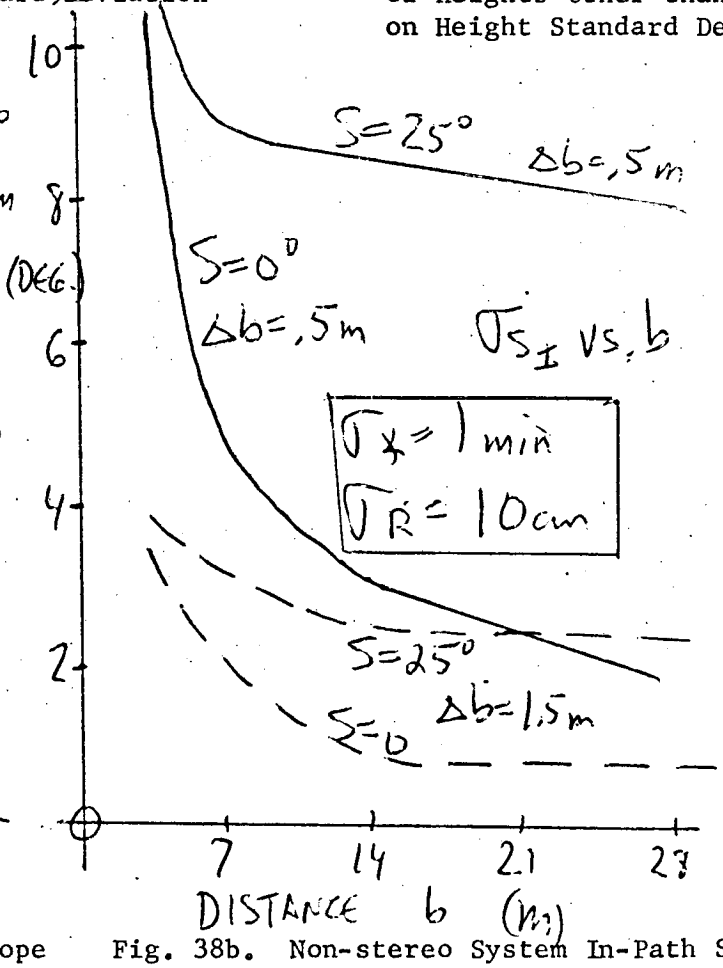

Fig. 38b. Non-stereo System In-Path Slope Standard Deviation vs Distance

C.2. Path Selection System Simulation and Evaluation - S. Boheim
Faculty Advisor: Prof. D. K. Frederick

In order to provide a means of evaluating proposed path selection systems, the preparation of a comprehensive digital computer program was undertaken 18 months ago. The primary objective of the task has been to be able to simulate the operation of a vehicle on realistic three-dimensional terrains in the presence of random effects, with a variety of path selection systems. A secondary objective was been to establish quantitative criteria for evaluating a path selection system's performance, as simulated by the computer program referred to above.

During the first academic year of work the general structure of the simulation was established and all of the essential elements were programmed, at least in an initial working version which was able to simulate one specific path selection system. The progress made in these two areas prior to July 1, 1972 has been summarized in Reference 22.

During the past six months, efforts have continued in the areas of simulation package improvements and path selection system design tradeoffs, and in compiling a cumulative technical report, Reference 23 and a user's guide for the simulation package. A brief discussion of these activities is presented below.

A. Simulation Package Improvements

Further attention has been directed towards the computer simulation package, as it was felt that a more powerful program would greatly aid in establishing improved evaluation criteria. The following additions and/or improvements were made to the simulation package:

1. Vehicle Model - In the past, the vehicle has been modeled as a point source. The vehicle model has been updated to include the dimensions of the vehicle in some areas of the simulation package. Further work is necessary before this improvement is completed.

2. Vehicle-Fixed Sensor - A sensor, with a fixed orientation with respect to the vehicle, has been simulated. This "vehicle-fixed" sensor is affected by the in-path and cross-path slopes of the terrain beneath the vehicle.*

3. Vertical-Fixed Sensor - In previous sensor simulators (see Reference 22), the mid-range sensor which is assumed to have a range of 3 to 30 meters, was considered to be mounted on an ideal level platform directly above

* The in-path slope is defined as the slope of the terrain measured in the direction of the vehicle's motion. The cross-path slope is measured in the direction perpendicular to the vehicle's motion. Both measurements are made by the vehicle.

the vehicle. The "vertical-fixed" sensor simulator has been improved so that the effects of in-path and cross-path slope on the location of the sensor can be simulated. The vertical-fixed and vehicle-fixed mid-range sensors are compared in Figure 40.

4. Range Measurement Simulation - Previous simulation methods (see Ref. 22) could calculate, with a resolution of only one meter, the length of the beam from the mid-range sensor to the beam impingement point on the surface. Using this inaccurate range calculation as a first guess, an interval-halving algorithm has been utilized to obtain as fine a resolution as desired. For a typical desired resolution of one centimeter, there was no noticeable increase in program execution time as compared to the time required to obtain one meter resolution. After further modifying the coding of sensor simulators, a saving of about 30% was realized in the execution time of these simulators.

5. Short-Sighted Vehicle - The user has the option of not using a mid-range sensor on the vehicle. In addition, this feature allows simulation of a failure of the mid-range sensor, if desired.

6. Terrain Display Block - The terrain contour map has been expanded to display a larger area. The computer coding has been streamlined so that no appreciable execution time penalty for this size increase is realized. Two other maps have also been added. The first is a vehicle path map, which displays the path chosen by the vehicle, initial vehicle location, and the target location (see Figure 41). An appropriate symbol is also used to indicate when the mid-range sensor is being used along the vehicle's path. The second map is an overlay of the vehicle path map onto the terrain contour map.

7. Vehicle Dynamics Simulation - Noise may be added to the in-path and cross-path slopes of the terrain beneath the vehicle to simulate small terrain irregularities. Additional noise may be added to simulate vehicle measurement error of these slopes. All noise addition is controlled by the user. The user may also limit the total simulation run time, thus preventing excessive costs when a path selection system becomes "lost" and wanders aimlessly (see Figure 41).

8. Intermediate Output - To further speed execution time, the display of certain parameters of interest during a particular simulation run (such as vehicle location, heading, etc.), can be deleted by the user as desired.

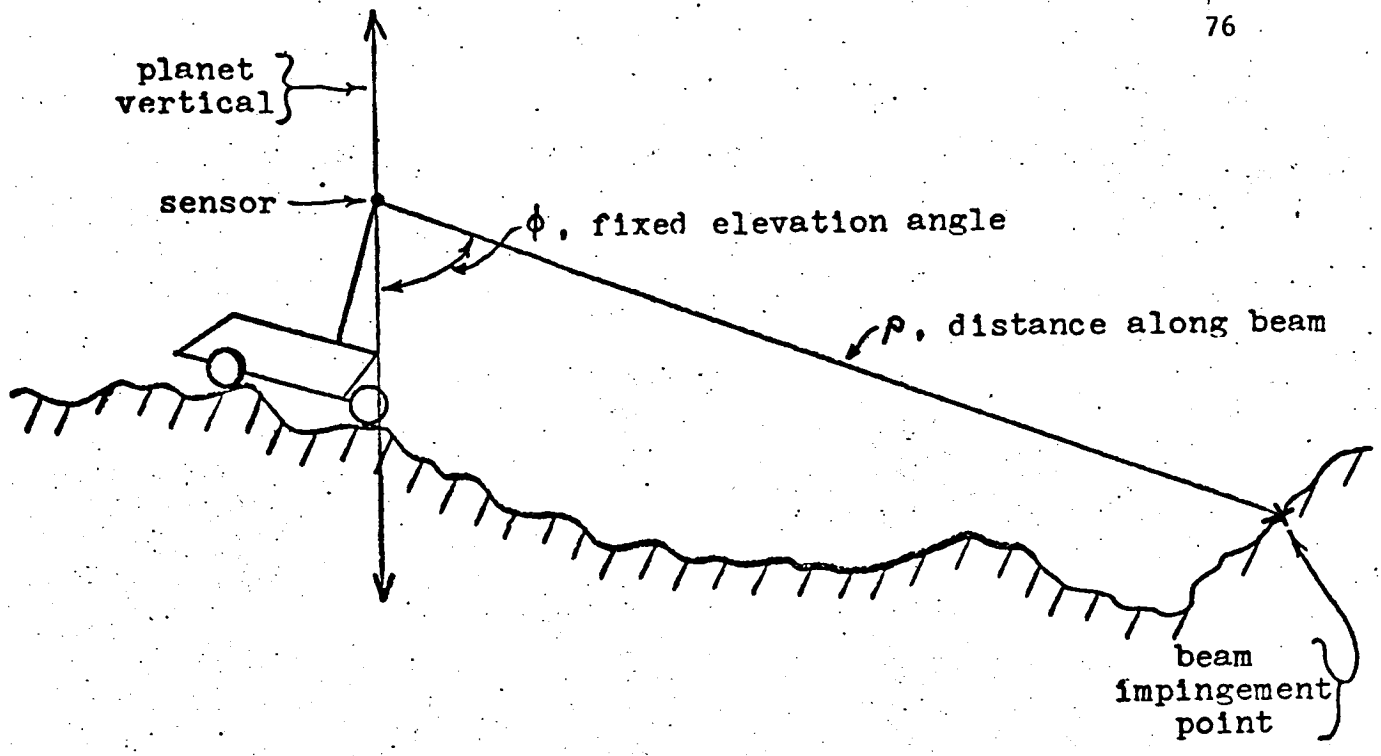

(A) Vertical-Fixed Sensor

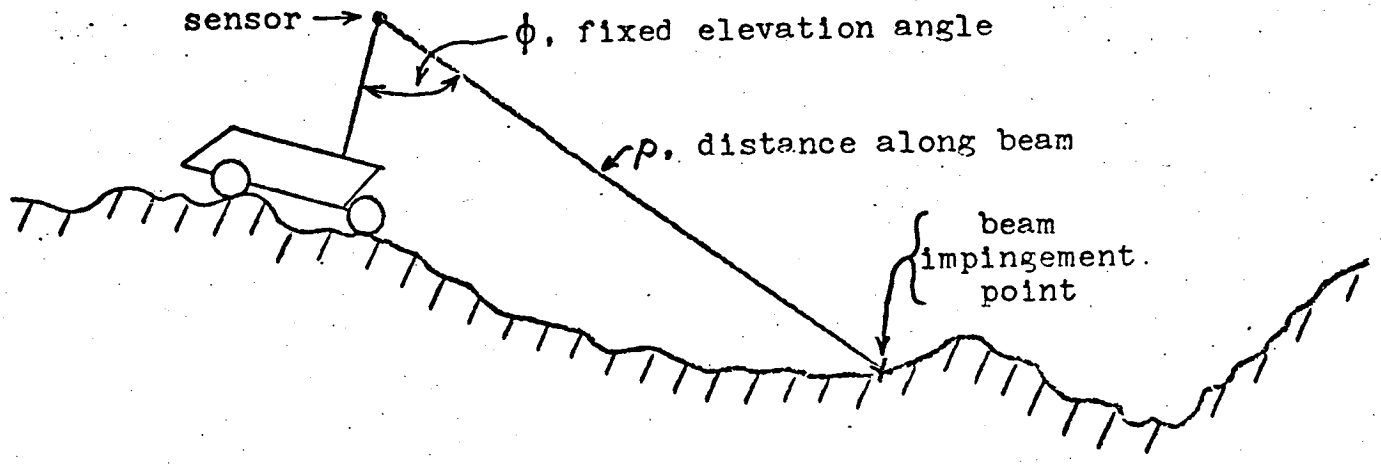

(B) Vehicle-Fixed Sensor

COMPARISON OF VERTICAL-FIXED AND VEHICLE-FIXED SENSORS

Figure 40

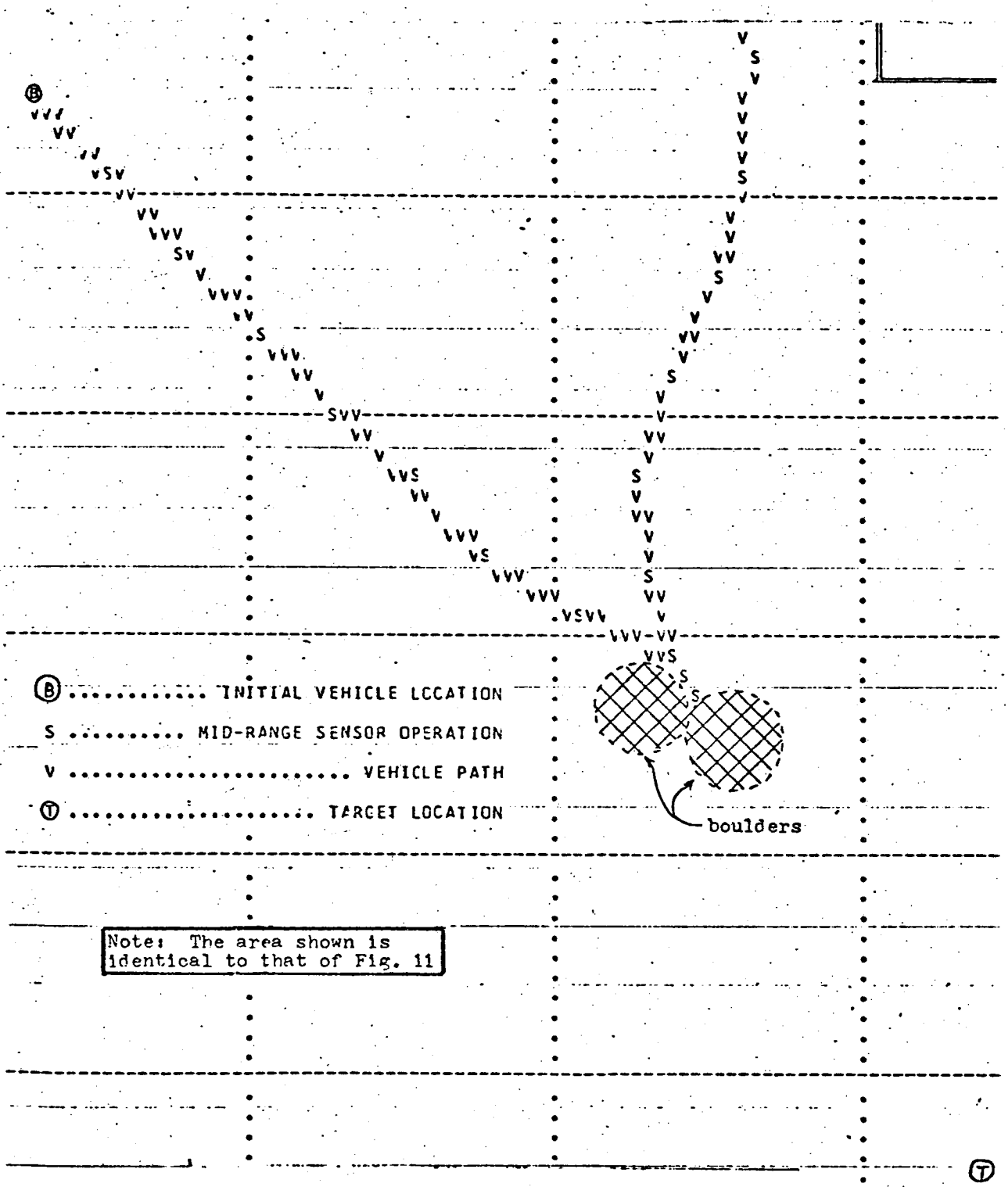

PERFORMANCE OF A 'CONFUSED' PATH SELECTION SYSTEM

Figure 41

B. Path Selection System Design Tradeoffs

The performance of three path selection systems has been evaluated to form some preliminary conclusions regarding the tradeoffs in designing a path selection system. These conclusions (three of which are stated below) are considered in detail in Reference 23.

1. When using slope type terrain models, the obstacle thresholds (slopes are compared to these thresholds to determine the existence of an obstacle) should not be as large as the vehicle's maximum traversable slope.

2. For slope type terrain models, increased use of the mid-range sensor allows better obstacle resolution, but may not be necessary if item 1 is satisfied.

3. Increasing the elevation angle of the sensor beam for slope type terrain models improves performance when in-path and cross-path slope effects are negligible. If these effects are not small, then the performance of the vehicle will be adversely affected. All of these situations are illustrated in Figure 42.

C. Technical Report and User's Guide

A technical report, Reference 23, has been prepared which summarizes all of the work done in this area of path selection system simulation and evaluation during the past 15 months. The development of the computer simulation package and the selection of evaluation criteria are discussed in detail. The performance of three different path selection systems is evaluated to determine the effectiveness of the simulation package, and to form some preliminary conclusions regarding the tradeoffs involved in designing a path selection system. Some of these conclusions were presented in the previous section. Finally, suggestions for future work in this area are presented and are summarized in the next section.

A user's guide has been prepared and will be available shortly. This text contains detailed information on how to use all of the available features in the simulation package, as well as the path selection systems presently implemented. Sections of the guide also specify guidelines for the user to follow when writing new path selection systems to be simulated and evaluated by the computer package. The derivation of all simulation formulas and methods used by the simulation package, as well as functional flowcharts, are included in the user's guide.

Future Work

1. Design Tradeoffs - Using the performance of three path selection systems, some preliminary conclusions

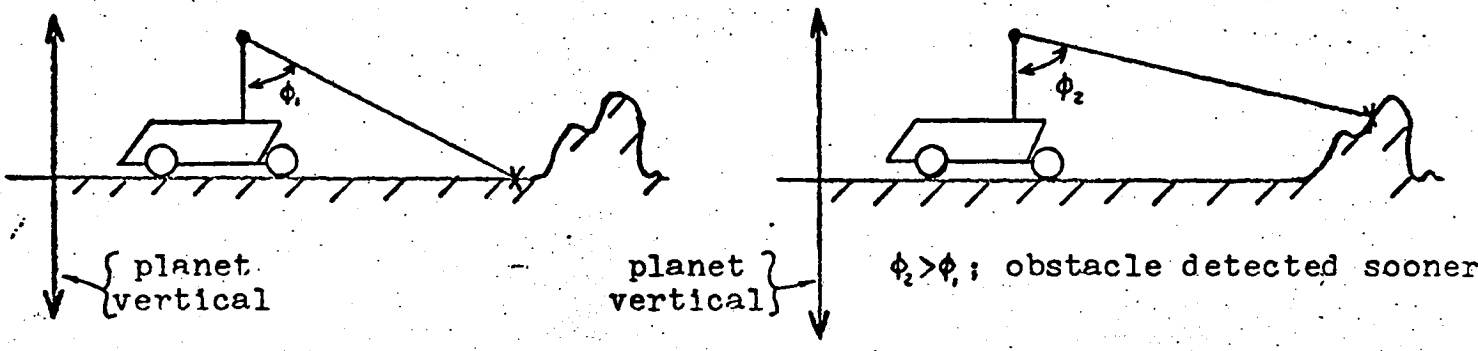

(A) Negligible In-Path and Cross-Path Slopes

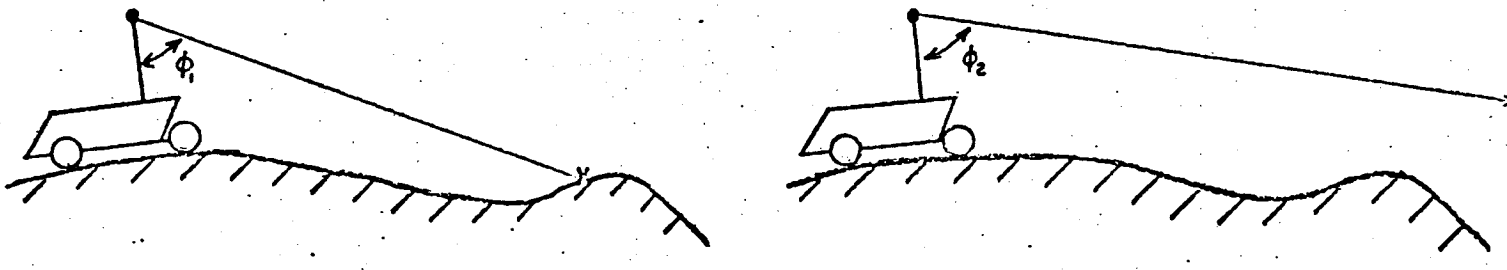

(B) Significant In-Path and Cross-Path Slopes

DESIGN CONSIDERATIONS FOR SENSOR BEAM ELEVATION ANGLES

Figure 42

regarding the tradeoffs involved in designing a path selection system have been made. More extensive analysis is required, however, before more meaningful and reliable results may be obtained. Of particular interest is the comparison of the performance of the vehicle-fixed sensor with the vertical-fixed sensor, a study which will be conducted next semester and concluded by May.

2. Evaluation Criteria - As path selection systems are evaluated, the desirability of these systems can be compared with the results of the simulation and evaluation package. A high degree of correlation is required between desirability and evaluation results, certainly higher than is presently available. Refinements and additions of evaluation criteria will be a continued effort that will become more effective as the number of evaluated path selection systems increase.

3. Path Selection Algorithms - A large effort has been made to realistically simulate mid-range sensors, and, to a smaller degree, terrain modelers. On the other hand, only very simple path selection algorithms have been implemented. Work done next semester will involve the simulation and evaluation of more advanced path selection algorithms.

Due to its modular arrangement, the program can be used to compare, by simulation, any number of path selection systems, regardless of their specific features. Hence, it is anticipated that the program will be used extensively in the future to compare the performance attainable with sensors, terrain modelers, and path selection algorithms originating at JPL, Cornell, and other establishments in addition to Rensselaer.

Task D. Chemical Analysis of Specimens

One important phase of the initial missions to Mars is the search for organic matter and living organisms on the martian surface. The present concept for attaining this objective consists of subjecting samples of the atmosphere and surface material to certain chemical and biochemical reactions and thereafter analyzing the products produced, probably in a combination gas chromatograph/mass spectrometer (GC/MS). The gas chromatograph is proposed for separating complex mistures evolved from the experiments into small groups of similar chemical species. Chemical analysis of these groups would be accomplished in the mass spectrometer. It is the objective of this task to provide engineering techniques and design criteria for designing such a system.

The overall concept of the chemical analysis system is shown schematically in Figure 43. Most of the previous effort has involved the systems analysis of the gas chromatograph using simulation, Ref. 24, 25. This technique uses mathematical models, which incorporate fundamental parameters

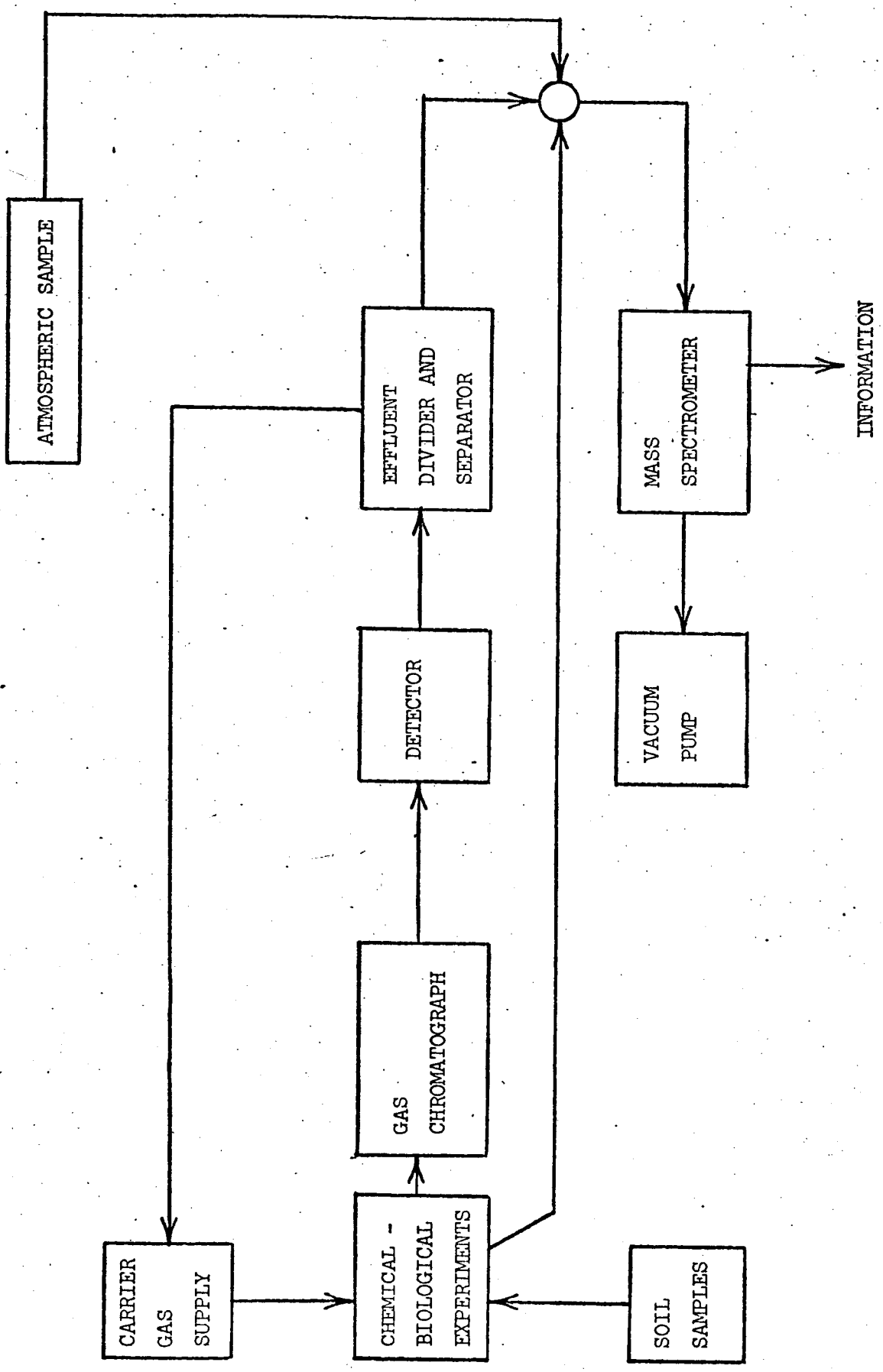

Figure 43. Schematic of Chemical Analysis System.

evaluated from reported experiments, to explore various concepts and to direct further experimental research. The objectives of the task have been extended to include preliminary studies of the entire chemical analysis system. System topics being considered include carrier gas generation and removal, and limitations imposed by and upon the mass spectrometer.

The task problems are being attached by a four-member team, each of whom is pursuing a specific assignment:

1. GC/MS system concepts
   a. Mass spectrometer system characteristics
   b. Carrier gas generation and removal
2. Chromatographic system analysis
   a. Multicomponent chromatography
   b. Chromatograph model improvement

D.1. GC/MS System Concepts

D.1.a. Mass Spectrometer System Characteristics - M. P. Badawy

Faculty Advisor: Prof. P. K. Lashmet

It is the function of the mass spectrometer to provide mass spectra for three different inputs (Figure 43): effluents from the gas chromatograph; direct samples from the life-determining experiments; and samples of the atmosphere. This subtask has as its objective the characterization of the major properties of the mass spectrometer, the resulting relations to provide direction in designing an instrument suitable for this space mission. In particular, those characteristics influencing power, weight, and volume requirements of the system are of primary concern in this study.

Prior work provided a parametric study of the coupling between the magnetic field and electrostatic potential in determining the ion masses to be detected (Ref. 26). Instrument resolution and the nature of the ionizing process are currently being investigated.

Resolution, or the ability of the instrument to differentiate among different masses at a given time, is estimated for the single focusing spectrometer as follows, Ref. 27, 28:

$$M/\Delta M = 1/\left[\frac{s'+s''}{a_m} + \left|\frac{\Delta V}{V}\right|\right]$$

where

s', s'' = slit widths at the source and detector ends, respectively.

a_m = magnetic field radius of curvature.

V = voltage used for deflection of mass M.

ΔV = voltage equivalent to range of masses emanating from the electrostatic field at different velocities.

ΔM = dispersion in mass detected.

Similar but more complicated results for the double focusing mass spectrometer have also been developed. These results emphasize the importance of the slit widths, the radius of curvature of the magnetic spectrum analyzer, and the energy spread of the instrument. Table 1 summarizes the physical parameters of three mass spectrometers and presents their respective mass resolutions as estimated from the above equations. Higher mass resolution can be achieved with more complicated designs, e.g. the toroidal electric sector field design, Ref. 29. However, for the current preliminary studies, the characteristics of the more simple single or double focusing designs are satisfactory for representing the basic instrument.

Instrument sensitivity or the minimum concentration level detectable is determined to a great extent by the ionization process, Ref. 34. The performance of the ionization chamber, based on an electron impact source, is characterized by the following equation, Ref. 30, 31.

$$I = b\, N \sigma\, s\, I_e$$

where

I, I_e = ion and electron currents, respectively

b = ion extraction efficiency

N = molecular density

σ = ionization cross-section

s = effective electron path length

Difficulty in determining the ionization cross-section limits the utility of the equation in the present study. Ionization cross-sections for single electron emission are available, Ref. 32. However, because knowledge of the components in the gas to be analyzed is uncertain, and determination of the ionization fragments is complicated, it appears that theoretical treatment of the ionization process is beyond the scope of this preliminary study. Experimental relations between the ion and electron currents will be sought to complete this phase of the task.

Further work will be concerned with determining the effect of the major design variables upon power consumption of the mass spectrometer. Figure 44 shows schematically the relation between the various power consuming elements of the instrument. Current studies involve estimates of power associated with the filament of the ionization chamber and with maintaining the accelerating potential. After these studies are completed, the vacuum pumping system and the magnet power supply will be considered.

D.1.b. Carrier Gas Generation and Removal - C. W. Jarva
Faculty Advisor: Prof. L. K. Lashmet

Carrier gas, which is relatively inert with respect to the samples

TABLE 1

Specific Parameters for Several Mass Spectrometers

		JPL	Hayden and Nier	Voorhies et. al.
Electrostatic field angle	ϕ_e	90.°	-	90°
Magnetic field angle	ϕ_m	90.°	-	60°
Source to electrostatic field length	l'_e	1.656 cm	0.8 cm	4.34 cm
Mass dispersion coefficient	$\Delta V/V$	$\pm$ 0.01	$\pm$ 0.02*	$\pm$ 0.02*
Magnetic field radius	a_m	3.82 cm	2.54 cm	25.4 cm
Electrostatic field radius	a_e	4.7 cm	4.27 cm	31.5 cm
Entrance slit width	S'	0.00507 cm	0.01 cm	0.00456 cm
Exit slit width	S''	0.00507 cm	0.038 cm	0.01524 cm
Mass resolution $M/\Delta M$	SF	(41.6)	(26.3)	1.25
	DF	180.9	47.31	(1.28)

* Assumed

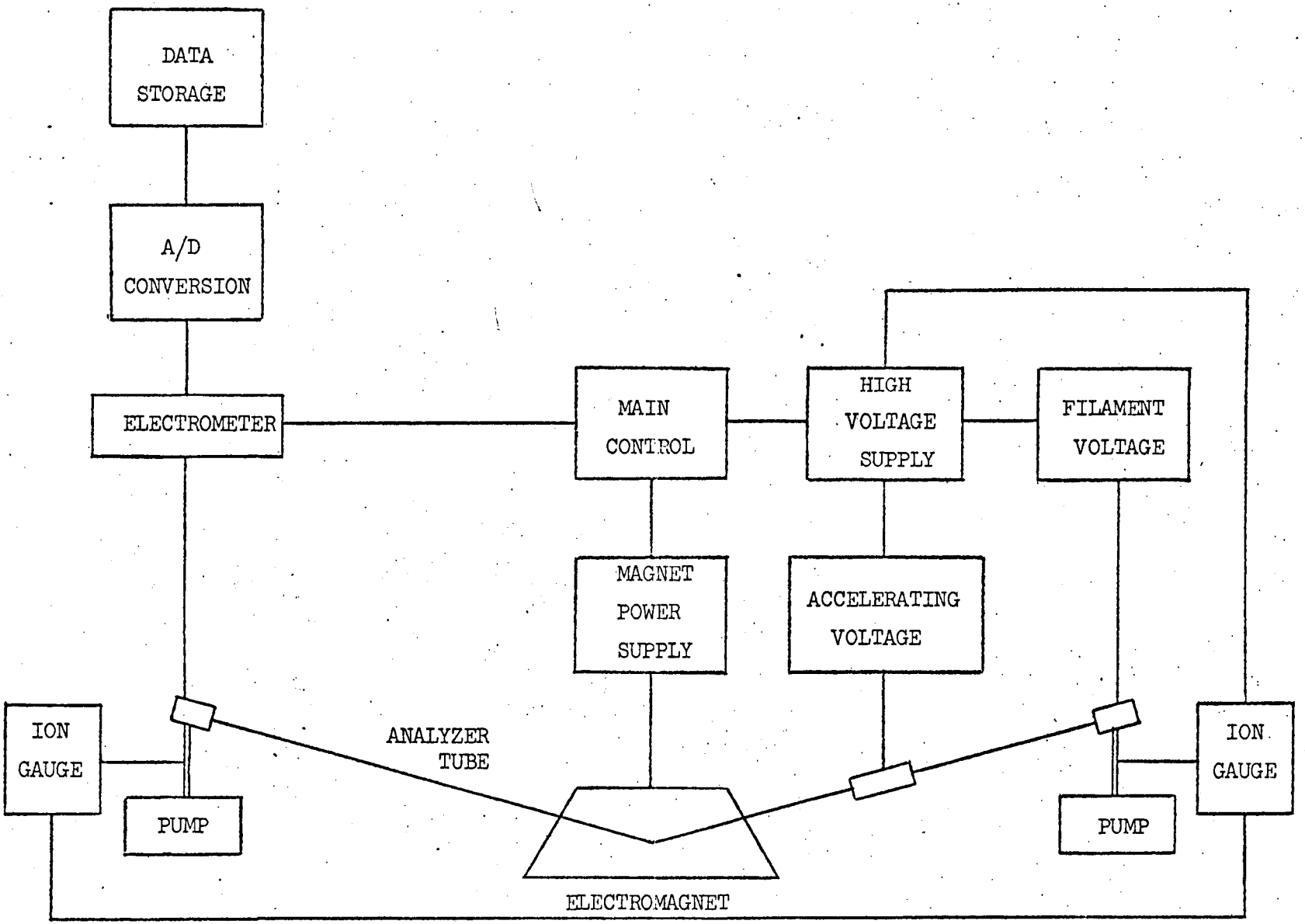

Figure 44. Power Consuming Components of Mass Spectrometer

being analyzed and which must be in supply for an appreciable part of the mission, is required to propel minute samples through the column of the gas chromatograph, Ref. 33. On arriving at the mass spectrometer, which operates at a low pressure ($< 10^{-4}$ torr), the major portion of this carrier gas must be separated from the sample and must be removed from the system. Thus the systems for generating, separating, and removing the carrier gas are important to overall system design and operation. It is the objective of this subtask to generate the basic characteristics and limitations of several promising concepts to aid in the design of the final overall system.

A study was undertaken to determine, as a function of the initial charge pressure, the physical characteristics of a spherical, high-pressure gas tank for storing the amount of carrier gas necessary for experimentation. Because of diffusion of the carrier gas, assumed to be hydrogen, through the vessel wall and its leakage through welds, valves, etc., Ref. 34, 35, the gas storage capacity was greater than the requirement for the experimentation. Diffusion rates were determined from reported data, Ref. 36. To estimate leakage through welds and valves, it was assumed the vessel would be subjected to helium leak detection when charged to a practical pressure taken as 34 atmospheres in this case. The minimum leak detectable by modern leak detectors, about 10^{-6} atm, cm^3/sec, Ref. 35, was extrapolated to account for hydrogen as the gas and for the actual charge pressure. The vessel wall thickness was estimated from standard equations, Ref. 37.

Estimates of vessel size and weights as affected by charge pressure and operating time are shown in Figures 45 and 46. These estimates are based on the following assumptions:

1. Construction - fiber reinforced stainless steel containing 1/3 metal by volume, Ref. 38.
2. Allowable working stress - 4.5×10^8 N/m^2 (66,000 psi), Ref. 38.
3. Gas flow rate for experiments - 2 std cm^3/min, Ref. 39.
4. Flight time to Mars - six months.
5. Maximum temperature - $300^{\circ}K$.

Although diffusion and leakage were considered in these studies, these processes contributed only about 1% to the vessel volume. The vessel weights, shown in Fig. 46 to be approximately independent of charge pressure, are for the shell only. The pressure regulator and its mounting boss will contribute an additional one kgm approximately.

It was a major objective of this study to examine the merits of the gas storage vessel especially relative to a water electrolyzing cell proposed earlier, Ref. 40. It is estimated that the gas storage tank will weigh approximately 60% more than a comparable electrolyzing cell system but will occupy about the same space depending upon the charge pressure. It thus appears that if reliable fiber-reinforced

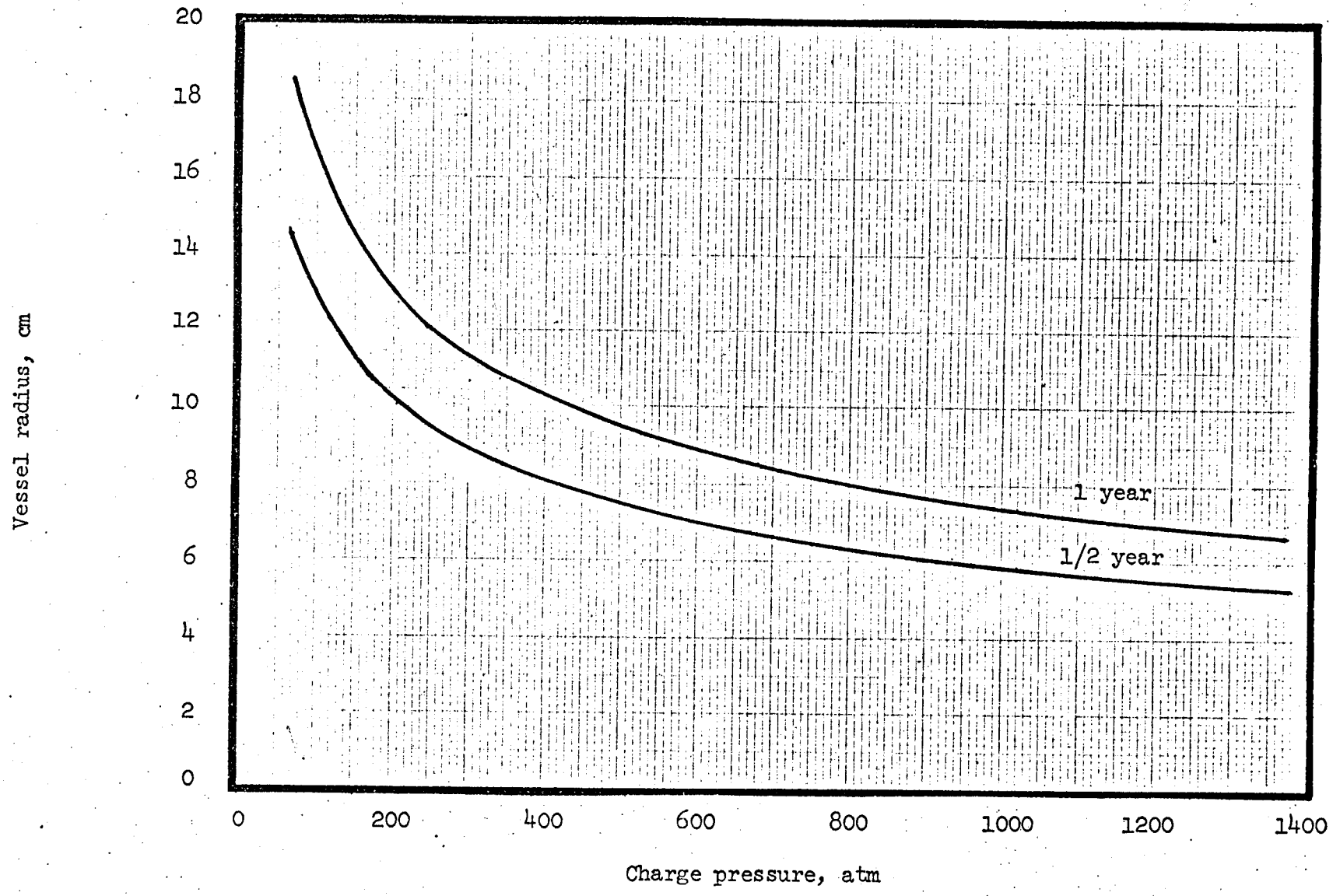

Figure 45. Effect of Charge Pressure and Operation Time on Size of Carrier Gas Sphere.

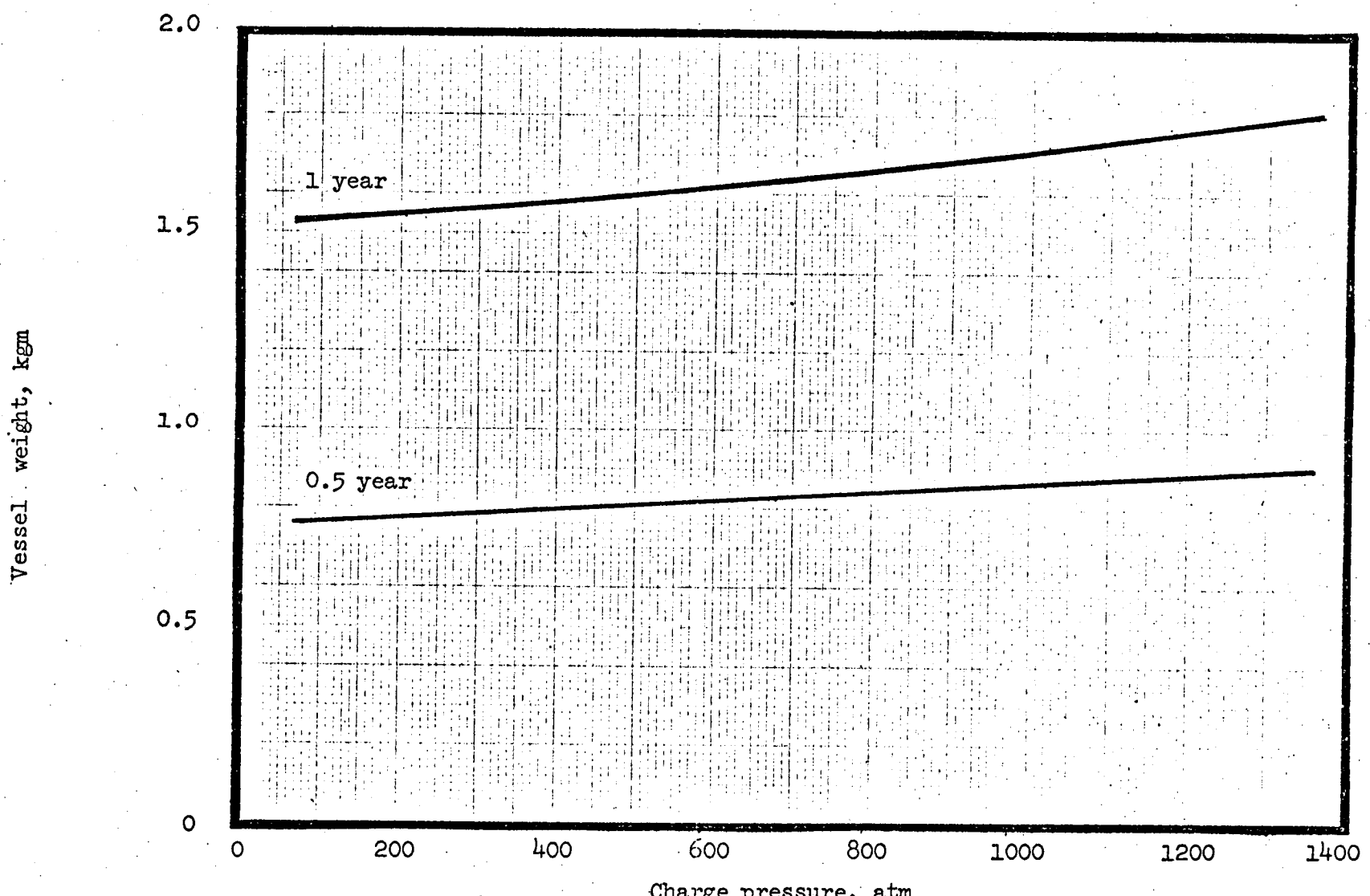

Figure 46. Effect of Charge Pressure and Operation Time on Shell Weight of Carrier Gas Sphere.

vessels having about four times the allowable working stresses of stainless steel, can be fabricated, the concept of the high-pressure storage vessel has promise, especially since the system is simple.

Except for possible minor improvements in the calculational procedures, this preliminary study has been completed.

A carrier gas removal system must be considered because the operating pressure of the mass spectrometer is about 10^{-7} times the pressure expected in the chromatograph, Ref. 41. The palladium-silver alloy/hydrogen gas separator has been proposed, Ref. 39. In such a system, hydrogen flowing in a palladium tube diffuses rapidly through the heated tubing wall in comparison to other gaseous materials. This subtask is concerned with developing technical procedures suitable for the design of such a unit as well as with assessing its merits.

At present the steady state behavior of the system is being considered using momentum balance and material conservation equations. Hydrogen diffusion rate through a palladium wall is proportional to the difference of the square roots of the hydrogen gas pressures at each face of the wall because of dissociation during diffusion, Ref. 42. A diffusivity particular to the system is also involved, Ref. 42. From this diffusion rate equation, a first order, nonlinear, differential equation has been developed which relates the rate of material flowing at any point in the tube to the rate the gas is diffusing out of the system. Combined with a second order nonlinear momentum balance equation, a describing set of equations for this system was formed which requires numerical solution. This analysis assumes laminar flow, pure hydrogen flowing through the palladium tube (no presence of sample), and radial flow of the diffusing gas through the palladium walls. Equations accounting for the presence of sample will be developed after the characteristics of this simple system have been determined.

In the present studies, the hydrogen pressure outside the palladium tube is assumed to be approximately zero. Pumping means such as combining the diffused hydrogen with oxygen on the tubing wall, Ref. 29, is a topic of future work. Other topics worthy of consideration if time permits include estimations of mechanical breakdown due to temperature and pressure cycling and chemical breakdowns due to contaminants.

D.2. Chromatographic Systems Analysis

D.2.a. Multicomponent Chromatography - A. J. Meisch

Faculty Advisor: Prof. P. K. Lashmet

Linear mathematical models of the chromatograph have been developed for single chemical components and have been solved analytically for an impulse input, Ref. 25, 43, 44. Other work, Ref. 24, which used data from a chromatographic test facility has shown that convolution of the actual input data with the theoretical normalized impulse response gives a reasonable representation of the actual chromatogram for a single component.

It is the objective of this subtask to experimentally evaluate the mathematical model for multicomponent chemical systems using superposition of a single component data. Specifically the equilibrium adsorption model, Ref. 44, is being considered:

$$Y(\theta) = \sqrt{\beta P_e / 4\pi\theta^3} \exp\left[- (P_e/4\beta\theta) (\theta - \beta)^2 \right.$$

where

β = $1 + (1/m R_o)$

θ = dimensionless time = vt/L

v = carrier gas velocity

t = time

L = column length

Pe = the Peclet number, a dimensionless measure of sample diffusion in the carrier gas

mR_0 = a thermodynamic parameter, specific to the chemical system considered

Y = composition response to a unit impulse.

This model assumes the gas at each point to be in equilibrium with the solid adsorbent; i.e., the column is very long. The Peclet number is a function of the fluid mechanics and the physical properties of the system and is predictable, Ref. 25. The parameter mR_0 is specific to the system and is determined from the system data using a curve fitting technique, Ref. 27.

Extension of the model to multicomponent chemical systems using superposition of pure component data was proposed. Experimental work reported earlier, Ref. 25 on the binary system n-pentane/n-heptane on a microporous adsorbent Chromosorb 102 column (see Table 2) showed superposition was only a first order approximation and large deviations were noted. This subtask has as its objective the verification of the previously observed discrepancies and the generation of additional multicomponent chromatographic data.

Chromatographic data for the system n-pentane/n-heptane on the Chromosorb 102 column have been obtained at 150 and 200°C and for mixtures containing 0, 1, 25, 50, 75, 99, and 100% n-pentane by weight. As shown in Figure 47, the peak times for the multicomponent system lagged peak times predicted from superposition of the pure component data. This time lag occurred for both compounds for all mixtures considered as shown in Table 3. The time lag increased as the component composition became more dilute.

The peak time is primarily related to the parameter mR_0, Ref. 44. As the peak time varies with sample composition, it is possible that mR_0 is composition dependent; i.e., although the component compositions

TABLE 2

COLUMN CHARACTERISTICS

	CHROMOSORB 102	POLYETHYLENE GLYCOL
LENGTH (CM)	100 CM	100 CM
O D	1/8 IN	1/8 IN
I D	0.22 CM	0.22 CM
MESH	60/80	60/80
PARTICLE SIZE	0.025/0.0177 CM	0.025/0.0177 CM
COMPOSITION	MICROPOROUS STYRENE-DIVINYL BENZENE POLYMERS	POLYETHYLENE GLYCOL (CARBOWAX 1500) 20% BY WEIGHT
TEMPERATURE RANGE	ROOM -250°C	ROOM-225°C
APPLICATION	SEPARATION OF LOW MOLECULAR WEIGHT, VERY POLAR SUBSTANCES SUCH AS WATER, ALCOHOLS, AMINES, ACIDS, ESTERS, KETONES, ETHERS, ALDEHYDES AND TO A LIMITED EXTENT LIGHT GASES.	SEPARATION OF HIGH BOILING POLAR COMPOUNDS. GENERAL PURPOSE COLUMN FOR POLAR SAMPLES.

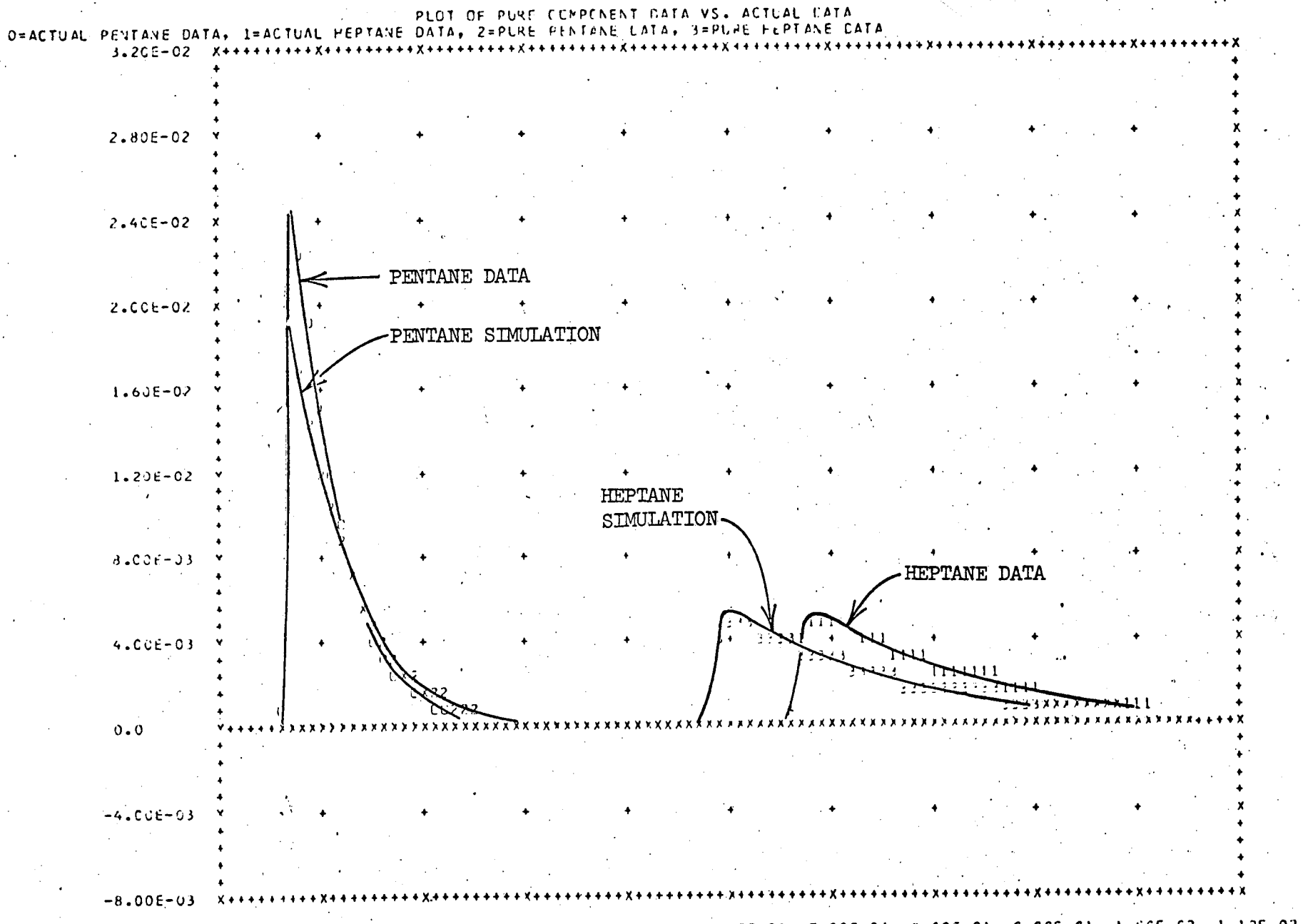

Figure 47. Comparison of Predicted and Actual Chromatograms for Pentane-Heptane System on Chromosorb 102 at 150° C.

TABLE 3

PENTANE - HEPTANE SYSTEM ON A CHROMASORB 102 COLUMN

HELIUM FLOW RATE OF 29.4 CC/MIN AT 150 DEG C

COMPOSITION (WGT %)	ACTUAL PENTANE PEAK *	ACTUAL HEPTANE PEAK *
100 H	-	285.5
99 H - 1 P	95.0	294.0
75 H - 25 P	88.5	307.5
50 H - 50 P	86.0	327.5
25 H - 75 P	84.0	364.0
1 H - 99 P	81.5	432.5
100 P	80.5	-

* TIMES ARE IN SECONDS

in the helium carrier gas are small ($\sim 10^{-5}$ mole fraction), there are possible interaction effects at the adsorbent surface.

Future work on the n-pentane/n-heptane system will include data generation at 175° C on the Chromosorb 102 column and at 75° to 125° C on a nonporous Carbowax 1500 column described in Table 2.

The chromatographic test facility described earlier, Ref. 45, is being modified to improve data handling. Automatic data processing as outlined in Figure 48 is being implemented to improve consistency in the data and to reduce the manual effort in handling. Oscillographic strip charting will be continued to verify the output from the more automated procedure.

Studies have also begun on the basic characteristics of the adsorbents used in the chromatographic columns. This work includes experimental determination of pore size distribution in the adsorbent particles and void fractions in the columns. These data are required for accurate prediction by the improved mathematical models being developed (see Task D.2.b.).

D.2.b. Chromatograph Model Improvement - P. T. Woodrow
Faculty Advisor: Prof. P. K. Lashmet

Prior to July, 1972 the mathematical model of the chromatographic column was based on a packing material which either was non-porous or which allowed pore diffusion and subsequent adsorption to occur at such a high rate that the resultant system dynamics were not significantly affected. Thus, in modeling the system, only interparticle and adsorbed phase mass balances were considered. The applicable partial differential equations, assumptions, initial conditions, and boundary conditions have been presented elsewhere, Ref. 25. These equations showed the predicted chromatogram to be a function of three variables:

mR_0 = a thermodynamic parameter, specific to the chemical system considered.

N_{tOG} = the number of transfer units, a dimensionless measure of diffusion rates to the adsorbent surface.

Pe = the Peclet number, a dimensionless measure of sample diffusion in the carrier gas.

Solutions to this system of equations have been reported, and cases of equilibrium adsorption ($y = y^*$; $N_{tOG} \rightarrow \infty$) and non-equilibrium adsorption ($y = y^*$; N_{tOG} is finite) have been compared with experimental data, Ref. 25. It was concluded that for the ranges of parameters encountered in typical chromatographs, consideration of a finite rate of mass transfer (N_{tOG} = finite) yields minor, at best, improvement in output chromatogram predictions. In addition, the predictions of peak height and spreading were inadequate for some experimental conditions and chemical systems. It appeared that another mechanism not considered in the model formulation was responsible for

FIGURE 48

CHROMATOGRAPHIC DATA PROCESSING

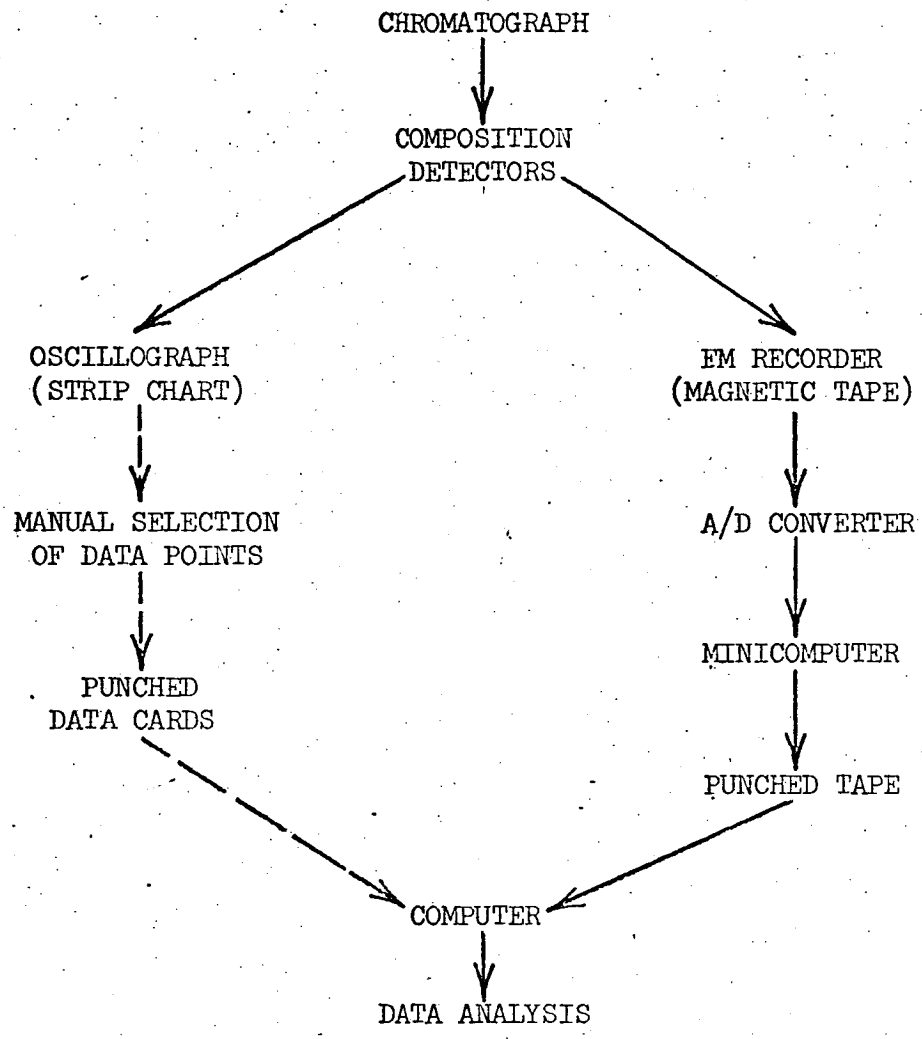

MANUAL PROCESSING -----

AUTOMATIC PROCESSING ——

the discrepancies between prediction and experiment. As the adsorbent (Chromosorb 102) was porous, Table 2, the mechanism of intraparticle diffusion warranted investigation.

Consideration of the intraparticle diffusion process as well as the rate of surface adsorption yielded a new system of equations shown in Fig. 49 and having the following parameters and variables not defined previously:

m = thermodynamic equilibrium constant.

N_{RU} = the number of reactor units, a dimensionless measure of the rate of adsorption.

Pe_A = intraparticle Peclet number, a dimensionless measure of diffusion rates within the particle.

Pe_E = interparticle Peclet number, a dimensionless measure of diffusion rates in the carrier gas.

L/R = ratio of column length to particle radius.

R_I = moles of fluid in particle per mole of adsorption sites.

r = intraparticle space variable, dimensionless.

x = adsorbed phase composition, dimensionless.

y = interparticle gas phase composition, dimensionless.

y_i = intraparticle gas phase composition, dimensionless.

y_i^* = equilibrium intraparticle gas phase composition, dimensionless.

z = longitudinal position in column, dimensionless.

As an aid to envisioning the various transport processes incorporated in this new chromatograph system formulation, Figure 50 is included. In the interparticle region, material is transported by convection (i.e., by carrier gas flow) and by turbulent and molecular diffusion in the axial direction, which is characterized by the interparticle Peclet group, Pe_E. The transport from the interparticle region to the intraparticle region is characterized by the dimensionless mass transfer coefficient, N_{tOG}. Transport by diffusion within the particle - the intraparticle region - is characterized by the intraparticle Peclet group, Pe_A. The rate of adsorption from the intraparticle gas phase to the adsorbed phase within the particle is characterized by N_{RU}, the number of reactor units.

The transfer function of the system of Figure 49 is given in Figure 51. Before attempting an inversion of the equations of Figure 51, a moment analysis of the model hereafter designated as the Inter-Intraparticle Adsorption Model was undertaken to determine gross behavior.

INTERPARTICLE PHASE MASS BALANCE:

$$\left(\frac{1}{Pe_E}\right) \frac{\partial^2 y}{\partial z^2} - \frac{\partial y}{\partial z} - N_{toG} \; (y-y_i)_{r=1} = \frac{\partial y}{\partial \theta}$$

INTRAPARTICLE PHASE MASS BALANCE:

$$\frac{1}{Pe_A} \left(\frac{L}{R}\right)^2 \left[\frac{\partial^2 y_i}{\partial r^2} + \left(\frac{2}{r}\right) \frac{\partial y_i}{\partial r}\right] - N_{RU} \; (y_i - y_i^*) = \frac{\partial y_i}{\partial \theta}$$

ADSORBED PHASE MASS BALANCE:

$$\left(\frac{1}{R_I}\right) \frac{\partial x}{\partial \theta} = N_{RU} \; (y_i - y_i^*)$$

THERMODYNAMIC RELATIONSHIP:

$$y_i^* = m \; x$$

Figure 49. System Equations for Inter-Intraparticle Model

Figure 50

CHROMATOGRAPHIC COLUMN

INTER-INTRAPARTICLE MODEL CONCEPTS

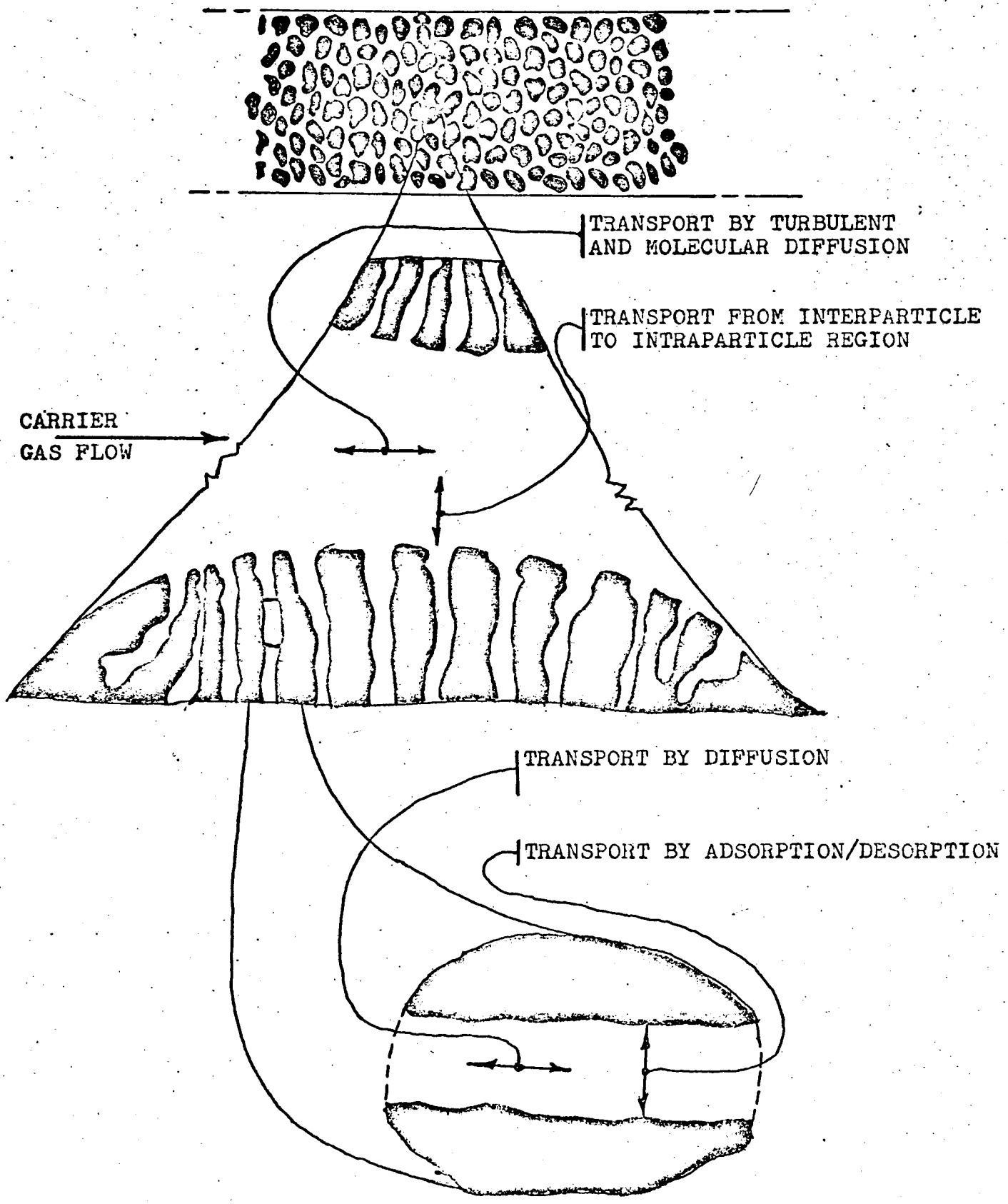

$$Y(1,s) = \exp\left\{\frac{Pe_E}{2} - \sqrt{\frac{Pe_E^2}{4} + \gamma(s)\, Pe_E}\right\}$$

where:

$$\gamma(s) = N_{toG}\,(1 - \lambda(s)) + s$$

$$\lambda(s) = \frac{b \sinh(\sqrt{a_1})}{[(b-1)\sinh(\sqrt{a_1}) + \sqrt{a_1}\cosh(\sqrt{a_1})]}$$

$$a_1(s) = \left\{\left[\frac{-N_{RU}^2\, mR_I}{(s + N_{RU} mR_I)} + N_{RU} + s\right](\frac{R}{L})^2\, Pe_A\right\}$$

$$b = \frac{N_{toG}}{3\,\frac{\beta\,(1-\epsilon)}{\epsilon}\,(\frac{L}{R})^2\,\frac{1}{Pe_A}}$$

β = Particle porosity

ϵ = Bed void fraction

Figure 51. Transfer Function of Chromatograph

This technique has been described earlier, Ref. 44.

Moments derived from the equations of Figure 51 provide characteristics of an impulse response. Because the inputs to the system are pulses of finite duration, equations relating the moments of the output chromatogram with the moments of the impulse response and input were derived:

$$A_Y = A_X$$

$$\mu 1_Y = \mu 1_X + \bar{\theta}$$

$$\bar{\mu} 2_Y = \bar{\mu} 2_X + \bar{\mu} 2_y$$

$$\bar{\mu} 3_Y = \bar{\mu} 3_X + \bar{\mu} 3_y$$

where

A_Y, A_X = areas under the output and input curves, respectively.

$\mu 1_Y, \mu 1_X$ = first moments about the origin of the output and input curves respectively.

$\bar{\theta}$ = first moment about the origin of the impulse response.

$\bar{\mu} 2_Y, \bar{\mu} 2_X$ = second moments about the mean of the output and input curves respectively.

$\bar{\mu} 2_y$ = second moment about the mean of the impulse response.

$\bar{\mu} 3_Y, \bar{\mu} 3_X$ = third moments about the mean of the output and input curves respectively.

$\bar{\mu} 3_y$ = third moment about the mean of the impulse response.

The three moments $\bar{\theta}$, $\bar{\mu} 2_y$, and $\bar{\mu} 3_y$ were derived from the equations of Figure 51, whereas the input moments $\mu 1_X$, $\bar{\mu} 2_X$, and $\bar{\mu} 3_X$ were computed directly from experimental data. A priori prediction of (L/R), Pe_A, Pe_E, and N_{toG} was possible from the experimental operating conditions. The parameters mR_0 and N_{RU} must be determined by curve-fitting procedures.

To determine qualitatively the capability of the new model of Figure 49 fore representing more adequately the chromatographic data, a parametric study of the moments was undertaken. Table 4 compares moments obtained for the ethylene system, Ref. 25, with predictions from the interparticle equilibrium adsorption model, Ref. 25, 44, and the new model. The new model more closely predicts the mean, $\mu 1$, although differences between the two models and the data are small.

TABLE 4

MOMENT ANALYSIS AND PARAMETRIC STUDY - ETHYLENE 50°C.

mR_0	$\mu_{1,observed}$	$\mu_{1,predicted}$ (1)	$\mu_{1,predicted}$ (2)
0.194	26.475	25.986	23.719

N_{RU}	$\bar{\mu}_{2_{observed}}$	$\bar{\mu}_{2_{predicted}}$ (1)	$\bar{\mu}_{2_{predicted}}$ (2)
100	7.024	13.283	0.388
200		6.973	
400		3.817	
800		2.240	
1600		1.451	
3200		1.056	
6400		0.859	
12800		0.760	
25600		0.711	

N_{RU}	$\bar{\mu}_{3_{observed}}$	$\bar{\mu}_{3_{predicted}}$ (1)	$\bar{\mu}_{3_{predicted}}$ (2)
100	19.623	13.049	0.191
200		3.519	
400		1.058	
800		0.403	
1600		0.219	
3200		0.163	
6400		0.144	
12800		0.137	
25600		0.134	

Pe_A = 9744

N_{toG} = 79750

$(L/R)^2/Pe_A$ = 436.2

(1) Inter-Intraparticle Adsorption Model
(2) Interparticle Equilibrium Adsorption Model

More importantly, the new model is capable of better predicting the dispersion, as represented by the second moment about the mean, $\bar{\mu}_2$, and more closely approximates the skew as represented by the third moment about the mean, $\bar{\mu}_3$. Values of N_{RU} necessary for good agreement between the moments are in reasonable accord with other independent data, Ref. 46. It thus appears that the proposed model will yield more adequate chromatogram predictions.

The solution to the equations of Figure 49 is presently being considered. It appears that inversion of the transfer function of Figure 51 is not feasible, and an analytical solution is probably not realizable. The simplified situation of negligible mass transfer resistance ($N_{tOG} \rightarrow \infty$) and equilibrium adsorption ($N_{RU} \rightarrow \infty$) was also investigated. It appears the resulting transfer function, while considerably less complicated, is not easily inverted. Future activities, therefore, will consider direct numerical solutions to the system equations.

REFERENCES

1. Moore, J.W., "An Exploratory Investigation of a 1979 Mars Roving Vehicle Mission," JPL Document No. 760-58, December 1, 1970.

2. Almstead, J.G., "Payload Design of an Unmanned Martian Roving Vehicle," a project report in partial fulfillment of the degree requirements of a Master of Engineering, RPI, Troy, N.Y., August 1972.

3. Uicker, J.J., "User's Guide, IMP, A Problem Oriented Language for the Computer Aided Design and Analysis of Mechanism," Department of Mechanical Engineering, Univ. of Wisconsin, Madison, Wisconsin, 1972.

4. Biezeno, C.B. and Grammel, R., Engineering Dynamics, Vol. II, D. Van Nostrand Co., Inc., 1956.

5. LTT Aerospace/Optical Division, Final Report to NASA for Lunar Rovering Vehicle Hazard Detection, May 1970, pages 3-9, 3-43.

6. Kuriger, W., "A Proposed Obstacle Sensor for a Mars Rover," Journal of Spacecraft and Rockets, Vol. 8, No. 10, October 1971, pages 1043-1048.

7. Fowler, V. J. and Schafer, J., "A Survey of Laser Beam Deflection Techniques," Proceedings of the IEEE, Vol. 54, No. 10, October 1966, pp. 1437-1443.

8. Advertisement by Coherent Optics, Inc., Laser Focus, Feb. 1970, pp. 13.

9. Kulcke, W. et al, "Digital Light Deflectors," Proceedings of the IEEE, Vol. 54, No. 10, October 1966, pp 1419-1429.

10. Nelson, T. J., "Digital Light Deflection," Bell System Technical Journal, Vol. 43, No. 3, May 1964, pp. 821-845.

11. Kuriger, W., "A Proposed Obstacle Sensor for a Mars Rover," Journal of Spacecraft and Rockets, Vol. 8, No. 10, October 1971, pp. 1043-1048.

12. Nikon Inc., Lens Catalogue.

13. Golden, J., "An Obstacle Detection System for Mid-Range Path Selection for an Autonomous Roving Vehicle," Annual Report to NASA, RPI, Troy, N. Y., June 1972.

14. Fox, E.A., Mechanics, Harper & Row, N.Y., 1967, p. 237.

15. Pavarini, C. and Chrysler, J.H., "Terrain Modeling and Path Selection by an Autonomous Martian Exploratory Vehicle," RPI Technical Report MP-14 NASA Grant 33-018-191, June 1970.

16. Rautio, A., "An Analysis of the Effect of Sensor Errors on a Long Range Terrain Modeling System and a Study of Short Range Terrain Modeling for an Autonomous Roving Vehicle, RPI Masters Project Report, June 1971.

17. DeRusso, P., Roy, R., and Close, C., State Variables for Engineers, John Wiley & Sons, Inc., N.Y. 1965, p. 457.

18. Bryson, A.E. and Ho, Y.C., Applied Optimal Control, Ginn-Blaisdell Publishing Co., 1969, Chapter 12.

19. Shen, C.N., "Random Variables, Gauss-Markov Random Sequences and Linear Discrete Optimal Filtering," unpublished notes, RPI, Troy, N.Y.

20. Golden, J., "An Obstacle Detection System for Mid-range Path Selection for an Autonomous Roving Vehicle," RPI Masters Project Report, June 1972.

21. Rautio, A.M., "An Analysis of the Effect of Sensor Error on Long Range Terrain Modeling System and a Study of Short-Range Terrain Modeling for an Autonomous Roving Vehicle," RPI Masters Project Report, June 1971.

22. Frederick, D.K. et al, "A Progress Report for July 1, 1971 to June 30, 1972, Analysis and Design of a Capsule Landing System and Surface Vehicle Control System for Mars Exploration" RPI Technical Report MP-28, Rensselaer Polytechnic Institute, Troy, N.Y., July 1972.

23. Boheim, S.L. and Purdon, W.C., "Path Selection System Simulation and Evaluation for a Martian Roving Vehicle," RPI Technical Report MP-29, December 1972.

24. Benoit, G.L., "Reduction of Chromatographic Data and Evaluation of a GC Model," RPI Technical Report MP-22, Rensselaer Polytechnic Institute, Troy, New York, June 1971.

25. Keba, P.S., and Woodrow, P.T., "A Comparison of Two Gas Chromatograph Models and Analysis of Binary Data," RPI Technical Report MP-27, Rensselaer Polytechnic Institute, Troy, New York, July 1972.

26. Frederick, D.K., Lashmet, P.K., Sandor, G.N., Shen, C.N., Smith, E.J., and Yerazunis, S.W., "Progress Report for July 1, 1971 to June 30, 1972," RPI Technical Report MP-28, Rensselaer Polytechnic Institute, Troy, New York, July 1972.

27. Mattuch, J., and Herzog, R., "Uber einen neuen Massen-spektrographen," Z. Phys., 89, 786-795 (1934).

28. Herzog, Richard, "Ionen-und elektronenoptische Zylinderlensen und Prismen, I., " Ibid., 89, 447-473 (1934).

29. Matsuda, H., Fukumoto, S., and Matsuo, T., "New Ion Optical System for a High-Resolution Mass Spectrometer,""Recent Developments in Mass Spectroscopy," (K. Ogata and T. Hayakawa, ed.), University Park Press, Baltimore, 1970, pp. 175-180.

30. Nier, A.O., "A Mass Spectrometer for Isotope and Gas Analysis," Rev. Sci. Instr., 18, 398-411 (1947).

31. Nier, A.O., "A Mass Spectrometer for Routine Isotope Abundance Measurements," Ibid., 11, 212-216 (1940).

32. Cooper, J.L., Pressley, G.A., and Stafford, F.E., "Electron Impact Ionization Cross-sections for Atoms," J. Chem. Phys., 44, 3946-3949 (1966).

33. Littlewood, A.B., Gas Chromatography, Principles, Techniques, and Applications," Academic Press, New York, 1970, pp. 1, 2.

34. Kubaschewski, O., Cibula, A., and Moore, D., "Gases and Metals," American Elsevier, New York, 1970, p. 94.

35. Burmeister, L., Loser, J., and Sneegas, E., "Advanced Valve Technology," Report NASA SP-5019, Natl. Aeronaut. Space Admin., Washington, D.C., 1967.

36. Dushman, S., "Scientific Foundations of Vacuum Technique," 2nd ed., (J.M. Lafferty, ed.), Wiley, New York, 1962, pp. 570-574.

37. Siemon, K., "Pressure Vessel Manual," Edwards Brothers, Ann Arbor, Mich., 1958, pp. 37-52.

38. Morris, E.E., "Glass-Fiber-Reinforced Metallic Tanks for Cryogenic Service," in "Advances in Structural Composites," Sci. Adv. Mater. Process Eng., 12, Paper No. AS-4, 1967.

39. "Engineering Model GC/MS Design Review: Gas Chromatograph Subsystem," pp. 6-1 to 6-29, Jet Propulsion Lab., Pasadena, Cal., Jan. 28, 1971.

40. Ibid., pp. 2-1 to 2-8.

41. "Dynamic Response of a Gas Chromatograph - Mass Spectrometer Combination," JPL Space Programs Summary 37-62, v. I, pp. 28-33, Jet Propulsion Lab., Pasadena, Cal., Mar. 31, 1970.

42. Crank, J., "The Mathematics of Diffusion," Clarendon Press, Oxford, 1956, pp. 62-64.

43. Sliva, T.F., "Chromatographic Systems Analysis: First-Order Model Evaluation," RPI Technical Report MP-1, Rensselaer Polytechnic Institute, Troy, New York, Sept. 1968.

44. Voytus, W.A., "Chromatographic Systems Analysis: Moment Analysis of the Equilibrium Adsorption Model," RPI Technical Report MP-9, Rensselaer Polytechnic Institute, Troy, New York, Aug. 1969.

45. Baer, S.R., and Benoit, G.L., "Chromatographic Test Facility," RPI Technical Report MP-19, Rensselaer Polytechnic Institute, Troy, New York, Mar. 1971.

46. Schneider, P., and Smith, J.M., "Adsorption Rate Constants from Chromatography," AIChE J., 14, 762-771 (1968).